



University of  
Stavanger

Faculty of Science and Technology

## MASTER'S THESIS

Study program/ Specialization:  Offshore Technology/ Marine- and Subsea Technology	Spring semester, 2014  Open / <del>Restricted access</del>
Writer: Fredrik Haugland Danielsen	..... (Writer's signature)
Faculty supervisor: Eiliv Fougner Janssen  External supervisor: Peter Ostrowski, A/S Norske Shell	
Thesis title:  Dynamic Loads on Telescopic Safety Joint for Workover Riser	
Credits (ECTS): 30p	
Key words: - Workover riser - Safety Joint - Weak link - Workover operation - Workover installation	Pages: 73  Stavanger, June 5 <sup>th</sup> 2014 Date/year

## ABSTRACT

The push in the industry towards increasing the weather window for marine operations offshore leads to a focus on new technology. When performing workover operations in a subsea well, the workover riser is a physical connection between the well and the floating workover vessel. A floating vessel will experience wave induced motion and is therefore equipped with a heave compensator to allow for this relative motion without increasing the load to the riser. If the heave compensator fails or if the heave of the vessel exceeds the stroke length of the heave compensator, the workover riser can be subjected to an excessive axial force that could rupture the riser and damage subsea well barriers.

A safety joint that is to be installed in the riser can improve the window for safe operation while reducing consequences if an accident were to occur. It is called the Telescopic Safety Joint (TSJ) and has been developed by FMC Technologies. The joint is designed to telescope when subjected to a predetermined axial force. The telescoping function of the joint will ensure that there is sufficient time for personnel onboard the vessel to activate the emergency disconnect function so that the riser can safely be disconnected from the well.

The safety joint is a weak link. During installation of the workover system, the riser experiences loading conditions exceeding that of normal operation. There is a concern that the safety joint may take plastic damage during this installation. Hence the TSJ is equipped with an over-ride function that temporarily can increase the strength of the joint. The over-ride function works by pumping hydraulic pressure into external cylinders. The increase in the strength of the joint from the over-ride function depends upon the hydraulic pressure. This thesis studies the effect the over-ride function has on the weather window for installation of a workover system, comparing a fully pressurized over-ride function to a semi-pressurized over-ride function.

Simulations in Orcaflex for various environmental conditions found the loads that the TSJ must be able to withstand for installation to be possible. A model of the joint was created in AUTODESK Inventor. Using ANSYS workbench, the model was tested to find out which loads that are acceptable and which loads leads to plastic damage of the joint both for the fully pressurized and semi-pressurized over-ride function.

Combining the results for the fully- and semi-pressurized over-ride function test, with the results from the dynamic simulations performed in Orcaflex revealed an increase in installation window when using the fully pressurized over-ride function. The joint using the full capacity of the over-ride function was able to withstand 620kNm before plastic damage took place. The joint using a semi-pressurized over-ride function began taking plastic damage at 400kNm. The over-ride function increases the bending moment capacity of the joint by 55%. Using the scatter diagram for the Draugen field to see how many observations has been made of the different sea states, the increased availability for installation when using the full capacity of the over-ride function, as opposed to the semi-pressurized joint was calculated. When installing the TSJ as the 2<sup>nd</sup> riser joint, the availability increased by 21,7%. Installing the TSJ as the 3<sup>rd</sup> joint increases the availability by 16,7%. Installation of the TSJ on the 4<sup>th</sup> and 5<sup>th</sup> joint gives an increase of respectively 2,8% and 0,3% when the full over-ride capacity is used. The over-ride functions proved to be so effective that the joint became stronger than the actual workover riser. Hand calculations showed that the riser would yield before the safety joint and thus the safety joint would not be a limiting factor for the workover installation activity if the over-ride function is active.

## ACKNOWLEDGEMENTS

Although this thesis only has one writer at the front page, it was by no means a one-man project. During the last five months I have received some great support while writing this thesis.

First of all, I would like to thank Tor-Øystein Carlsen and Svein Kjenner from FMC Technologies. In the early face of the project they took the time to meet with me to define a scope for the thesis that would be of interest for FMC Technologies, Norske Shell and I. They gave me a thorough presentation of the Telescopic Safety Joint which gave me an insight that would be difficult to achieve only by reading. Tor-Øystein has also been very helpful whenever I needed some expert judgement or information. Thank you for the invitation OTC in Houston, I would have loved to go. Perhaps I'll see you there some time in the future.

Thank you to my university supervisor Eiliv Fougner Janssen. You were a terrific motivation while writing this report and I always looked forward to our meetings. I appreciate all the help you gave me throughout the semester, I found it very helpful.

I would like to express my sincere gratitude to my external supervisor Peter Ostrowski at Norske Shell. It was Peter whom first came up with the idea of using the Telescopic Safety Joint as the topic for my thesis and even took the time to travel to Asker with me, to meet with Tor-Øystein and Svein. He showed a genuine interest in the work I have been performing and was always a great help when I had questions. I could not have asked for a more dedicated supervisor. Thank you.

Last of all; thank you to my classmates at room D-207. It surely made writing my thesis more fun by having great friends around me while doing so.

Fredrik Haugland Danielsen  
University of Stavanger  
June 4<sup>th</sup> 2014

## TABLE OF CONTENT

Abstract .....	i
Acknowledgements .....	ii
List of Symbols .....	3
List of Abbreviations .....	4
List of Figures .....	5
List of Tables.....	6
1.1 Introduction .....	7
1.2 Scope of the Thesis .....	8
1.3 Methodology.....	8
1.4 Structure of the Thesis .....	9
1.5 Limitations for This Thesis.....	9
2.1 Riser Types .....	10
2.2 The Workover Riser System .....	11
2.3 Technology Background .....	12
2.3.1 Operational Risks .....	12
2.3.2 Benefits of The Telescopic Safety Joint.....	13
2.3.3 Concerns When Installing a Safety Joint.....	13
2.4 Workover Riser Loads .....	14
2.4.1 Operational Loads.....	14
2.4.2 Installation Loads .....	16
2.5 Design of the Telescopic Safety Joint from FMC Technologies .....	19
2.6 Situations Requiring a Weak Link.....	23
2.6.1 Vessel Drift-off .....	23
2.6.2 Heave Compensator Lock up/Stroke out.....	23
3.1 Orcaflex 9.7 .....	24
3.2 Workover Vessel Data .....	24
3.3 Environmental Data Settings.....	25
3.3.1 Scatter Diagram .....	25
3.3.2 Current.....	25
3.3.3 Wave Spectrum .....	26
3.3.4 Wave Settings .....	26
3.4 The Workover Riser .....	27
3.4.1 Boundary Conditions .....	27
3.4.2 Dimensions .....	27
3.4.3 Added Mass .....	28
3.4.4 Drag Coefficient .....	28
3.4.5 Segment Length .....	33
3.5 The Xmas Tree Stack .....	34
3.5.1 Dimensions .....	34
3.5.2 Added Mass to Xmas Tree Stack.....	35
3.5.3 Added Mass Coefficient.....	38
3.5.4 Drag Coefficient .....	38
3.5.5 Mass Coefficient .....	39
3.5.6 Mass Moment of Inertia .....	39
3.5.7 Volume of the Stack.....	40
3.6 Summary of Orcaflex Input .....	40

3.7 Orcaflex Simulations .....	41
3.8 Ansys Workbench 13.0.....	41
3.8.1 Autodesk Inventor Model.....	42
3.8.2 Acceptance Criteria.....	43
3.8.3 Bolt Pretension Settings.....	43
3.8.4 Tensile Bolts.....	45
3.8.5 Simulation .....	46
4.1 Sensitivity Analysis .....	47
4.1.1 Time Step Sensitivity Test .....	47
4.1.2 Current Sensitivity Test.....	48
4.1.3 Point of Maximum Bending Moment .....	48
4.1.3 Point of Maximum Effective Riser Tension .....	49
4.2 Results of the Dynamic Simulations .....	50
4.2.1 Test 1 – Results for the 26m Riser Simulation (2 <sup>nd</sup> joint deployed) .....	50
4.2.1 Test 2 – Results for the 39m Riser Simulation (3 <sup>rd</sup> joint deployed) .....	52
4.2.2 Test 3 – Results for the 52m Riser Simulation (4 <sup>th</sup> joint deployed) .....	55
4.2.3 Test 4 – Results for the 65m Riser Simulation (5 <sup>th</sup> joint deployed) .....	57
4.3 Results from Ansys Workbench .....	60
4.3.1 Results of the Semi-pressurized Over-ride Function Test.....	60
4.3.2 Results of the Fully-pressurized Over-ride Function Test .....	61
4.4 Weather Window .....	61
4.4.1 Installation Window for the TSJ as the 2 <sup>nd</sup> Riser joint .....	62
4.4.2 Installation Window for the TSJ as the 3 <sup>rd</sup> Riser Joint.....	62
4.4.3 Installation Window for the TSJ as the 4 <sup>th</sup> Riser Joint.....	63
4.4.4 Installation Window for the TSJ as the 5 <sup>th</sup> Riser Joint.....	63
4.5 Summary of Results.....	64
4.6 Strength of the Riser .....	64
5.1 Discussion.....	67
5.2 Conclusions .....	68
5.3 Recommendations for Future Work .....	68
Reference list .....	69

## LIST OF SYMBOLS

$A_0$	– added mass for a rectangular plate
$A_{mSX}$	– added mass for a solid block – translational motion along the x-axis
$A_{mSY}$	– added mass for a solid block – translational motion along the y-axis
$A_{mSZ}$	– added mass for a solid block – translational motion along the z-axis
$A_{mX}$	– added mass for a perforated block – translational motion along the x-axis
$A_{mY}$	– added mass for a perforated block – translational motion along the y-axis
$A_{mZ}$	– added mass for a perforated block – translational motion along the z-axis
$A_p$	– area of the submerged part of an object projected on a horizontal plane
$A_R$	– cross sectional area for added mass
$A$	– cross sectional area
$C_A$	– added mass coefficient
$C_{AX}$	– added mass coefficient in x direction
$C_{AY}$	– added mass coefficient in y direction
$C_{AZ}$	– added mass coefficient in z direction
$C_d$	– drag coefficient
$C_m$	– mass coefficient
$C_{mx}$	– mass coefficient in x direction
$C_{my}$	– mass coefficient in y direction
$C_{mz}$	– mass coefficient in z direction
$D$	– diameter
$d$	– water depth
$g$	– gravity constant
$H_{max}$	– maximum wave height
$H_s$	– significant wave height
$h$	– height
$I_x$	– mass moment of inertia about x-axis
$I_y$	– mass moment of inertia about y-axis
$I_z$	– mass moment of inertia about z-axis
$I$	– moment of inertia
$K_c$	– Keulegan-Carpenter number
$k_s$	– stiffness of the spring
$k$	– surface roughness
$L_p$	– length of pendulum
$L$	– wave length
$M_{max}$	– maximum bending moment
$m_A$	– added mass per meter
$m$	– mass
$p$	– perforation percentage
$R_{p0,2}$	– offset yield point
$T_{bolt}$	– maximum tension capacity of each tensile bolt
$T_{eff}$	– effective riser tension
$T_{max}$	– maximum effective riser tension
$T_p$	– natural period of pendulum motion
$T_s$	– natural period of a spring
$T_z$	– zero up-crossing period
$T$	– wave period

$u_{max}$	– maximum horizontal water particle velocity
$u$	– horizontal water particle velocity
$V$	– volume
$y$	– distance from the neutral line to the point furthest from the center
$z$	– water depth of the water particle velocity
$\xi_0$	– wave amplitude
$\sigma_b$	– bending stress
$\sigma_t$	– axial stress
$\rho$	– density of fluid
$\tau$	– shear stress
$\nu$	– kinematic viscosity
$\omega$	– wave frequency

## LIST OF ABBREVIATIONS

BOP	– Blow Out Preventer
EDP	– Emergency Disconnect Package
EQD	– Emergency Quick Disconnect
ID	– Inner Diameter
JONSWAP	– Joint North Sea Wave Project
LMRP	– Lower Marine Riser Package
LRP	– Lower Riser Package
OD	– Outer Diameter
TSJ	– Telescopic Safety Joint
XT	– Xmas Tree

## LIST OF FIGURES

- Figure 1.1 The Telescopic Safety Joint prototype by FMC Technologies
- Figure 2.1 The drilling riser
- Figure 2.2 The workover system configuration
- Figure 2.3 The Telescopic Safety Joint installed in the riser
- Figure 2.4 Location of the TSJ in the workover riser
- Figure 2.5 Bending moments in riser due to vessel offset
- Figure 2.6 Example of bending moment distribution along a riser during operation
- Figure 2.7 Forces contributing to the motion of the equipment stack
- Figure 2.8 Pendulum from an elastic band
- Figure 2.9 The Telescopic Safety Joint by FMC Technologies
- Figure 2.10 Simplified assembly of the TSJ
- Figure 2.11 Assembly of the TSJ with tensile bolts
- Figure 2.12 Configuration of the pressure compensating cylinders in the TSJ
- Figure 2.13 Configuration of the long pressure balance cylinders in the TSJ
- Figure 2.14 Configuration of the over-ride cylinders in the TSJ
- Figure 2.15 Long sea pressure cylinders
- Figure 3.1 Picture of the Transocean Arctic
- Figure 3.2 The JONSWAP spectrum compared to the Pierson-Moskowitz spectrum
- Figure 3.3 Wave train settings from OrcaFlex
- Figure 3.4 Boundary conditions for the riser
- Figure 3.5 Drag coefficients as a function of Reynolds number and surface roughness
- Figure 3.6 Segment lengths for the workover riser in OrcaFlex
- Figure 3.7 The geometry of the model used for the OrcaFlex simulations
- Figure 3.8 Rotational axis of the equipment stack
- Figure 3.9 The workover vessel seen in OrcaFlex
- Figure 3.10 Autodesk Inventor model of the retracted TSJ
- Figure 3.11 Close-up of the Tensile and Over-ride bolts
- Figure 3.12 Section cut view of the interface between the upper and lower sections of the joint
- Figure 3.13 Reaction forces from the bolt pretension
- Figure 3.14 Location of the three tensile bolts in the model
- Figure 3.15 Forces applied to the joint in ANSYS
- Figure 4.1 Sensitivity analysis of the time step in OrcaFlex
- Figure 4.2 Comparison of bending moment in the riser with and without sea current
- Figure 4.3 Distribution of bending moment along the workover riser
- Figure 4.4 The distribution of effective tension along the riser
- Figure 4.5 The workover vessel with two riser joints deployed.
- Figure 4.6 The bending moment as a function of wave period (26m test)
- Figure 4.7 The bending moment as a function of the significant wave height (26m test)
- Figure 4.8 The workover vessel with three riser joints deployed
- Figure 4.9 The bending moment as a function of wave period (39m test)
- Figure 4.10 The bending moment as a function of the significant wave height (39m test)
- Figure 4.11 The workover vessel with four riser joints deployed
- Figure 4.12 The bending moment as a function of wave period (52m test)
- Figure 4.13 The bending moment as a function of the significant wave height (52m test)



Figure 4.14	The workover vessel with five riser joints deployed
Figure 4.15	The bending moment as a function of wave period (65m test)
Figure 4.16	The bending moment as a function of the significant wave height (65m test)
Figure 4.17	Yielding of tensile bolt at 400kNm
Figure 4.18	Yielding of tensile bolt at 620kNm
Figure 5.1	Acceptable bending moment for TSJ vs workover riser

## LIST OF TABLES

Table 3.1	Wave heights – wave periods for Draugen
Table 3.2	Dimensional values for the workover riser
Table 3.3	Added mass for a cylinder
Table 3.4	Maximum wave height for the different sea states
Table 3.5	Horizontal water particle velocity for all waves.
Table 3.6	Reynolds numbers for all waves
Table 3.7	Keulegan-Carpenter numbers for each significant wave height
Table 3.8	Drag coefficients for each significant wave height
Table 3.9	Dimensions for the equipment stack used in OrcaFlex
Table 3.10	DNV table for calculation of added mass for square prisms
Table 3.11	DNV table for calculation of added mass for flat plates
Table 3.12	Input data for the workover riser
Table 3.13	Drag coefficients for the workover riser
Table 3.14	Input values for the equipment stack
Table 3.15	Data table for the tensile bolts
Table 3.16	Pretension values to be used in ANSYS workbench
Table 4.1	Maximum bending moments in the riser for different waves – test 1
Table 4.2	Maximum effective riser tensions for different waves – test 1
Table 4.3	Maximum bending moments in the riser for different waves – test 2
Table 4.4	Maximum effective riser tensions for different waves – test 2
Table 4.5	Maximum bending moments in the riser for different waves – test 3
Table 4.6	Maximum effective riser tensions for different waves – test 3
Table 4.7	Maximum bending moments in the riser for different waves – test 4
Table 4.8	Maximum effective riser tensions for different waves – test 4
Table 4.9	Data table for the Semi-pressurized Over-ride function test
Table 4.10	Data table for the Fully-pressurized Over-ride function test
Table 4.11	Installation window for the TSJ as the 2 <sup>nd</sup> joint
Table 4.12	Installation window for the TSJ as the 3 <sup>rd</sup> joint
Table 4.13	Installation window for the TSJ as the 4 <sup>th</sup> joint
Table 4.14	Installation window for the TSJ as the 5 <sup>th</sup> joint
Table 4.15	Availability for installation of EDP, LRP and Xmas tree at Draugen
Table 4.16	Shear force in the workover riser

# 1. INTRODUCTION

## 1.1 INTRODUCTION

Technology that will enable larger weather windows for offshore activities whilst maintaining/increasing safety is of great interest for the industry. Marine operations in more challenging environmental conditions will amplify the motion of vessel and equipment so that there is an enlarged risk of accidental loads or impact. To reduce these risks the industry must implement extra safety measures to fulfill the rules and regulations for safe operation offshore. An activity that may be delayed due to weather is workover operations. During workover the vessel is connected to the well through a workover riser. The workover riser provides a conduit for fluid and equipment to be transferred between the vessel and the well without direct contact to the sea. The riser is a rigid steel pipe and workover vessels use heave compensators that enable heave motion of the vessel relative to the well. If however, this relative movement between the vessel and seabed is too large an excessive force may be exerted to the workover riser. A force with a magnitude that can lead to rupture of the riser, damage to the vessel or subsea equipment installed down with the well. Such an accident can result in devastating consequences for the involved companies and personnel, but also environmental pollution. Various safety functions are implemented onboard the vessel and at the seabed to avoid such a situation, but the risk of accidents can never be neglected.

A new type of weak link developed by FMC Technologies can improve the weather window for safe operation and greatly reduce the consequences if accidents were to occur. A weak link in a riser is designed to break off before an accidental axial load can damage any other equipment, thus the only damage to the system will be to the weak link itself. The FMC developed weak link is called the Telescopic Safety Joint (TSJ) and is shown in figure 1.1. At a predetermined axial tension this link splits and begins to slide apart. It never fully disengages, but telescopes. The joint is designed so that its telescoping stroke length always exceeds any heave motion of the vessel. While the joint is stroking there will be no discharge of the fluid contained within the workover riser to the external environment. Once an accident has occurred and the joint has begun telescoping, the TSJ provides sufficient time for the personnel onboard to safely disconnect the riser from the well.



Figure 1.1 The Telescopic Safety Joint prototype by FMC Technologies (FMC Technologies, 2014)

A challenge when using such a weak link is the loads it is subjected to during installation of the workover equipment. The workover riser may be used as running tool for installation of a Xmas tree, a Lower Riser Package (LRP) and an Emergency Disconnect Package (EDP). These tools combined has a dry weight exceeding 100 tonnes. When using the workover riser as a running tool the tension and bending moment in the riser will be far above that of normal operational loads. This requires extra attention to the weak link as this is the most vulnerable point along the riser. The FMC developed TSJ is equipped with four over-ride cylinders that can temporarily increase the strength of the joint so that it does not take damage during installation. The over-ride cylinders work by applying an external hydraulic pressure. The magnitude of this pressure determines the

pretension in the joint and thus increases its strength. This thesis will study how these over-ride cylinders can increase the weather window for installation of a workover system, compared to installation using a weak link without the same over-ride capability.

## 1.2 SCOPE OF THE THESIS

During installation of an EDP, a LRP and a Xmas tree (hereafter referred to as the “equipment stack” or “stack”) the workover riser is used as a running tool. As the stack is lowered through the sea it is subjected to hydrodynamic forces. The forces exerted on the equipment stack along with its own weight generate load conditions in the riser that are larger than the operational loads. If the TSJ is to be installed in the riser it must be able to withstand these loads without taking damage. The TSJ is designed to be the weakest link along the riser and when it is subjected to an axial load above a certain magnitude it will begin to separate. The axial loads during installation will exceed the predetermined operational breaking load due to the large equipment stack connected to the riser. The TSJ is equipped with an over-ride function that temporarily increases the axial and bending stiffness of the joint. This makes the joint more suited to cope with the installation loads without taking plastic damage.

The purpose of this thesis is to study the loads that the TSJ is subjected to during installation and to verify the effect of using the over-ride function in such cases. The effect of the bending moment to the TSJ will be of particular interest. The alternative to using the TSJ is to install a traditional weak link in the riser. The aim is to show how the over-ride function increases the weather window for installation of the Xmas tree stack.

## 1.3 METHODOLOGY

A model of the applicable installation scenario is created in ORCAFLEX 9.7. This model will be used for the dynamic simulations. The first task of creating a good model for the simulations is to calculate all relevant input data to OrcaFlex. Dimensions, coefficients for added mass and drag, mass moment of inertia etc. must be imported to the model data sheet for the riser and the equipment connected to this. A workover vessel must be chosen and its Response Amplitude Operator (RAO) will be plotted into the vessels data sheet. This thesis is written for Norske Shell and so a water depth that would be relevant for one of their fields in the Norwegian Sea is to be used. Once the model is complete, the simulations will show the loads in the workover riser during installation. A combination of different significant wave heights and zero up-crossing periods are going to result in different bending moments and axial tensions in the riser. The environmental data for the chosen field is supplied by Shell. The length of the riser will have an effect on the bending moment, so different riser lengths must be used. Once the location and magnitude of the largest loads have been found they can be presented in matrices showing their dependence of significant wave heights and zero up-crossing periods.

Once the distribution of dynamic loads in the workover riser is found, the next step will be to see how they are going to affect the TSJ if it was installed at the point exposed to the largest loads. AUTODESK Inventor will be used to create a model of the joint with dimensions supplied by FMC Technologies. With the help of ANSYS Workbench 13.0, this model can be used for a static structural simulation in order to see how much bending moment and tension the joint can withstand before taking plastic damage. The TSJ has an over-ride function that temporarily increases its load capacity. By comparing the ANSYS Workbench results of the joint with fully pressurized over-ride cylinders to a joint with semi-pressurized over-ride cylinders, it should be possible to see how much effect the over-ride function has on the strength of the joint. When the strength of the joint is known the installation window can be found using the results from OrcaFlex. Using the scatter diagram, the increased availability for installation of the workover system can be calculated.

The following five tasks sums up the work to be performed in this thesis:

1. A workover installation using an 8 5/8" outer diameter, 7" inner diameter workover riser is chosen.
2. Create a model of an installation scenario where an EDP, a LRP and a Xmas tree is being installed by the workover riser. Perform dynamic simulations in OrcaFlex 9.7 to find bending moments and axial forces that the safety joint will be subjected during installation.
3. Test different values for significant wave heights and zero up-crossing periods that are applicable for the chosen area, along with different riser lengths. (environmental data from Shell metocean data)
4. Perform finite element analysis using ANSYS of a simplified model of the TSJ to verify the effect of the over-ride cylinders. The analysis will compare the strength of the joint subjected to bending moments and increased axial loads when using the full capacity of the over-ride cylinders, to a version of the joint that has a reduced over-ride capacity.
5. To show how the over-ride cylinders increase the weather window and whether the safety joint will limit the installation window.

## 1.4 STRUCTURE OF THE THESIS

This thesis is divided into five chapters. The first chapter contains the introduction to the scope of this thesis. This is to give the reader an understanding of the purpose of the simulations to be performed. The chapter will briefly clarify the reasons for installing a weak link in a workover riser. There is also a section explaining the limitations of the work performed.

Chapter two provides further insight to reasons why such a weak link is critical to a workover system. This chapter shows how the workover riser is exposed to different loads during installation than for operation. The joint is described in sufficient detail for the reader to gain understanding of its various components and their function. The purpose of the over-ride system is described and how this system should increase the weather window for installation.

Chapter three describes how the installation scenario will be modeled using the OrcaFlex software and which parameters that are used for the simulations. This includes the calculation of various coefficients and input values for the OrcaFlex simulations. The chapter also contains a description of the ANSYS workbench model.

Chapter four presents the results from the OrcaFlex and the ANSYS workbench simulations. The data obtained from these simulations are used to conclude when installation of a workover system using the TSJ is acceptable and when it is not. The strength of the workover riser with respect to bending moment is calculated in order to see whether the TSJ will be the limiting factor when performing the installation.

Chapter five contains the conclusions with discussion. The section includes recommendations for future work.

## 1.5 LIMITATIONS FOR THIS THESIS

This thesis will focus on an installation case where a Xmas tree is installed along with a LRP and an EDP at the Draugen field located in the Norwegian Sea, 150km north of Kristiansund. The steel workover riser is used as a running tool and has the dimensions; OD 8 5/8" and ID 7". The water depth is 250m. Simulations are going to be performed for significant wave heights up to 5m, with zero up-crossing periods applicable for the Draugen field. All waves have a 0° heading towards the vessel. The RAO data for the Transocean Artic is used for the workover vessel. The thesis will only focus on the load effect on the TSJ and the workover riser during installation. Other components of the system that might take damage will not be covered. The final conclusion with acceptable installation conditions will only show which weather conditions that does and does not lead to plastic damage to the TSJ. Operational loads are not covered.

## 2. STATE OF THE ART

This chapter describes the functional requirements of the Telescopic Safety Joint and also argues why the safety joint should be located close to the bottom end of the riser as opposed to being installed close to the mean water level. The chapter describes the different loading conditions the riser is subjected to during installation and operation.

### 2.1 RISER TYPES

There are two types of risers used for marine operations. The drilling riser (often referred to as a marine riser) and the workover riser. The difference between the two is explained briefly.

#### THE DRILLING RISER/MARINE RISER

For subsea wells the Blow Out Preventer (BOP) is situated at the seabed. The drilling riser is an extension of the well from the BOP to the drilling vessel. The drilling riser enables transfer of fluid and equipment from the vessel to the well without interaction with the sea. For drilling operations, the drilling riser guides the drill string while the annulus provides a conduit which permits the return of drilling fluid and cuttings to the surface. The drilling riser is only designed to withstand hydrostatic pressure and so the pressure from the well must never enter the riser bore. Hydrocarbons should hence never enter the riser. The drilling riser will serve as a running and retrieving string for the BOP stack. Drilling risers are large diameter pipes, often with a nominal diameter exceeding 21". (Baker, 1991, p.537) The drilling riser is usually used together with a Lower Marine Riser Package (LMRP) and BOP as seen in figure 2.1.

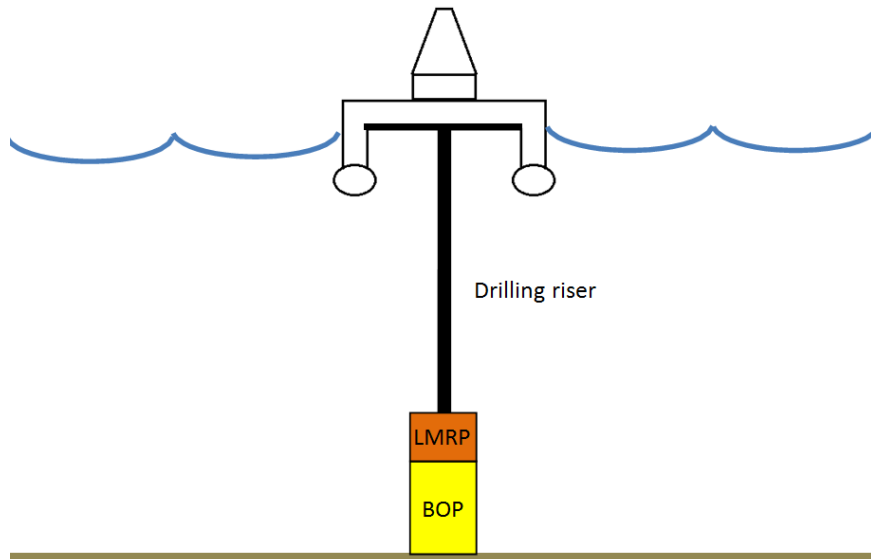


Figure 2. 2 The drilling riser

#### THE WORKOVER RISER

A workover riser has many of the same applications as a drilling riser. The workover riser is an extension of the well from the seabed to the workover vessel. The riser enables transfer of fluid and equipment from the vessel to the well without interaction with the sea and serves as a running tool for equipment being installed or removed from the seabed. Unlike a drilling riser, the workover riser is designed to be in direct contact with the well stream. This means that the workover riser is exposed to well pressure and hydrocarbons. The workover

riser has a smaller diameter than a drilling riser. The outer diameter for the riser used in this report will be 8 5/8". The workover riser can be installed along with an Emergency Disconnect Package (EDP) and a Lower Riser Package (LRP), as seen in figure 2.2.

## 2.2 THE WORKOVER RISER SYSTEM

Performing a workover operation will not always include installation of a Xmas tree. If the Xmas tree is already installed, the workover operation only requires a LRP and an EDP in order to safely enter the well. A sketch of how the workover system is configured when installing a Xmas tree is shown in figure 2.2. For the reader not familiar with the system, a brief description of the relevant components and their function is given. (Subsea1, 2014)

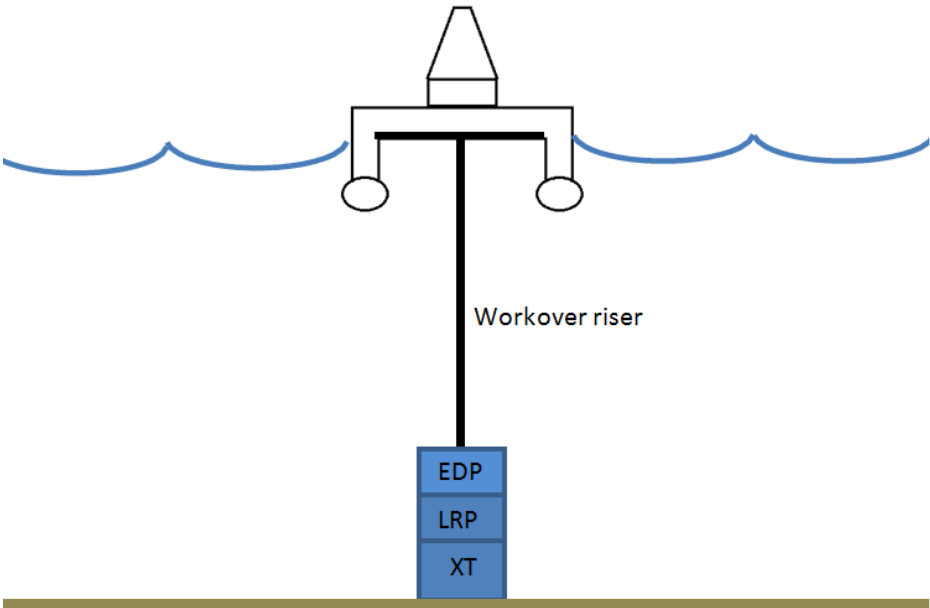


Figure 2.2 The workover system configuration

### The Emergency Disconnect Package

The EDP makes up a part of the well barrier together with the LRP during operations. It has a retainer valve situated in the main bore which is the main barrier of the EDP. If the workover vessel for some reason has to quickly abort the workover operation and disconnect from the well, it provides facilities for safe Emergency Quick Disconnect (EQD) of the workover riser from the LRP. As the name suggest, the EDP should only be used for emergency situations. (Subsea1, 2014)

### The Lower Riser Package

The LRP is installed together with the EDP on top of the Xmas tree during the workover operations. The LRP is a part of the well barrier. Typically it comprises of minimum an isolation valve and a shear seal ram situated in the main bore. Both of these valves have the ability to contain well pressure, but can also sever any wireline or coiled tubing the might be located inside the bore during an emergency. (Subsea1, 2014)

### The Xmas tree

The Xmas tree will act as a barrier between the well and the environment. It is a pressure vessel for well flow and will have accommodation for flow control elements and various systems for the well. (Subsea1, 2014)

## 2.3 TECHNOLOGY BACKGROUND

(Tømmermo et al., 2014, p.1)

### 2.3.1 OPERATIONAL RISKS

When workover operations are being performed the heave compensator onboard the workover vessel allows for relative vertical movement between the vessel and the riser. If the heave compensator fails or the heave of the vessel exceeds the stroke length of the heave compensator cylinders, a tremendous force will be exerted on the workover riser.

During workover operations the workover riser makes up a part of the primary well barrier. If the workover riser is damaged, the primary well barrier is damaged. If excessive loads are applied to the riser, the integrity of the subsea equipment at the bottom can be compromised. Damage to the subsea equipment will also mean damage to the well barriers.

The NORSOK standard for System Requirements Well Intervention Equipment states:

*“System and equipment are to provide two independent levels of protection to prevent or minimize the effects of a single malfunction or fault in the process equipment and piping system, including their controls.”* (NORSOK D-002, 2000, p.8)

A riser without any form of weak link would be vulnerable to such a failure. A malfunction in the heave compensator could directly result in large damage to important safety functions and barriers.

The EDP is installed to disengage the riser from the LRP in order to avoid damage to rig and equipment in case of a situation that requires rapid disconnection. This disconnect sequence must be activated from rig personnel. If a situation where the workover riser very rapidly is exposed to extreme loads without warning, rig personnel might not be able to activate the emergency disconnect sequence quickly enough to avoid damage. There is also the unpredictable factor of human error. There may be hesitation or they may not even be aware of the situation until it is too late. Such a failure could occur if the vessel heave is too large for the heave compensator or the heave compensator locks up. This is what happened to Statoil's deep water Trym in 1998 (Statoil, 1998). The heave compensator suddenly locked and the riser was exposed to over 500 tonnes of tensile load of a period of five seconds. This led to the riser breaking in six places and there were large damages to the drill floor. This all happened so quickly that the rig personnel did not have time to activate the emergency disconnect sequence.

For several years, weak links have been used in risers as a physical barrier to prevent damage to subsea well barriers in an emergency situation. If extreme heave amplitudes of the vessel or failure/stroke out of the heave compensators occur, large tensile loads shall not be able to damage the integrity of the well barriers. A weak link installed in a drilling or workover riser prevents such a load from being transferred. The traditional weak link is designed so that it will rupture and split under a predetermined load lower than the critical load the well barriers can withstand. By doing so, the well can safely be controlled if an accidental load from topside were to occur. However, the riser recoil from such a rupture could damage the vessel and riser content will be released to the sea. This can lead to damage to the rig, personnel and also environmental discharge. The economic consequences of such a situation with respect to the well are also a major concern. Retrieval of the severed riser section for instance.

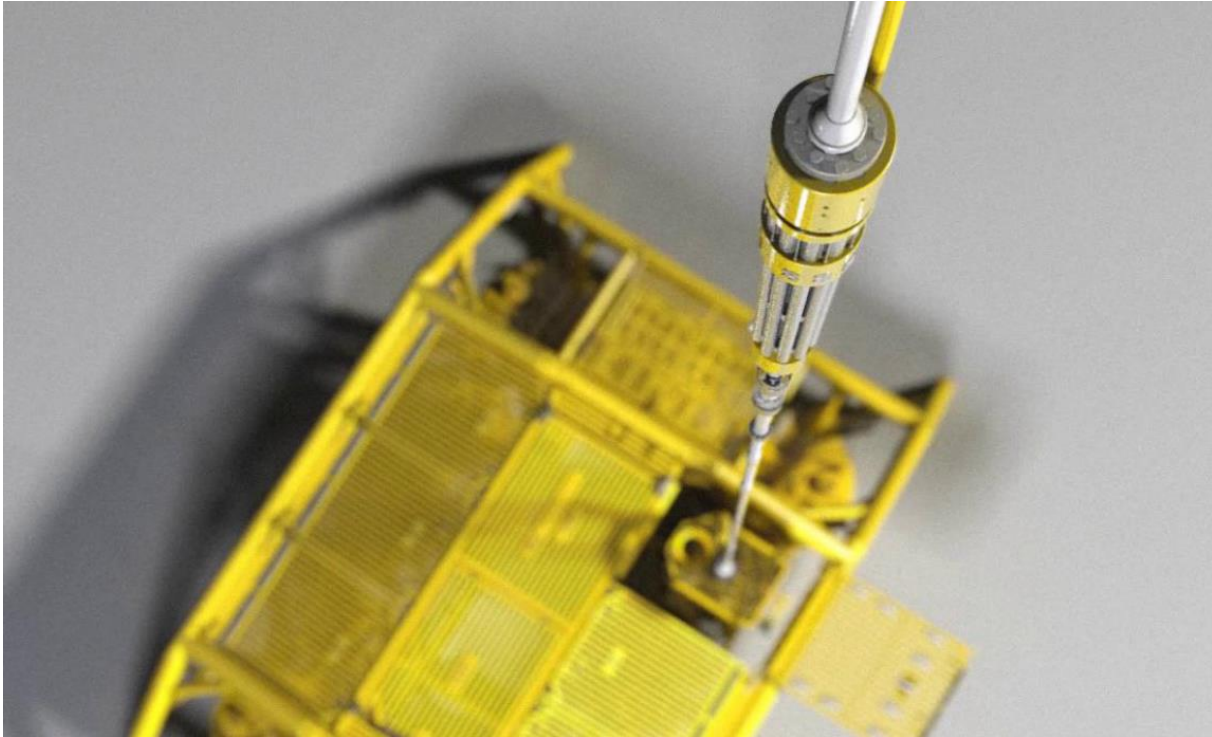


Figure 2.3 The Telescopic Safety Joint installed in the riser (Tømmermo et al., 2014, p.11)

FMC has developed a Telescopic Safety Joint (TSJ) that does not rupture, but telescopes once subjected to excessive loading conditions. The safety joint is going to be installed as a riser joint in the workover riser, see figure 2.3. This will provide enough time to safely activate the emergency disconnect sequence and disconnect the riser from the Xmas tree stack properly without spillage and riser recoil. (Tømmermo et al., 2014, p.1)

### 2.3.2 BENEFITS OF THE TELESCOPIC SAFETY JOINT

The installation of a safety joint will be an independent layer of protection that minimizes the consequences of a heave compensator lockup. Most modern workover risers are installed with a weak link that breaks before damaging the equipment or drill floor, but there are other potential hazards that could occur if the riser link were to completely break. Riser recoil is an example that could lead to damage of the workover vessel.

The pressure balanced TSJ from FMC is designed to be activated when subjected to a predetermined axial load. The joint is designed so that during normal operation the TSJ is retracted and behaves passively as a standard riser joint. When activated the joint begins telescoping while the contents of the riser bore are retained. Pressure compensating cylinders ensures that tension is kept in the riser; this is explained in more detail in section 2.5. The stroke length of the joint is set to be larger than the largest expected heave of the vessel. Once the TSJ has been activated the telescopic function gives rig personnel sufficient time to active the emergency disconnect sequence. Alternatively the safety joint can automatically disconnect the EDP when activated.

### 2.3.3 CONCERNS WHEN INSTALLING A SAFETY JOINT

A limitation when installing such a weak link in a workover riser may be the installation procedure. The workover riser can be used as a running tool for an equipment stack consisting of an EDP, a LRP and a Xmas tree. This equipment has a dry weight of 100 tonnes and will result in a temporary increased axial load to the workover riser and thus the safety joint. Since the safety joint is designed to be the weakest link along the riser, it may also be the most vulnerable to these increased loads. A safety joint may therefore become a restricting factor concerning when workover installation can, and cannot be performed.



## 2.4 WORKOVER RISER LOADS

### 2.4.1 OPERATIONAL LOADS

This section describes various load cases a workover riser is subjected to during operation. The purpose is to provide the reader with an understanding of the forces that the workover riser will encounter and why a safety joint should be located at the lower end as shown in figure 2.4.

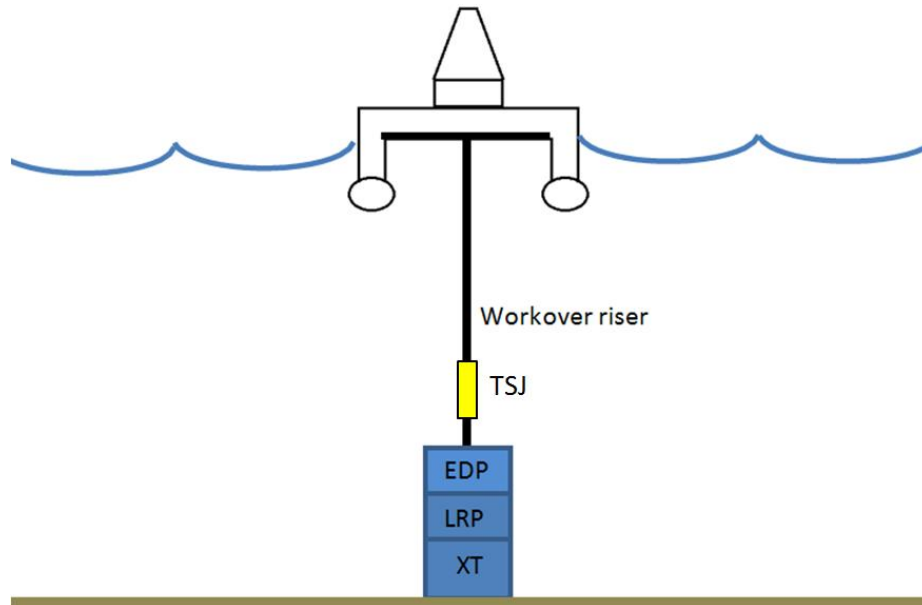


Figure 2.4 Location of the TSJ in the workover riser

#### AXIAL LOADS

The workover vessel will have some heave relative to the seabed and a heave compensation system enables vertical movement of the vessel without applying an extreme tension in the riser.

If sufficient tension is not applied to the riser when the vessel is in the wave trough there is a risk that the riser might experience compressional forces and buckle. The riser tension declines with water depth so the bottom of the riser will have the least amount of tension. The bottom of the riser will therefore be the most vulnerable to buckling if the top tension is too low. A floating drilling unit will be equipped with a riser tensioning system to ensure that tension is kept at all sections throughout the riser. This will normally be based on a pneumatic spring principle. Large piston cylinder arrangements coupled to the top of the drilling riser using cables. The air pressure in the cylinder supports the weight of the riser and in addition applies a tension force so that there is a certain over-pull at the EDP/LMRP. Sufficient over-pull is required in order to ensure that the emergency disconnection sequence can be properly engaged. If over-pull is too low the EDP/LMRP may not be pulled away quickly enough and might therefore collide with the LRP/BOP after detachment. (Baker, 1991, p.537)

#### LATERAL FORCES

Waves and ocean currents will generate lateral forces in the riser. The current velocity varies with time but this happens so slowly that it can be considered to be a steady force. This lateral force can create bending moments in the riser, but also result in vortex induced vibrations that can lead to fatigue. The current does not necessarily change with water depth which means that the drag force from the current on the riser can be as large or larger closer to the seabed.

Waves create oscillating forces on the riser that will only be at its largest for a short period at a time. Wave forces also make the riser vulnerable to fatigue. Unlike the current, waves forces decrease exponentially with water depth. Even large waves will have a negligible impact on the section of the riser located close to the seabed in a deep water situation.

## BENDING MOMENTS

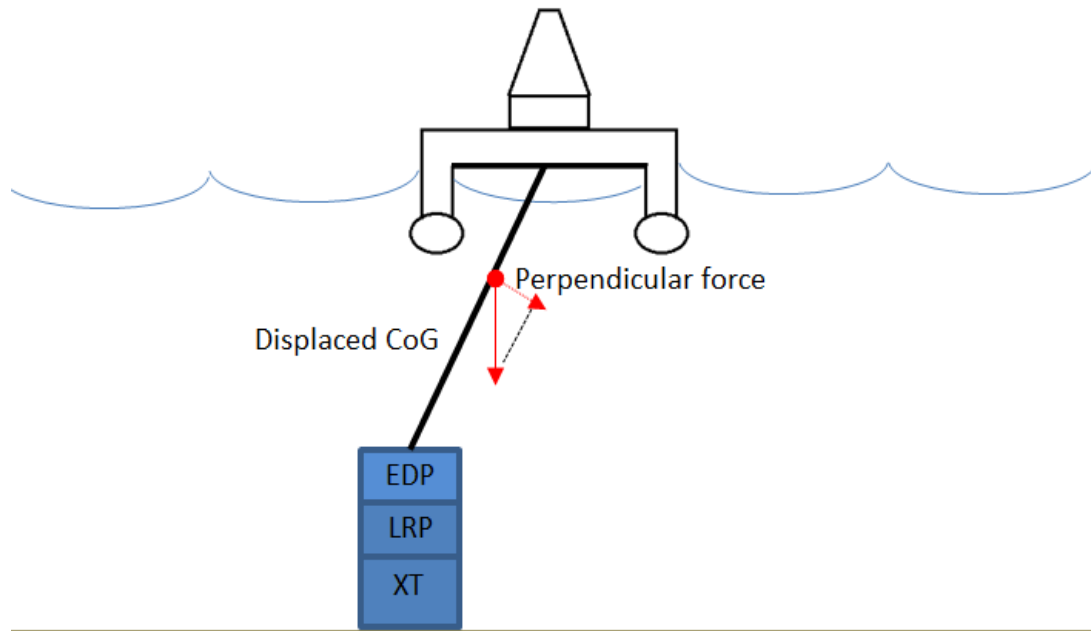


Figure 2.5 Bending moments in riser due to vessel offset

Vessel offset may result in bending moments in the riser. The workover riser is equipped with slip joints at the top and bottom which allows some angular displacement. A vessel situated in deep water will be able to have a larger offset than a vessel in shallow water. However, one effect of the offset is that an inclination in the riser will displace the center of gravity such that a small arm occurs. By decomposing this displaced force vector, the effect of the vessel offset can be regarded as a force acting perpendicular to the riser, this is illustrated in figure 2.5.

When plotting the curve for the bending moment in riser the curve normally has two maxima. One located close to the water line and another closer to the bottom. This curve varies according to several parameters. In constant water depth the maxima increases linearly with vessel offset. For increasing water depth and increasing top tension, the maxima decrease. Buoyancy elements along the riser provide a lifting force. This will result in a decrease in the lower bending moment maxima to the point where it becomes non-existing. By increasing mud weight while keeping top tension constant, the lower bending maxima increase rapidly while the upper bending maxima stays constant. If however the top tension is adjusted to compensate for the heavier mud, there is not going to be a significant change in lower bending maxima.

An example of how the bending moment may be distributed under certain circumstances is shown in figure 2.6. The bending moment curve will vary according to factors such as weight of the content, top tension, current, drift off or water depth. The TSJ should be located in a section of the riser where bending moments are low and is normally installed two or three riser lengths over the EDP, above the lower bending moment peak. (Azar & Soltveit, 1978, p.1)

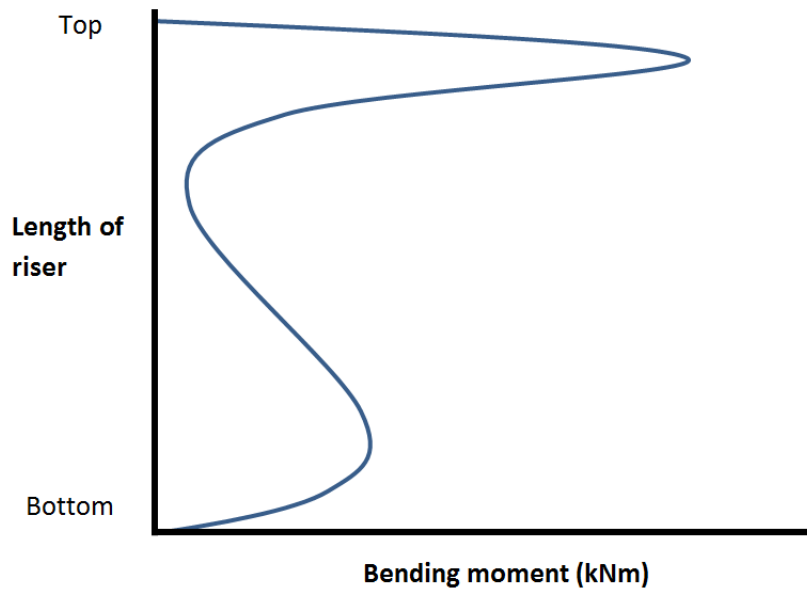


Figure 2.6 Example of bending moment distribution along a riser during operation (Azar & Soltveit, 1978, p.41)

#### 2.4.2 INSTALLATION LOADS

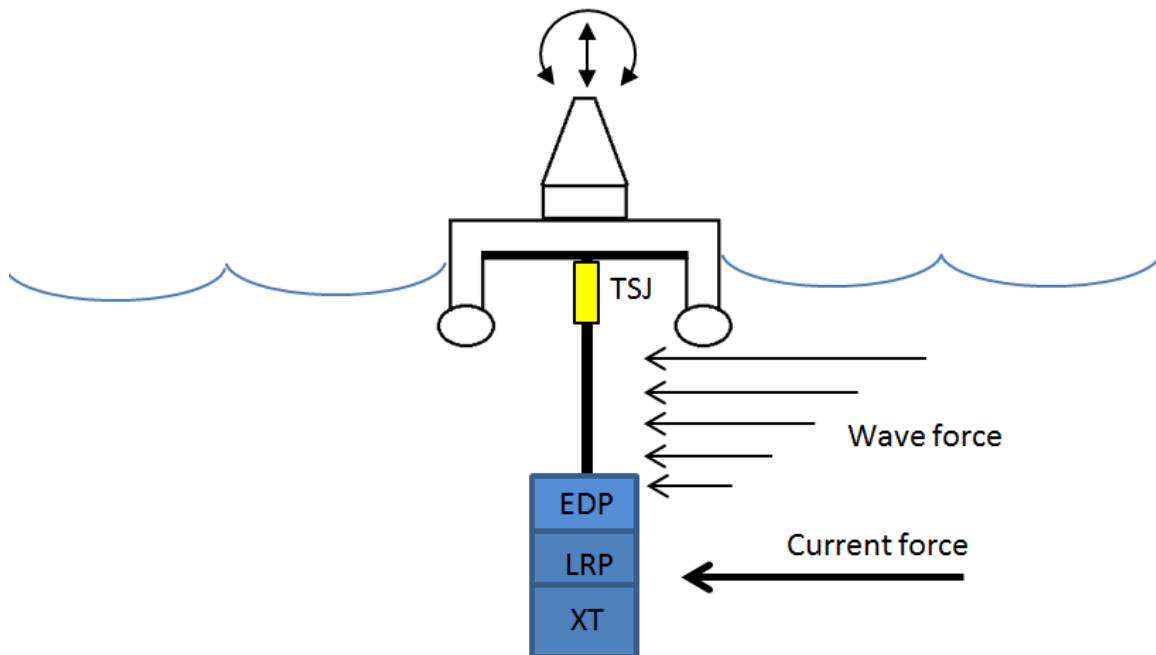


Figure 2.7 Forces contributing to the motion of the equipment stack

An installation scenario is illustrated in figure 2.7. The workover riser is used as a running tool for the Xmas tree, LRP and the EDP. The workover riser is assembled joint by joint on the deck. While each joint is installed there is a period where the equipment package is suspended from the vessel, hanging from the deployed section of the riser. During installation of the equipment stack the TSJ will be exposed to larger loads and stresses than normal operations.

---

## AXIAL LOADS

During installation the workover riser is going to be subjected to an increased axial load due to the weight of the equipment stack being lowered towards the seabed. At this point the heave compensator is not active, so the top section of the riser can be regarded as fixed to the vessel. No relative motion of the equipment stack and the vessel can occur at this point without bending/stretching of the riser. As the heave of the vessel forces the equipment package to follow the vertical motion, an increased tension force in the riser will be present due to the added mass and the inertia of the stack.

---

## LATERAL FORCES

Once the equipment stack has been lowered through the splash zone it is subjected to dynamic loads from waves, currents and the vessels movement. All these loads are transferred through the riser. Since the equipment stack is suspended in mid-water there is a risk that the wave and current forces may result in large motions of the stack. Waves with period close to the systems natural frequency will be the most critical. These waves can create harmonic motions described in more detail in the latter. The wave forces declines exponentially with water depth and so as the equipment stack is lowered through the water, the forces from the waves are reduced. The current can have a damping effect on the equipment stack, but in small waves the lateral force from the current will apply a bending moment to the riser.

---

## HARMONIC MOTIONS OF SYSTEM

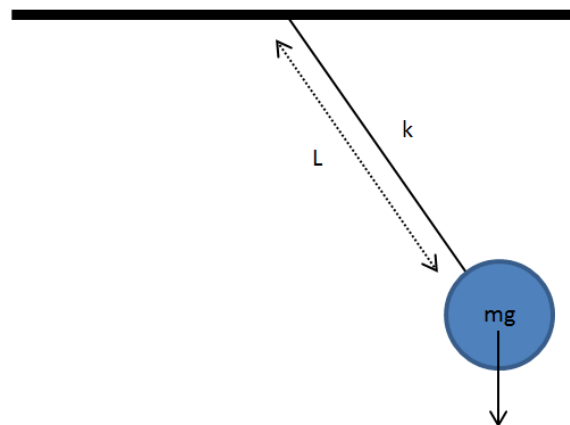


Figure 2.8 Pendulum from an elastic band

Where:

- $L_p$  is the length of the pendulum [ $m$ ]
- $k_s$  is the axial stiffness of the spring [ $N/m$ ]
- $m$  is the mass of the pendulum [ $kg$ ]

The workover riser is basically a long steel pipe. When a steel pipe is subjected to a tensile force its behavior can be compared to that of a very stiff rubber band. As long as the force is within the elastic range of the rubber band, it will go back to its initial length once the load is removed. The same applies for the steel pipe. The elastic modulus for the steel is far greater than that of rubber and so the elongation is not going to be as apparent. The tensile load in this case is applied by the weight of the equipment lowered through the sea. The complicating factor for this is that the workover riser is subjected to dynamic loads due to the waves and current. The model of the equipment stack connected to a can be compared to a pendulum hanging from an elastic band, seen in figure 2.8.

The natural period of a pendulum is described by:

$$T_p = 2\pi \sqrt{\frac{L_p}{g}} \quad (2.1)$$

Where:

$T_p$  is the natural period of the pendulum [s]

Waves with periods close to the natural frequency of the vessel and riser system will induce harmonic motion which can lead to large amplitudes of the equipment. This can increase the stress in the riser. The pendulum motion can be critical with respect to bending moment.

Another degree of freedom for the equipment stack is the vertical motion of the system. The workover riser has a certain stiffness. If a vertical force (like accelerations during heave of the vessel for instance) or motion is exerted the natural period of the system is:

$$T_s = 2\pi \sqrt{\frac{m}{k_s}} \quad (2.2)$$

Where:

$T_s$  is the natural period of the spring [s]

The system can be modelled as a combination of both a pendulum and a spring. When the two respective natural periods fulfill the following relationship:

$$T_p \sim 2T_s$$

By combining equations 2.1 and 2.2, the following relationship is found:

$$\sqrt{\frac{L_p}{g}} \sim 2 \sqrt{\frac{m}{k_s}}$$

$$L_p \sim 4 \frac{mg}{k_s} \quad (2.3)$$

When the length of the pendulum reaches this point, the system alternates between a pendulum motion and a vertical spring motion. When this occurs there is an increasing risk when installing in waves close to the natural period of the system. Even a small heave of the vessel can result in unwanted pendulum motion of the equipment stack. (Gudmestad, 2013)

The complexity of the system makes foreseeing such a wave period more challenging. The damping of the system is going to reduce the amplitude of the heave of the equipment. The added mass of the equipment will also be difficult to accurately estimate.

## 2.5 DESIGN OF THE TELESCOPIC SAFETY JOINT FROM FMC TECHNOLOGIES

(Tømmermo et.al, 2014, p.4)

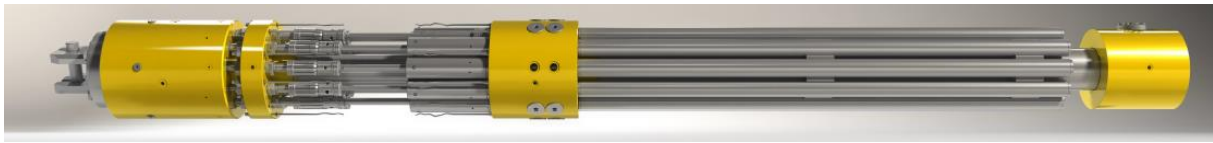


Figure 2.9 The Telescopic Safety Joint by FMC Technologies (Tømmermo et.al, 2014, p.11)

The Telescopic Safety Joint developed by FMC Technologies is shown in figure 2.9. The following section presents the different properties of the TSJ. The properties are presented one by one in order to give the reader a better understanding of the function for each different component. The TSJ contains all of the components presented, although the sketches do not contain all details. This simplification has been done for the sake of the reader due to the complexity of the joint.

### The assembly

The TSJ can be viewed as the assembly of two components shown by the upper and lower section in figure 2.10. In passive mode these two sections are locked together and begin to slide apart (telescope) once a predefined axial load has been applied to the joint. As the two sections separate the content within the bore is not released to the external environment.

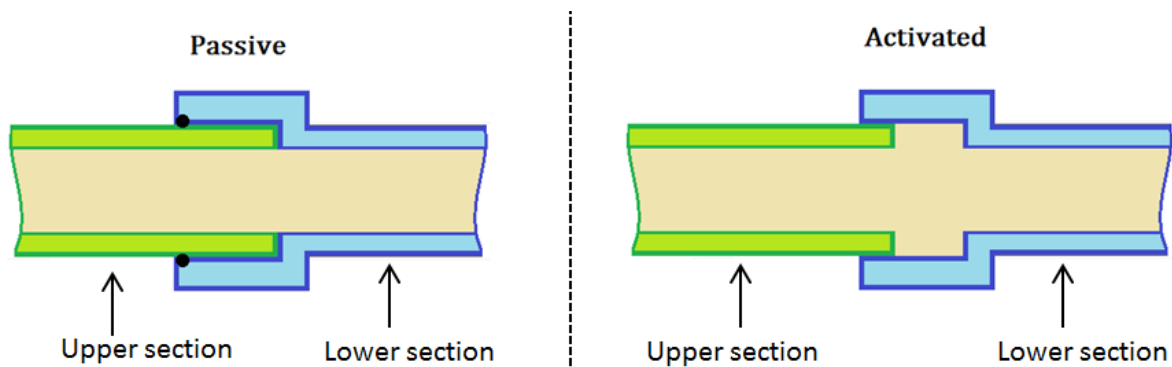


Figure 2.10 Simplified assembly of the TSJ

### Tensile bolts

When in retracted (passive) mode the TSJ is equipped with ten ductile tensile bolts; they are presented as red in figure 2.11. Any increased tension to the workover riser will be applied to these bolts. The bolts are ductile and are able to be elongated within their elastic regime before they rupture. By being ductile the chance of unplanned activation of the safety joint is reduced. The bolts are dimensioned to rupture at a predetermined axial load. Each bolt may be 1m long and can elongate 100mm before breaking. The tensile bolts are pre-tensioned in order to avoid fatigue and unwanted movement of the piston in the pressure compensating cylinders described in the latter.

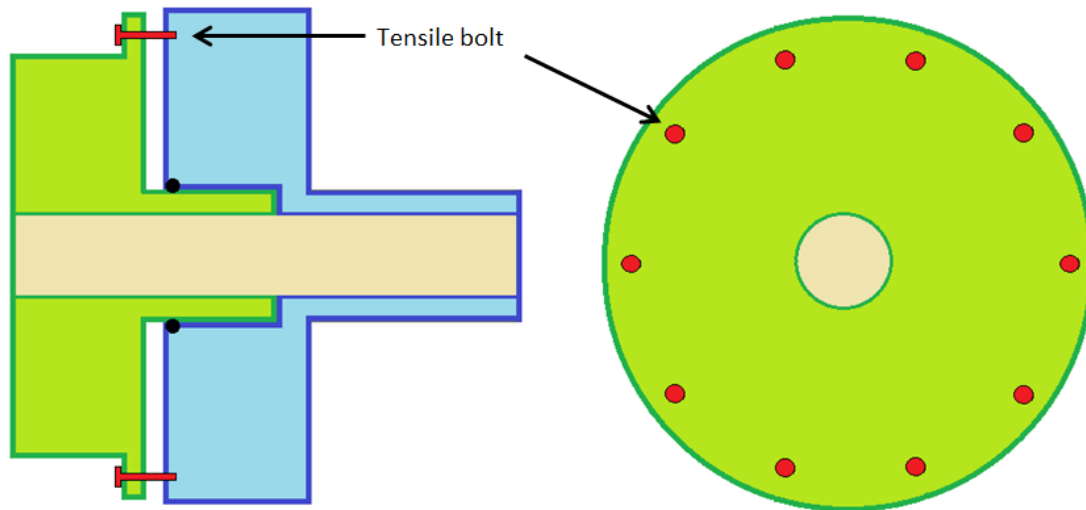


Figure 2.11 Assembly of the TSJ with tensile bolts

### Pressure compensating cylinders

Internal pressure in a pipe will exert a longitudinal force on the pipe walls. This is known as the end-cap effect (Guo, Song, Ghalambor & Lin, 2014, p.65). To avoid fluctuations in the internal pressure of the safety joint from affecting the capacity of the tensile bolts, the TSJ is pressure balanced. Being pressure balanced, meaning that the TSJ uses the internal pressure that initially creates the end-cap effect, to counteract this very force. This is achieved by external short cylinders around the joint. Each cylinder is attached to the lower section whilst a piston is connected to the upper section.

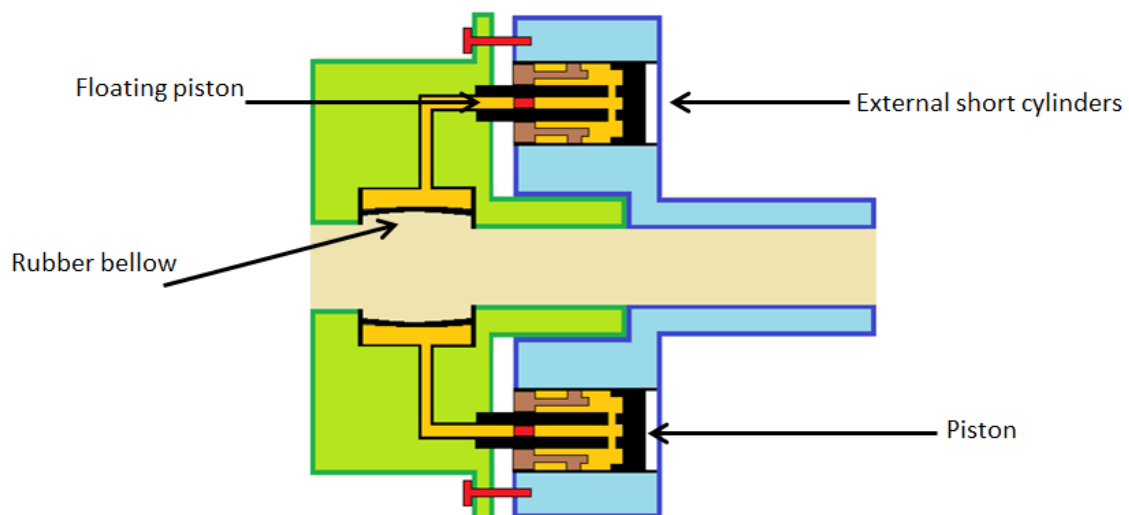


Figure 2.12 Configuration of the pressure compensating cylinders in the TSJ

Figure 2.12 shows the location of the pressure compensating cylinders. The internal pressure from the joint is communicated to the short cylinders. The pressure will apply a force to the backside of each piston. Because the piston is connected to the upper section of the TSJ, this force pulls the two sections together, reducing the tension in the bolts. As the internal pressure rise, the force on the pistons increase and thus the tension in the bolts are not affected by the bore pressure in the riser. There are enough external short cylinders to ensure that their combined cross sectional area equals the cross sectional area of the safety joint bore.

Although pressure is communicated between the well bore and the cylinders, no actual fluid transfer occurs. The fluid from the riser bore may contain impurities from the well stream that could clog up the cylinders. The pressure is transferred via a rubber bellow inside the bore. The internal surface of the bellow is in direct contact with the well fluids, while the outer surface is in contact with the clean hydraulic fluid. If any of these cylinders fail (i.e. leakage) a floating piston above the cylinder will travel to an end stop and isolate that cylinder from the others. This ensures that functionality is maintained with an acceptable reduction in compensation force.

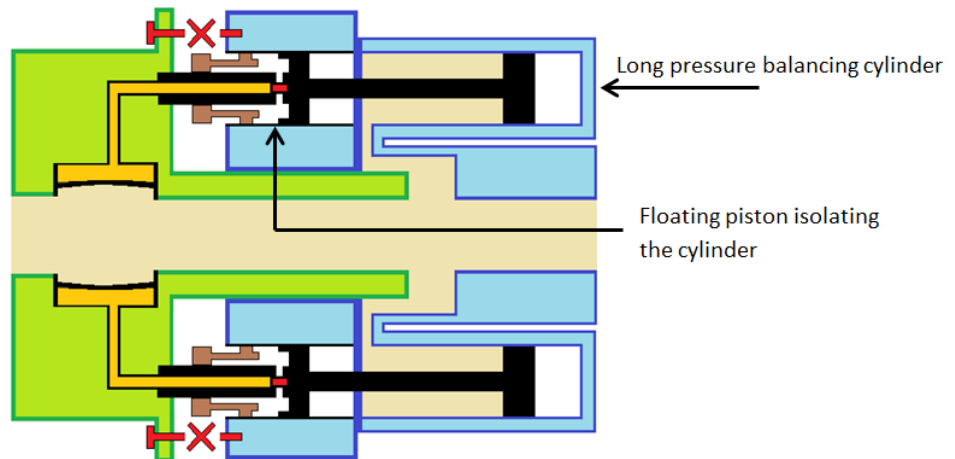


Figure 2.13 Configuration of the long pressure balance cylinders in the TSJ

### Long pressure balance cylinders

In the event of an accidental load where the tensile bolts rupture, the TSJ begins to stroke. In figure 2.12 the long cylinders are not shown. Their configuration can be seen in figure 2.13. The short pressure compensating cylinders are not designed for the long strokes that occur once the joints begin to telescope and so they become disabled. As the short cylinders are disabled, the long external cylinders are activated to provide the required stroke. These long cylinders provide the same pressure compensation effect as the shorter cylinders, but enables far longer stroke length. Below the piston of the long cylinders there is an under-pressure. Above the piston these cylinders are in direct communication with the well bore meaning that dirty well fluid can enter the cylinders. This is however an emergency situation and once the TSJ have begun to stroke, engaging the long cylinders; the EDP must be activated as quickly as possible.

### The over-ride system

There are temporary loading conditions that exceed that of normal operation. Such a condition will be when installing the Xmas tree with a LRP/EDP using the workover riser as a running tool. The dry weight of this equipment can reach 100 tonnes and this may be tripled during dynamic motions. If the tensile bolts were strong enough to carry these loads, they would not be weak enough to rupture at the required load. Therefore the TSJ has a separate set of over-ride cylinders that increases the load bearing capacity of the TSJ during installation faces. These cylinders are in principal the same as the pressure compensating cylinders, but they can be connected to an external high pressure hydraulic source (see figure 2.14). This hydraulic pressure simulates a high pressure inside the bore. The cylinders generate a compressive force in the joint without the end-cap force being present. This makes the joint able to withstand the extra tension from the heavy equipment package without excessive tension being applied to the bolts. The over-ride cylinders are spaced evenly around the safety joint. This increases its resistance towards bending moments that may occur during installation. The thesis studies the effect these cylinders have on the joints resistance towards bending moment in particular.



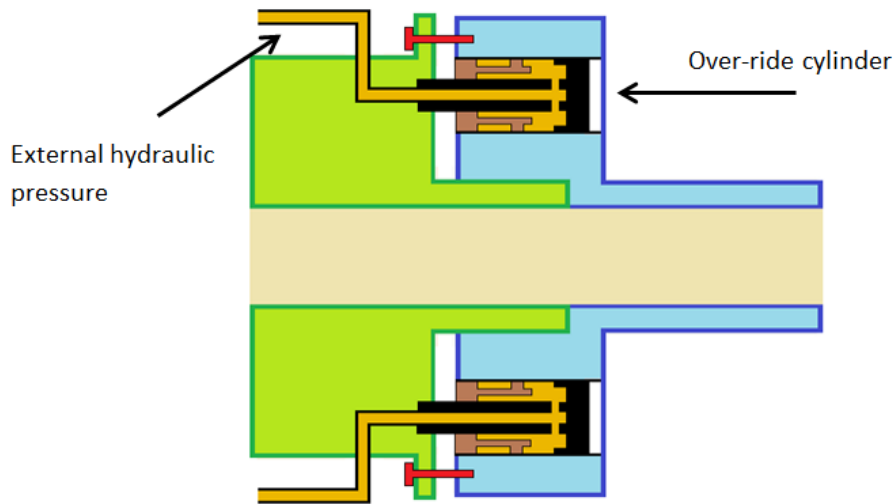


Figure 2.14 Configuration of the over-ride cylinders in the TSJ

### Long sea pressure cylinders

In order to ensure structural stability of the workover system as well as to being able to properly perform EQD, tension must be maintained in the riser at all times. An over-pull of 20-30 tonnes on the EDP is not unusual. The TSJ have therefore been provided with a function to maintain riser tension using the hydrostatic pressure of the surrounding sea water. Long cylinders with vacuum chambers similar to the long pressure balancing cylinders are open to the sea (see figure 2.15).

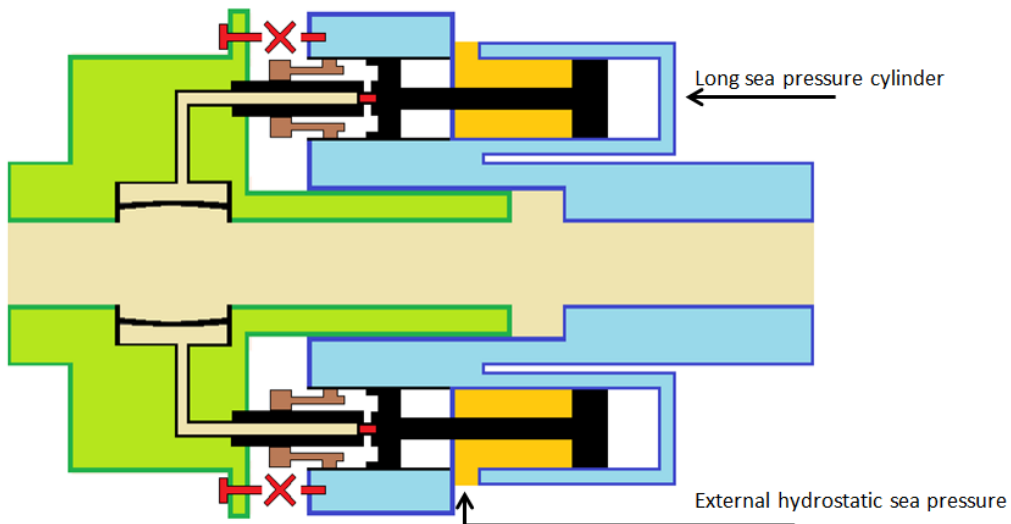


Figure 2.15 Long sea pressure cylinders

The hydrostatic pressure exerts a force above the vacuum chamber. Therefore a constant tension is kept in the piston extending from the cylinder even though riser pressure drops. This function is only activated when the TSJ is in telescoping mode.

## 2.6 SITUATIONS REQUIRING A WEAK LINK

### 2.6.1 VESSEL DRIFT-OFF

One situation where a TSJ would reduce consequences is during vessel drift off. Dynamic positioning has become common practice on workover vessels. The vessel is equipped with thrusters that can rotate 360 degrees. Using GPS the vessel is kept stationed above the well by using its thrusters to account for wind, waves and currents that normally would make the vessel drift. Dynamic positioning systems are very reliable and have backup systems, but the risk of unintentional drift off cannot be excluded. There may be emergency events on board the vessel such as a fire or explosion that can cause the dynamic positioning system to malfunction. One of the consequences of the explosion onboard the Deepwater Horizon was the damage to the dynamic positioning system that led to the vessel unintentionally drifting off. Although there were several other factors leading to the large consequences of this accident, it is nevertheless an example that dynamic positioning systems can fail. If the vessel drifts off, the increased tension in the riser will at some point rupture the tensile bolts in the joint and it will begin to telescope. By telescoping the TSJ extends the time for the crew onboard the vessel to activate the EQD system. Alternatively the TSJ can be equipped with a function that automatically activates the EDP once the joint has begun telescoping.

### 2.6.2 HEAVE COMPENSATOR LOCK UP/STROKE OUT

All floating vessels experience heave motion when situated in waves and must be equipped with a heave compensating system to allow for relative motion between the vessel and well. The heave compensator system must function properly to avoid damaging loads to the riser and subsea equipment. A heave compensator has a finite stroke length and so workover operations should not be performed in certain sea states where there is a risk that the heave of the vessel may exceed this stroke. If an unforeseen large wave were to occur, the vessel could be lifted to a point where the heave compensator exceeds its maximum stroke length. In such a situation the vessel would pull the riser with an extreme force. A similar situation would occur if the heave compensator locks up. The damage in both of these cases would be eliminated by having installed a safety joint that would telescope and allow sufficient time to safely disconnect the riser from the well.

The workover riser is a steel pipe. The elasticity of a steel pipe can be compared to a very stiff rubber band. How far the riser can be elongated within the elastic region depends upon the length of the riser. A short riser is not able to be stretched as far as a long riser. A workover riser in deep water has the ability to elongate far more than a workover riser situated in shallow water. This means that if the heave compensator lockup occurs in deep water there is a chance that the workover riser is able to stretch sufficiently without plastic damage to the riser itself, or its connection points. In shallow water the heave compensator lockup is far more likely to result in plastic damage and thus the installation of a safety joint is going to be even more vital in shallow water areas.

# 3. METHOD

This chapter contains all input values that have been plotted into the OrcaFlex model as well as a description of the ANSYS workbench simulations.

## 3.1 ORCAFLEX 9.7

The dynamic simulations will be performed using OrcaFlex 9.7. OrcaFlex is developed by Orcina. The program is used for dynamic simulations of vessels and other installations offshore. The program allows the user to choose between different wave spectrums, water depths, vessels, mooring lines, risers and more (Orcina, 2014). This enables the user to create an offshore model and then perform dynamic simulations to find the forces, stress, displacements, velocities and accelerations etc. of the model. There is a wide range of applications for OrcaFlex. Among these are simulations of risers, hose systems, mooring, installation analysis, towing etc. For this project OrcaFlex will be used to simulate the loads in a workover riser when used as a running tool for installation of an equipment stack consisting of a vertical Xmas tree, a LRP and an EDP. The riser is suspended from a floating vessel that is subjected to waves and current. The waves are going to create a movement of the vessel as well as applying a force to the riser and the equipment. The combination of these motions and their resulting loads along the riser can then be obtained.

In order to get an accurate model of the installation scenario, several input values must be plotted into OrcaFlex. The following sections will show which values that have been used for the OrcaFlex model and how they are calculated.

## 3.2 WORKOVER VESSEL DATA

### THE TRANSOCEAN ARTIC



Figure 3.1 Picture of the Transocean Arctic (offshore.no, 2014)

The workover vessel to be used in the simulations is the semi-submersible Transocean Arctic seen in figure 3.1. It is rated to a water depth of up to 500m and its size is 83m x 67m. Operational displacement is 36 260 tonnes. In order to get the correct motions of the vessel during waves, the Response Amplification Operator (RAO) for all 6 degrees of freedom has been plotted into OrcaFlex.

### 3.3 ENVIROMENTAL DATA SETTINGS

The settings for the environmental data are described in the following sections. If there are any settings for the environmental data sheet that is not described here, the default settings from OrcaFlex has been not been changed.

Often used terminology for this thesis (DNV-RP H103, 2011, p.13):

#### The significant wave height, $H_s$

*“The significant wave height,  $H_s$  is approximately equal to the average wave height (trough to crest) of the highest one-third waves in the indicated time period”*

#### The zero up-crossing period, $T_z$

*“The zero-up-crossing period,  $T_z$  is the average time interval between two successive up-crossings of the mean sea level”*

#### 3.3.1 SCATTER DIAGRAM

Wave and current data supplied by Shell are used for the analysis. In agreement with Shell and FMC Technologies the upper limit for the dynamic simulations is the significant wave height,  $H_s = 5m$ . Table 3.1 shows the combination of wave heights and periods taken from the all year scatter diagram from Shell’s metocean data. The green cells show which significant wave height/zero up-crossing period combinations has been observed at the Draugen area.

Table 3.1 Wave heights – wave periods for Draugen (Shell, 2009)

		Scatter diagram for Draugen														
		Tz (sec)														
		2	3	4	5	6	7	8	9	10	11	12	13	14	15	16
Significant wave height $H_s$ (m)	5,0															
	4,5															
	4,0															
	3,5															
	3,0															
	2,5															
	2,0															
	1,5															
	1,0															
	0,5															

#### 3.3.2 CURRENT

The current may have a damping effect on the equipment stack. There is a possibility that installation without any sea current may result in larger motion and thereby larger stresses in the workover riser. A sensitivity analysis will be performed to find out if the absence of current results in larger loads on the riser.

The current for the area can vary in intensity and the current profile as a function of the water depth will also change. The current speed is set to 0,5m/s for these simulations. The current speed does not change with water depth in these tests.

### 3.3.3 WAVE SPECTRUM

Various wave spectrums can be chosen in OrcaFlex when performing a simulation. The location for the installation is the Draugen field, 150km north of Kristiansund. This area is located in the Norwegian Sea. Since it is in close proximity to the North Sea, the JONSWAP (Joint North Sea Wave Project) spectrum is chosen. This spectrum is an empirical relationship that defines the energy distribution with frequency within the ocean. The typical spectrum for the North Atlantic is the Pierson-Moskowitz spectrum. This spectrum is applicable for areas where the fetch length is so large that the waves can fully develop. North Sea conditions have more restricted fetch length and so the waves cannot fully develop. The JONSWAP spectrum has a narrower peak. The difference between JONSWAP and the Pierson-Moskowitz spectrum can be seen in figure 3.2. Only the significant wave height and zero up-crossing periods are plotted into the OrcaFlex settings once the JONSWAP spectra has been chosen. The spectral parameters automatically provided by the program are used. (Stewart, 2005)

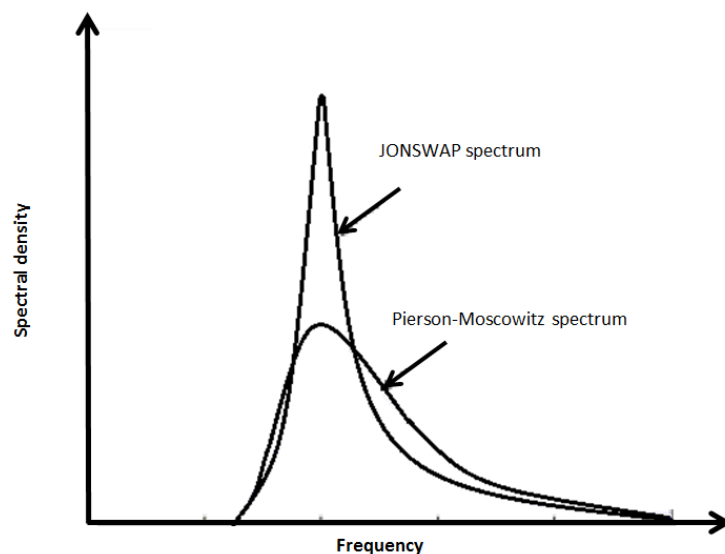


Figure 3.2 The JONSWAP spectrum compared to the Pierson-Moskowitz spectrum

### 3.3.4 WAVE SETTINGS

Data for Wave Train: Wave 1

Wave Data:

Direction (deg)	Hs (m)	Tz (s)	Wave Origin		Wave Time Origin (s)	Wave Type	Number of wave directions
			X (m)	Y (m)			
180,00	1,00	14,00	0,00	0,00	0,000	JONSWAP	1

Spectral Parameters: Automatic

$\gamma$	$\alpha$	$\sigma_1$	$\sigma_2$	f <sub>m</sub> (Hz)	T <sub>p</sub> (s)
0,9000	34E-6	0,0700	0,0900	0,0504	19,8382

Components:

Seed	Number	Relative frequency range		Maximum component frequency range (Hz)
		Minimum	Maximum	
12345	100	0,30	10,00	~

Figure 3.3 Wave train settings from OrcaFlex.

The wave settings can be seen in figure 3.3. The significant wave height ( $H_s$ ) and zero up crossing period ( $T_z$ ) will change depending the sea state to be tested. The number of wave components is chosen to be 100. Each component represents the part of the energy in the wave spectrum and covers a range of wave frequencies. If there are relatively few components, each one is trying to represent a fairly wide range of frequencies. The greater the number of components the longer the program takes to perform each simulation. 100 components are usually sufficient to cover the whole frequency range.

### 3.4 THE WORKOVER RISER

This section contains input values for the workover riser used in OrcaFlex. The workover riser is modeled as a homogenous steel pipe. The data sheet for the riser in OrcaFlex requires various parameters in order to perform the simulations correctly. All the values that have been plotted into the data sheet are shown in the following section. If there are any parameters on the riser data sheet that has not been shown here, the default settings from the software have not been changed.

#### 3.4.1 BOUNDARY CONDITIONS

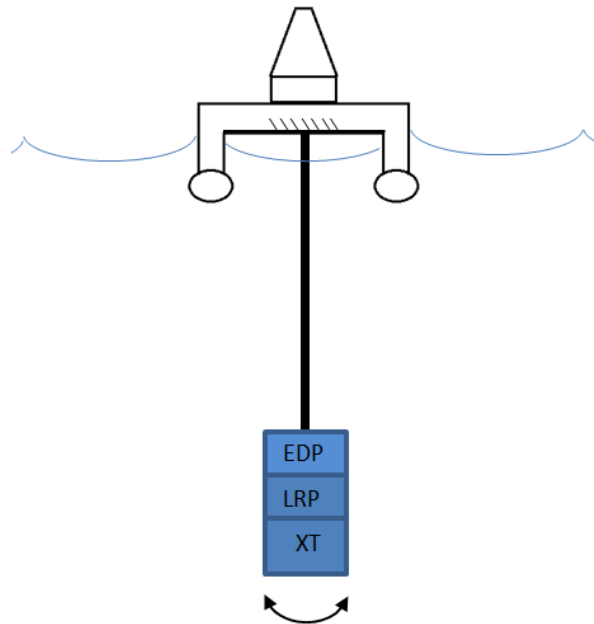


Figure 3.4 Boundary conditions for the riser

The workover riser in OrcaFlex is suspended from the workover vessel, which in this case will be the Transocean Arctic. During installation the heave compensator is not active so the equipment stack has the same heave as the vessel. The connection between the riser and the vessel is fixed so that no angular displacement between the top section of the riser and the vessel can occur. Any horizontal displacement of the equipment relative to the rig are going to result in bending of the riser. Figure 3.4 shows how the top end of the riser has a completely stiff connection to the rig deck. The lower end of the riser has a stiff connection to the equipment stack. Nevertheless, it is expected that the largest bending moments are found at the very top of the workover riser.

#### 3.4.2 DIMENSIONS

The dimensions for the workover riser are shown in table 3.2. This also includes surface roughness that is going to be used for calculation of drag coefficients later in this chapter.

Table 3.2 Dimensional values for the workover riser

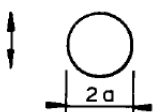
Outer diameter (OD)	8 5/8" (0,219m)
Inner diameter (ID)	7" (0,178m)
Surface roughness (k)	$3 \times 10^{-3}m$

### 3.4.3 ADDED MASS

(DNV RP-C205, 2010, p.116)

The added mass for the riser is found using DNV Recommended Practice for Environmental Conditions and Environmental Loads. The relevant cross section is shown in table 3.3.

Table 3.3 Added mass for a cylinder (DNV RP-C205, 2010, p.116)

Section through body	Direction of motion	$C_A$	$A_R$	Added mass moment of inertia [(kg/m) × m <sup>2</sup> ]
		1.0	$\pi a^2$	0

$$C_A = 1.0$$

The added mass per meter of workover riser can be found using the formula:

$$m_A = \rho C_A A_R \quad (3.1)$$

Where:

$A_R$  is the cross sectional area of the displaced water column [m<sup>2</sup>]  
 $\rho$  is the density of sea water [kg/m<sup>3</sup>]

Hence the added mass is:

$$m_A = 1025 \frac{kg}{m^3} \cdot 1,0 \cdot \pi \cdot \frac{(0,219m)^2}{4}$$

$$m_A = \underline{\underline{38,6 \frac{kg}{m}}}$$

### 3.4.4 DRAG COEFFICIENT

The workover riser is going to be exposed to the water particle velocity from the waves. Therefore the drag coefficient cannot be found using only data relevant for steady current. The ISO standard for Petroleum and natural gas industries - Fixed steel offshore structures propose a method of estimating the drag coefficient for a cylinder in un-steady current. This method is relevant for post-critical flow.

#### Post critical flow

For a certain Reynolds number, there is a distinct drop in the value of the drag coefficient (DNV RP-C205, 2010, p.56). This drop is dependent on the roughness of the cylinder. The roughness factor is found by dividing the surface roughness of the cylinder by its outer diameter. For applicable workover riser, the surface is assumed to be in the highly corroded steel range.

The roughness factor calculated using values from table 3.2:

$$\frac{k}{OD} = 1,4 \times 10^{-2}$$

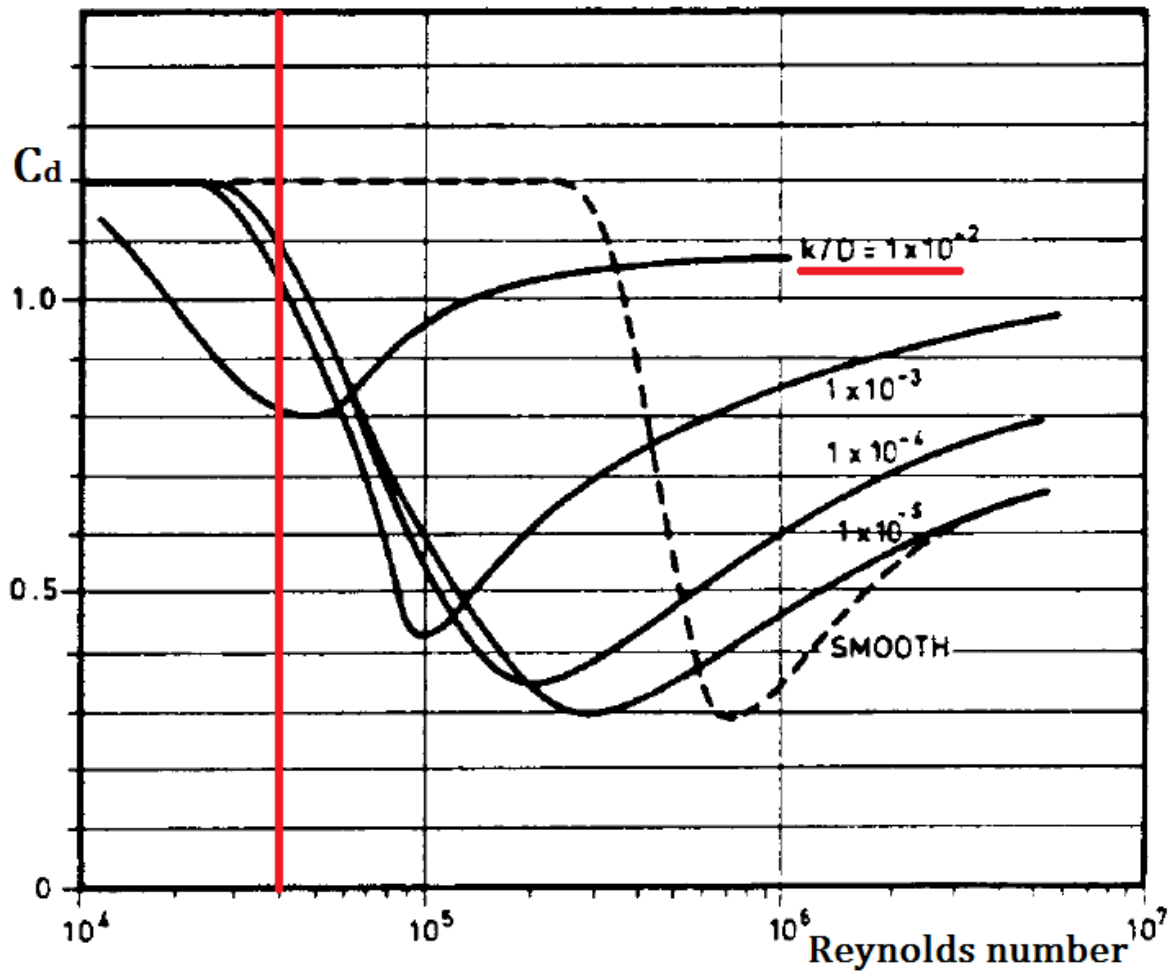


Figure 3.5 Drag coefficients as a function of Reynolds number and surface roughness (DNV RP-C205, 2010, p.56)

Figure 3.5 shows the drag coefficients for a cylinder as a function of the Reynolds number. The curve for the drag coefficient will depend upon the surface factors. For the workover riser used in this thesis, the critical flow for a cylinder with this roughness factor occurs for  $Re > 4 \times 10^4$ . To ensure that post-critical flow can be assumed for all simulations, the Reynolds numbers for the all wave conditions must be calculated.

#### The Reynolds number:

The Reynolds number is a dimensionless number that is used to describe flow patterns in fluid mechanics. The Reynolds number can be calculated from the relationship between the velocity of a fluid, the diameter of its obstruction and its kinematic viscosity (Finnemore & Franzini, 2002, p.236):

$$Re = \frac{uD}{\nu} \quad (3.2)$$

Where:

- $Re$  is the dimensionless Reynolds number
- $u$  is the horizontal water particle velocity [m/s]
- $D$  is the outer diameter of the cylinder [m]
- $\nu$  is the kinematic viscosity of the sea water [m<sup>2</sup>/s]



The horizontal water particle velocity will vary with different wave heights and periods. The various velocities are calculated in the following sections.

### Maximum wave height (Gudmestad, 2013)

To calculate the largest water particle velocities that occur for each wave condition, the maximum wave height must be used. The significant wave heights and zero up-crossing periods are shown in table 3.1. The maximum wave height for a 6 hour storm is approximately:

$$H_{max} = 1,9H_s$$

Table 3.4 shows the maximum wave heights used for the further calculations.

Table 3.4 Maximum wave height for the different sea states

$H_s$	0,5m	1,0m	1,5m	2,0m	2,5m	3,0m	3,5m	4,0m	4,5m	5,0m
$H_{max}$	1,0m	1,9m	2,9m	3,8m	4,8m	5,7m	6,7m	7,6m	8,6m	9,5m

### Linear wave theory for deep water waves (Gudmestad, 2013)

In order to use deep water linear wave theory for calculating the water particle velocity, following criteria must be fulfilled:

$$\frac{d}{L} > 0,5$$

Where:

- $d$  is the water depth [m]
- $L$  is the horizontal distance of the wave measured from crest to crest [m]

To calculate the wave length, the dispersion relation for deep water is assumed:

$$L = \frac{g}{2\pi} \cdot T^2 \quad (3.3)$$

Where:

- $T$  is the wave period [s]

The wave with the largest period will also be the longest. The zero up-crossing periods from the scatter diagram is used as the wave period for these calculations. The largest  $T_z$  in the scatter diagram has a period of 16 seconds, thus the longest wave is calculated to be (Eq. 3.3):

$$T = 16s$$

$$L = \frac{9,81 \text{ m/s}^2}{2\pi} \cdot (16s)^2 = 400m$$

The water depth for the Draugen area is approximately 250m  $\rightarrow d = 250m$

$$\frac{d}{L} = 0,625 > 0,5$$

Linear wave theory for deep water can be used for all waves.

**Horizontal water particle velocity** (Gudmestad, 2013)

The horizontal water particle velocity for a deep water wave is:

$$u = \frac{\xi_0 \cdot k \cdot g}{\omega} \cdot e^{kz} \cdot \sin(\omega t - kx) \quad (3.4)$$

Where:

- $\xi_0$  is the wave amplitude [m]
- $\omega$  is the frequency [ $s^{-1}$ ]
- $k$  is a constant [ $m^{-1}$ ]
- $z$  is the water depth where the velocity is calculated (mean water level is  $z = 0$ ) [m]

The maximum horizontal water particle velocity ( $u_{max}$ ) at mean water level for a deep water wave:

$$u_{max} = \frac{\xi_0 \cdot k \cdot g}{\omega} \quad (3.5)$$

$$k = \frac{2\pi}{L} \quad (3.6)$$

$$\omega = \frac{2\pi}{T} \quad (3.7)$$

$$\xi_0 = \frac{H_{max}}{2} \quad (3.8)$$

The horizontal water particle velocities are shown in table 3.5

Table 3.5 Horizontal water particle velocity for all waves

<b>u - Horizontal water particle velocity (m/s)</b>															
	<b><math>T_z</math>(s)</b>														
	<b>2</b>	<b>3</b>	<b>4</b>	<b>5</b>	<b>6</b>	<b>7</b>	<b>8</b>	<b>9</b>	<b>10</b>	<b>11</b>	<b>12</b>	<b>13</b>	<b>14</b>	<b>15</b>	<b>16</b>
<b><math>\xi_0</math> (m)</b>															
<b>4,750</b>					5,0	4,3	3,7	3,3	3,0	2,7	2,5	2,3	2,1	2,0	1,9
<b>4,275</b>				5,4	4,5	3,8	3,4	3,0	2,7	2,4	2,2	2,1	1,9	1,8	1,7
<b>3,800</b>				4,8	4,0	3,4	3,0	2,7	2,4	2,2	2,0	1,8	1,7	1,6	1,5
<b>3,325</b>				4,2	3,5	3,0	2,6	2,3	2,1	1,9	1,7	1,6	1,5	1,4	1,3
<b>2,850</b>			4,5	3,6	3,0	2,6	2,2	2,0	1,8	1,6	1,5	1,4	1,3	1,2	1,1
<b>2,375</b>			3,7	3,0	2,5	2,1	1,9	1,7	1,5	1,4	1,2	1,1	1,1	1,0	0,9
<b>1,900</b>			3,0	2,4	2,0	1,7	1,5	1,3	1,2	1,1	1,0	0,9	0,9	0,8	0,7
<b>1,425</b>		3,0	2,2	1,8	1,5	1,3	1,1	1,0	0,9	0,8	0,7	0,7	0,6	0,6	0,6
<b>0,950</b>	3,0	2,0	1,5	1,2	1,0	0,9	0,7	0,7	0,6	0,5	0,5	0,5	0,4	0,4	0,4
<b>0,475</b>		1,0	0,7	0,6	0,5	0,4	0,4	0,3	0,3	0,3	0,2				

Using the water particle velocities, the Reynolds numbers has been calculated in table 3.6 using  $OD = 0,219m$  and kinematic viscosity  $\nu = 1,35 \times 10^{-6}$

Almost all values for the Reynolds number in table 3.6 are larger than  $10^5$  which exceeds the critical limit. The smallest Reynolds numbers occur at the lowest wave amplitude ( $\xi_0 = 0,475m$ ), when  $T_z$  is larger than 5s. The minimum value for the Reynolds number is 40 359, larger than  $4 \times 10^4$ . Hence all wave conditions can be assumed to be in the post critical flow.

Table 3.6 Reynolds numbers for all waves

Reynolds number for different waves										
	$\xi_0$ (m)									
$T_z$	4,750	4,275	3,800	3,325	2,850	2,375	1,900	1,425	0,950	0,475
(s)										
2									484 309	
3								484 309	322 873	161 436
4					726 464	605 386	484 309	363 232	242 155	121 077
5		871 756	774 895	678 033	581 171	484 309	387 447	290 585	193 724	96 862
6	807 181	726 464	645 745	565 027	484 309	403 591	322 873	242 155	161 436	80 718
7	691 870	622 683	553 496	484 309	415 122	345 935	276 748	207 561	138 374	69 187
8	605 386	544 848	484 309	423 770	363 232	302 693	242 155	181 616	121 077	60 539
9	538 121	484 309	430 497	376 685	322 873	269 061	215 248	161 436	107 624	53 812
10	484 309	435 878	387 447	339 016	290 585	242 155	193 724	145 293	96 862	48 431
11	440 280	396 253	352 225	308 197	264 169	220 140	176 112	132 084	88 056	44 028
12	403 590	363 232	322 873	282 514	242 155	201 795	161 436	121 077	80 718	40 359
13	372 545	335 291	298 036	260 782	223 527	186 273	149 018	111 764	74 509	
14	345 935	311 342	276 748	242 155	207 561	172 968	138 374	103 781	69 187	
15	322 872	290 585	258 298	226 011	193 724	161 436	129 149	96 862	64 575	
16	302 693	272 424	242 155	211 885	181 616	151 347	121 077	90 808	60 539	

#### Drag coefficient for steady state flow

Using the roughness factor for the workover riser, the steady state drag coefficient can be found. (ISO 19902:2007, 2011, p.295)

A roughness factor of  $1,4 \times 10^{-2}$  gives:

$$C_{ds} = 1,07$$

#### Drag coefficient for un-steady flow

The drag coefficient can be read graphically (ISO 19902:2007, 2011, p.297). The drag coefficient here is plotted as a function of the Keulegan-Carpenter number. This graph applies for  $K_c > 12$

The Keulegan-Carpenter number is defined as:

$$K_c = \frac{uT}{D} \quad (3.9)$$

Where:

$D$  is the outer diameter (OD) of the pipe [m]

The values for  $K_c$  are shown in table 3.7

Table 3.7 Keulegan-Carpenter numbers for each significant wave height

$H_s$	5,0m	4,5m	4,0m	3,5m	3,0m	2,5m	2,0m	1,5m	1,0m	0,5m
$K_c$	136	123	109	95	82	68	54	41	27	14

It should be noted that the Keulegan-Carpenter number does not change with the wave period.

All values for  $K_c > 12$

The drag coefficients corresponding to each value for  $K_c$  are shown in table 3.8

Table 3.8 Drag coefficients for each significant wave height

$H_s$	5,0m	4,5m	4,0m	3,5m	3,0m	2,5m	2,0m	1,5m	1,0m	0,5m
$C_d$	1,07	1,07	1,07	1,07	1,11	1,12	1,20	1,20	1,30	1,60

### 3.4.5 SEGMENT LENGTH

An important setting for the simulations is the length of each segment in the riser. In OrcaFlex, bending of a line occurs at the nodes of each line. Each segment line will act as a rigid stick and so the bending occurs only at the nodes between the sticks. If a segment (stick) is too long, the line is not be able to bend into the shape that it naturally should due to the moment acting on it, the result of this is that both the deformation and the values for the bending moment becomes incorrect. The more segments a line is divided into, the more accurate the deformation and bending moment distribution becomes. However, the more segments to a line, the longer the simulations take to perform. The best way to decide the length of each segment is to perform simulations and use shorter segments each time. The bending moment values will start to converge towards a certain value at some point. The segment length should then be set small enough so that the output value is close to this converged value, but still long enough so that the simulations do not take too much time to perform (Orcina, 2014). Testing with the model showed that the largest bending moments occurred at the top section of the riser and so this section must be divided into smaller segments than the middle and lower section. The workover riser for the OrcaFlex model is therefore divided into 1m long segments at the 5m top section of the riser. The rest of the riser is divided into 5m section. Figure 3.6 shows the line segments in the 52m riser.

Sections:  Total length = 52,000m

No.	Line Type	Section Length (m)	Target Segment Length (m)	Number of Segments	Cumulative Values Length (m)	Segments
1	8 5/8" RISER	5,000	1,000	5	5,000	5
2	8 5/8" RISER	47,000	5,000	9	52,000	14

Figure 3.6 Segment lengths for the workover riser in OrcaFlex

### 3.5 THE XMAS TREE STACK

The true Xmas tree/LRP/EDP configuration is a quite complex structure with parameters and coefficients that are not easily available. Due to this the equipment stack used for the dynamic simulations in OrcaFlex must have a simplified geometry. Parameters in the data sheet have been found using various standards and assumptions. The following section provides explanation of how all values for the equipment stack plotted into the data sheet, have been found. Any values in the data sheet that are not calculated in the following section will be a default value from the OrcaFlex software.

#### 3.5.1 DIMENSIONS

The OrcaFlex model of the equipment stack is simplified to be a 6D buoy with the shape of a rectangular prism. In reality the EDP, LRP and Xmas do not all have the same width and length. Because only one value for the added mass and drag coefficients can be implemented, the equipment stack has the average width and length of the overall stack as a basis for the model. The height used will be the cumulative height. Dimensions are shown in table 3.9.

Table 3.9 Dimensions for the equipment stack used in OrcaFlex

	EDP	LRP	Xmas tree	Model
Length (Y)	4,2m	3,8m	4,5m	4,2m
Width (X)	3m	3m	3m	3m
Height (Z)	2,25m	4,5m	3m	10m
Mass	$25 \cdot 10^3 kg$	$45 \cdot 10^3 kg$	$40 \cdot 10^3 kg$	$11 \cdot 10^4 kg$

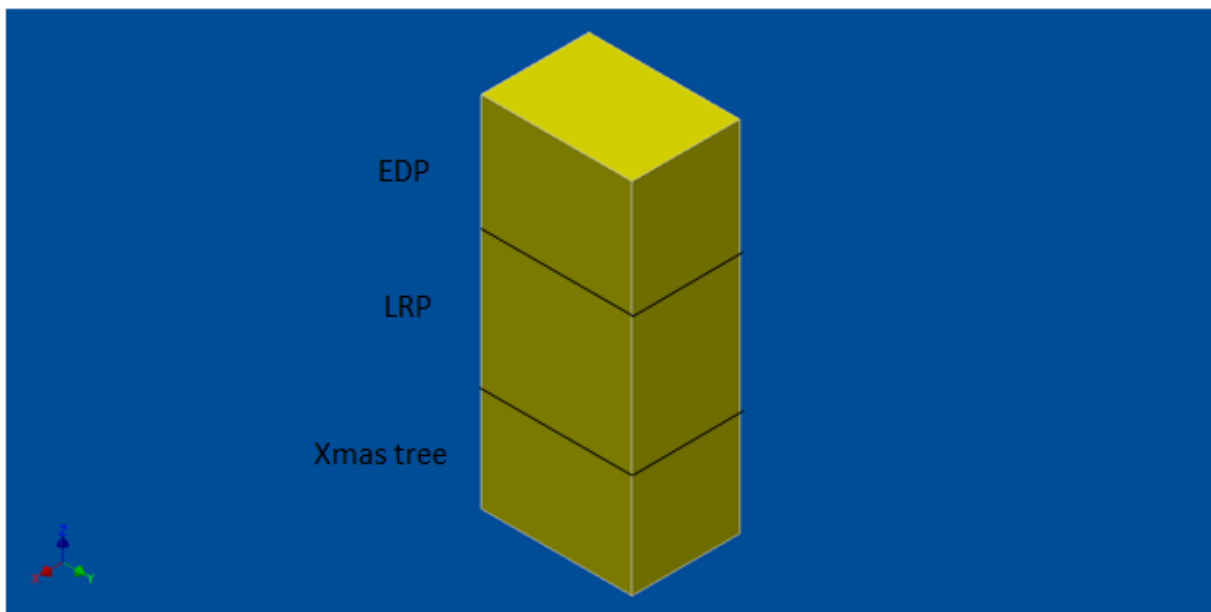


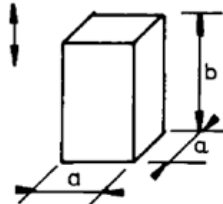
Figure 3. 7 The geometry of the model used for the OrcaFlex simulations

The equipment stack as it will appear in OrcaFlex is seen in figure 3.7.

### 3.5.2 ADDED MASS TO XMAS TREE STACK

The Xmas tree stack will experience the effect of added mass in all directions of freedom. Rotational motion is not applicable since the stack is not going to be able to rotate in the simulations. Table 3.10 is taken from DNV Recommended Practice - Modelling and Analysis of Marine Operations. This table only applies for motion normal to a square cross section. The prism used for this model does not have a square cross section in any directions and hence a different approach is used for the added mass estimation.

Table 3.10 DNV table for calculation of added mass for square prisms (DNV RP-H103, 2011, p.141)

Body shape		Direction of motion	$C_A$		$V_R$
Square prisms		Vertical	$b/a$	$C_A$	$a^2 b$
			1.0	0.68	
			2.0	0.36	
			3.0	0.24	
			4.0	0.19	
			5.0	0.15	
			6.0	0.13	
			7.0	0.11	
			10.0	0.08	

An alternative estimation is found from the same DNV document. This simplified approximation for the added mass in heave for a three dimensional body with vertical sides is (DNV RP-H103, 2011, p.70):

$$A_{mS} = \left[ 1 + \sqrt{\frac{1 - \lambda^2}{2(1 + \lambda^2)}} \right] \cdot A_0 \quad (3.10)$$

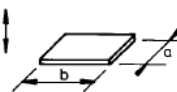
$$\lambda = \frac{\sqrt{A_p}}{h + \sqrt{A_p}} \quad (3.11)$$

Where:

- $A_{mS}$  is the solid added mass (solid mass for non-perforated structure) [kg]
- $A_0$  is the added mass for a rectangular plate [kg]
- $h$  is the height of the object [m]
- $A_p$  is the area of the submerged part of an object projected on a horizontal plane [m<sup>2</sup>]

The added mass for a rectangular plate can be seen in table 3.11.

Table 3.11 DNV table for calculation of added mass for flat plates (DNV RP-H103, 2011, p.141)

Rectangular plates	Vertical	$b/a$	$C_A$	$b/a$	$C_A$	$\frac{\pi}{4} a^2 b$
			1.00	0.579	3.17	
		1.25	0.642	4.00	0.872	
		1.50	0.690	5.00	0.897	
		1.59	0.704	6.25	0.917	
		2.00	0.757	8.00	0.934	
		2.50	0.801	10.00	0.947	
		3.00	0.830	$\infty$	1.000	

The added mass for rectangular plates:

$$A_0 = \rho C_A \frac{\pi}{4} a^2 b \quad (3.12)$$

**Translational motion along the z-axis:**

The cross sectional area of the stack normal to the z-axis is calculated by:

$$b/a \sim 1,5 \rightarrow C_A = 0,69$$

Where  $b$  is the width of the cross section, in this plane the length along the y-axis. The height of the cross section, the value  $a$  is the length along the x-axis.

With the added mass calculated from Eq. 3.12

$$A_0 = 1025 \text{ kg/m}^3 \cdot 0,69 \cdot \frac{\pi}{4} \cdot (3\text{m})^2 \cdot 4,2\text{m}$$

$$A_0 = 21\,000\text{kg}$$

$$A_p = a \cdot b = 4,2\text{m} \cdot 3\text{m} = 12,6\text{m}^2$$

From Eq.11

$$\lambda = \frac{\sqrt{12,6\text{m}^2}}{10\text{m} + \sqrt{12,6\text{m}^2}} = 0,26$$

From Eq.10

$$A_{mSZ} = \left[ 1 + \sqrt{\frac{1 - (0,26)^2}{2(1 + (0,26)^2)}} \right] \cdot 21\,000\text{kg} = 34\,857\text{kg}$$

**Translational motion along the x-axis:**

The cross section of the stack normal to the x-axis has the following ratio:

$$b/a \sim 2,5 \rightarrow C_A = 0,801$$

For this projection, the width  $b$  is the length along the z-axis. The height  $a$  is the length along the y-axis.

Added mass calculated from Eq. 3.12

$$A_0 = 1025 \text{ kg/m}^3 \cdot 0,801 \cdot \frac{\pi}{4} \cdot (4,2\text{m})^2 \cdot 10\text{m}$$

$$A_0 = 113\,748\text{kg}$$

$$A_p = a \cdot b = 4,2\text{m} \cdot 10\text{m} = 42\text{m}^2$$

From Eq.11

$$\lambda = \frac{\sqrt{42\text{m}^2}}{3\text{m} + \sqrt{42\text{m}^2}} = 0,68$$

From Eq.10

$$A_{msX} = \left[ 1 + \sqrt{\frac{1 - (0,68)^2}{2(1 + (0,68)^2)}} \right] \cdot 113\,748\,kg = 162\,213\,kg$$

**Translational motion along the y-axis:**

The cross section normal to the y-axis has the following ratio:

$$b/a \sim 3,17 \rightarrow C_A = 0,84$$

The width  $b$  is the length of the stack along the z-axis. The height  $a$  is the length along the x-axis.

Added mass calculated from Eq. 3.12

$$A_0 = 1025 \frac{kg}{m^3} \cdot 0,801 \cdot \frac{\pi}{4} \cdot (3m)^2 \cdot 10m$$

$$A_0 = 60\,860\,kg$$

$$A_p = a \cdot b = 3m \cdot 10m = 30m^2$$

From Eq.11

$$\lambda = \frac{\sqrt{30m^2}}{4,2m + \sqrt{30m^2}} = 0,57$$

From Eq.10

$$A_{mSY} = \left[ 1 + \sqrt{\frac{1 - (0,57)^2}{2(1 + (0,57)^2)}} \right] \cdot 60\,860\,kg = 91\,736\,kg$$

**True added mass due to perforation:**

The value  $A_m$  describes the added mass for a solid prism. The true Xmas tree stack is not a solid block, but is perforated. The true added mass for the prism can be estimated as a function of the perforation of the stack. (DNV RP-H103, 2011, p.71)

When  $p \leq 5$

$$A_m = A_{mS} \tag{3.10}$$

When  $5 < p < 34$

$$A_m = A_{mS} \cdot \left( 0,7 + 0,3 \cdot \cos \left[ \frac{\pi \cdot (p - 0,5)}{34} \right] \right) \tag{3.13}$$

When  $34 \leq p \leq 50$

$$A_m = A_{mS} \cdot e^{\frac{10-p}{28}} \tag{3.14}$$

Where:

- $A_{mS}$  is the solid added mass (solid mass for non-perforated structure) [kg]
- $p$  is the perforation rate [%]



A perforation of  $p = 20\%$  is assumed for the Xmas tree stack. Thus Eq.3.13 is used for the added mass calculations:

$$A_m = A_{mS} \cdot \left( 0,7 + 0,3 \cdot \cos \left[ \frac{\pi \cdot (20 - 5)}{34} \right] \right) = 0,76 \cdot A_{mS}$$

$$A_{mZ} = 26,5 \cdot 10^3 \text{ kg}$$

$$A_{mX} = 12,3 \cdot 10^4 \text{ kg}$$

$$A_{mY} = 69,7 \cdot 10^3 \text{ kg}$$

### 3.5.3 ADDED MASS COEFFICIENT

The added mass coefficient is defined as (DNV RP-H103, 2011, p.23):

$$C_A = \frac{m_A}{\rho A} \quad (3.15)$$

Where:

$A$  is the cross section normal to the motion [ $m^2$ ].

The added mass coefficient for motion along the x-, y- and z-axis using Eq.15:

$$C_{AZ} = \frac{26\,491 \text{ kg}}{1025 \text{ kg/m}^3 \cdot 4,2 \text{ m} \cdot 3 \text{ m}} = 2,05$$

$$C_{AX} = \frac{123\,281 \text{ kg}}{1025 \text{ kg/m}^3 \cdot 4,2 \text{ m} \cdot 10 \text{ m}} = 2,86$$

$$C_{AY} = \frac{69\,719 \text{ kg}}{1025 \text{ kg/m}^3 \cdot 10 \text{ m} \cdot 3 \text{ m}} = 2,26$$

### 3.5.4 DRAG COEFFICIENT

The true equipment stack has a complex geometry and its drag coefficient cannot easily be found. Unless specific CDF studies or model tests have been performed, the following guideline for drag coefficients on typical subsea structures in oscillatory flow is (DNV RP-H103, 2011, p.70):

$$C_D \geq 2,5$$

### 3.5.5 MASS COEFFICIENT

The mass coefficient is defined as (DNV RP-C205, 2010, p.52):

$$C_m = 1 + C_A \quad (3.16)$$

For the Xmas tree stack the mass coefficients using Eq.3.16:

$$C_{Mz} = 3,05$$

$$C_{Mx} = 3,86$$

$$C_{My} = 3,26$$

### 3.5.6 MASS MOMENT OF INERTIA

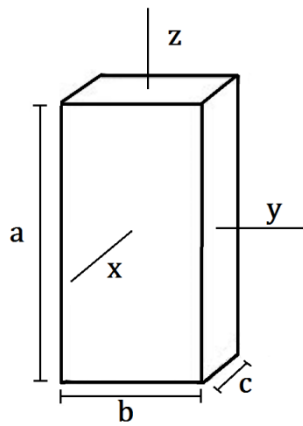


Figure 3.8 Rotational axis of the equipment stack

Figure 3.8 shows the axis of rotation for the equipment stack. The mass moment of inertia is calculated by:

$$I_x = \frac{1}{12} m(a^2 + b^2) \quad (3.17)$$

$$I_y = \frac{1}{12} m(c^2 + a^2) \quad (3.18)$$

$$I_z = \frac{1}{12} m(c^2 + b^2) \quad (3.19)$$

Where:

$m$  is the mass of the object [kg]

Dimensions from table 3.9 give the following mass moment of inertia:

$$I_x = 1,08 \cdot 10^6 \text{ kgm}^2$$

$$I_y = 1 \cdot 10^6 \text{ kgm}^2$$

$$I_z = 2,44 \cdot 10^3 \text{ kgm}^2$$

### 3.5.7 VOLUME OF THE STACK

Using the dimensional values for the stack, the volume of the equipment would be  $126 m^3$ . Such a volume will displace so much water that the equipment stack would become buoyant. The actual equipment has large gaps between the pipes and its protective frame. For this simulation the true volume of the equipment is assumed to be 50% of the calculated volume.

$$V = 63m^3$$

### 3.6 SUMMARY OF ORCAFLEX INPUT

The input data for the riser calculated in this chapter are shown in table 3.12.

Table 3.12 Input data for the workover riser

Riser data	
Outer diameter	8 5/8" (0,219m)
Inner diameter	7" (0,178m)
$C_A$	1,0
Content	Sea water ( $1025 kg/m^3$ )
Material	Steel

Since the drag coefficient varies according to wave velocity, the drag coefficients shown in table 3.13 are used for the corresponding wave condition.

Table 3.13 Drag coefficients for the workover riser

Drag coefficients										
$H_s$	5,0m	4,5m	4,0m	3,5m	3,0m	2,5m	2,0m	1,5m	1,0m	0,5m
$C_d$	1,07	1,07	1,07	1,07	1,11	1,12	1,20	1,20	1,30	1,60

All input values used for the Xmas tree stack that were calculated in section 3.5 are shown in table 3.14.

Table 3.14 Input values for the equipment stack

Equipment stack data	
Weight (dry)	$1,1 \cdot 10^5 kg$
Dimensions	$4,2m \times 3m \times 10m$
True Volume	$63m^3$
Added mass x direction	$12,3 \cdot 10^4 kg$
Added mass y direction	$69,7 \cdot 10^3 kg$
Added mass z direction	$26,5 \cdot 10^3 kg$
$C_{AZ}$	2,05
$C_{AX}$	2,86
$C_{AY}$	2,26
$C_D$	2,50
$C_{Mz}$	3,05
$C_{Mx}$	3,86
$C_{My}$	3,26
$I_x$	$1,08 \cdot 10^6 kgm^2$
$I_y$	$10^6 kgm^2$
$I_z$	$2,44 \cdot 10^3 kgm^2$

### 3.7 ORCAFLEX SIMULATIONS

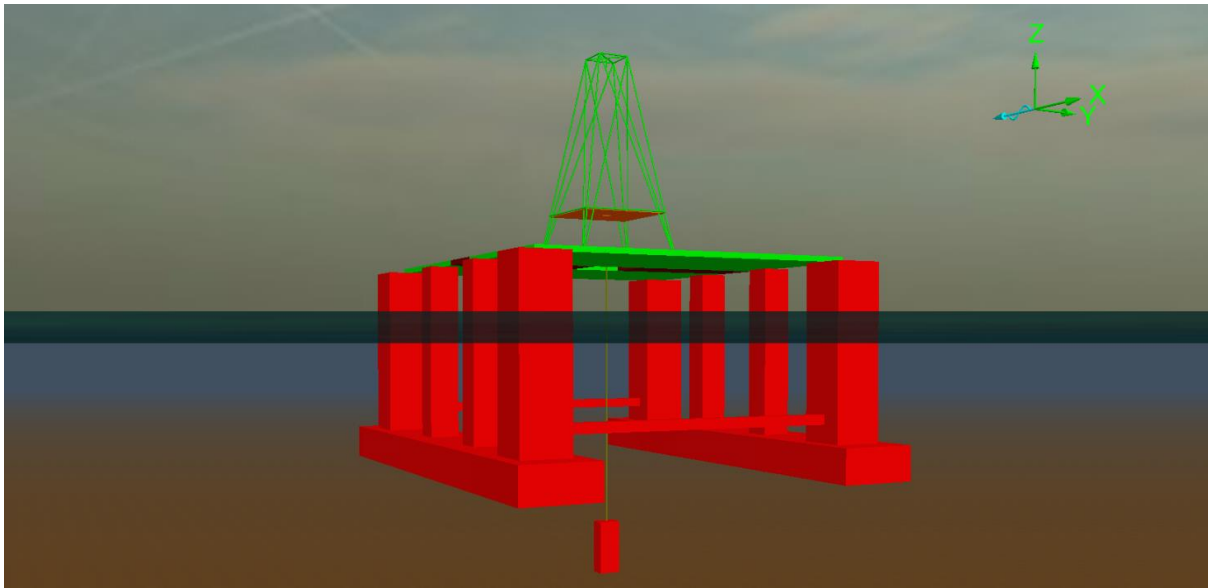


Figure 3. 9 The workover vessel seen in OrcaFlex

Figure 3.9 shows how the vessel with the suspended riser and equipment stack is displayed in OrcaFlex. Each riser joint is 13m long. Every simulation will test a situation where  $x$  number of riser joints has been deployed with an attached equipment stack consisting of an EDP, a LRP and a Xmas tree at the end. While a new riser joint is being installed on deck, the suspended riser section and equipment stack is exposed to waves and currents. These OrcaFlex simulations will reveal the bending moment and effective tension along the riser.

The simulations are going to be run for different riser lengths in order to see its effect on the bending moment. This may clarify whether TSJ will be exposed to larger stresses if it, for instance, were to be installed as the 2<sup>nd</sup> joint as opposed to the 5<sup>th</sup> joint. Gaining knowledge of these loads to the riser can help to determine which points along the riser the TSJ could safely be installed for the different sea states. As an example; the dynamic simulation may reveal that if the TSJ is installed as the 5<sup>th</sup> riser joint, installation should not be performed for  $T_z > y$  when  $H_s = z$ .

### 3.8 ANSYS WORKBENCH 13.0

To conclude which wave conditions that are acceptable for the installation, the TSJ must be tested to find out which loads it can withstand. Using ANSYS workbench the loads from the dynamic simulations can be applied to a model of the joint in order to see which wave conditions that do not damage the joint. The model of the TSJ will be analyzed twice; one time when using the full capacity of the over-ride cylinders and another time using a lower pretension value. The aim is to see how/if these cylinders increase the joints resistance with respect to bending moment. If so, the OrcaFlex results can be used to find out what environmental conditions that is appropriate for installation with respect to the safety joint.

### 3.8.1 AUTODESK INVENTOR MODEL



Figure 3.10 Autodesk Inventor model of the retracted TSJ

Figure 3.10 shows the assembled model of the upper and lower section from Autodesk Inventor. This model is simplified in comparison to the real TSJ as it does not contain any of the external pressure compensating cylinders. The ten tensile bolts are equally spaced in a ring, each bolt being 328mm from the center of the joint. As for the over-ride cylinders, they are not in the model. To simulate their effect, large bolts will be used with a given pretension that is going to be of the same magnitude that the over-ride cylinders would apply. Each over-ride bolt is located 250mm from the center.

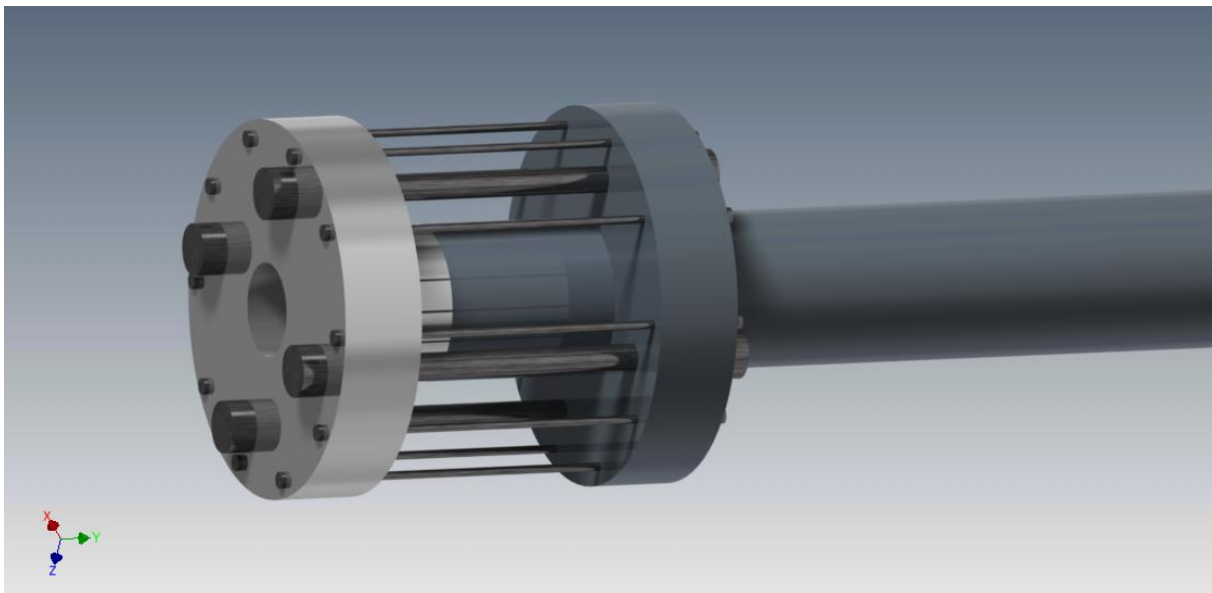


Figure 3.11 Close-up of the Tensile and Over-ride bolts

The assembly interface is shown in closer detail in figure 3.11. The bolts can also be seen here. The four largest diameter bolts represents the over-ride cylinders. The ten smaller bolts are the tensile bolts. It is this section of the joint that will be of interest during the static simulations in ANSYS.

Figure 3.12 shows the cross section of the joint assembly. The interface between the upper and lower segment is visible here. It is worth noting that the contact surface between the upper and lower joint sections does not extend all along the length of the joint. There is a gap between the inner pipe (the upper section) and the outer pipe (the lower section). The bolts prevent the assembly from sliding apart due to the applied axial tension in the joint. The simulations will show how the applied bending moment to the joint affects the stress in the tensile bolts that are located the furthest from the neutral axis. The bore of the joint is not pressurized and so

the end cap effect will not be present. The short external pressure balancing cylinders are not included in the model, nor are any of the long stroke cylinders.

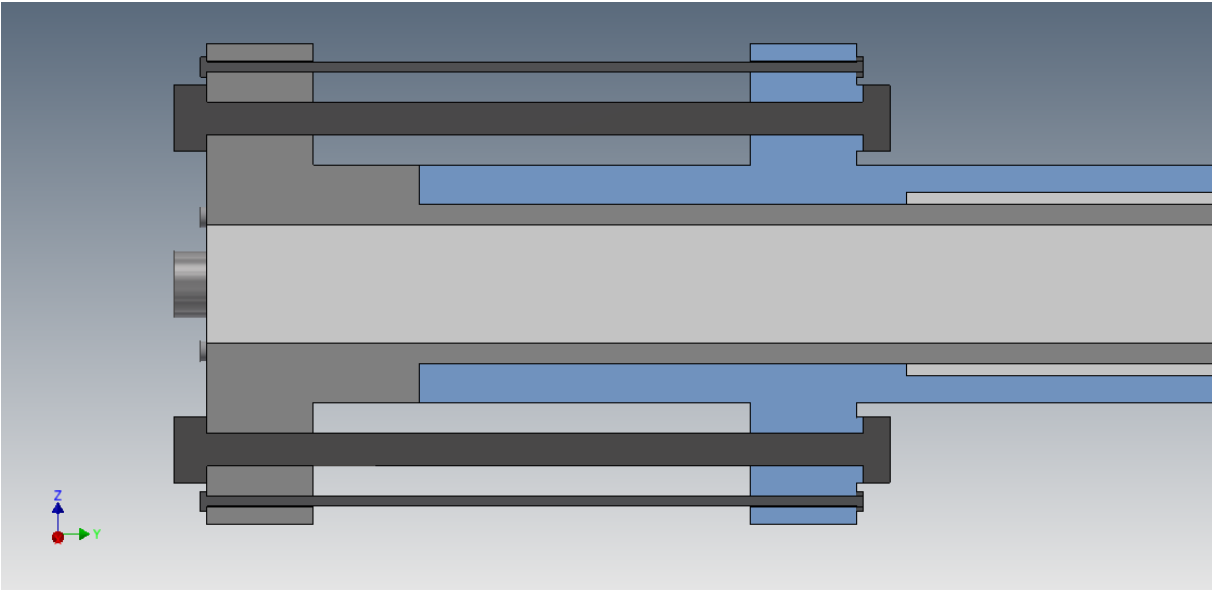


Figure 3.12 Section cut view of the interface between the upper and lower sections of the joint

### 3.8.2 ACCEPTANCE CRITERIA

If the tensile bolts were to take plastic damage during installation they would no longer be able to function as intended. The purpose of the simulations is to find out at which magnitude of the bending moment the tensile bolts will begin to yield. The acceptable bending moment in the riser is the largest bending moment that can be applied to the joint without plastic deformation of the tensile bolts. Material properties and dimension for the tensile bolts are given in table 3.15. This information is provided by FMC Technologies.

Table 3.15 Data table for the tensile bolts

Number of tension bolts	Diameter	$R_{p0,2}$	Pretension
10	15,6mm	634MPa	66kN

The applied bending moment to the joint will be acceptable as long as the maximum equivalent Von-Mises stress in all the bolts are within the elastic regime:

$$\sigma_{Von-Mises} < R_{p0,2} = 634MPa$$

### 3.8.3 BOLT PRETENSION SETTINGS

Bolts with pretension are used in order to simulate the effect of the tensile bolts and the over-ride cylinders. To reduce the complexity of the model the “no bolt simulation” is used for most of the bolts. This means that instead of adding the actual bolts in the model, the reaction forces from the bolts are placed at the washer surface. This gives the same pretension force as if bolts were to be used. When the tension in the joint increases the tension in each bolt would normally increase linearly due to its stiffness. The stiffness is defined by the Young’s modulus of the material. The “no bolt simulation” does not provide the effect from the bolt stiffness. Figure 3.13 shows where the reaction forces from the bolts will be placed on the model.

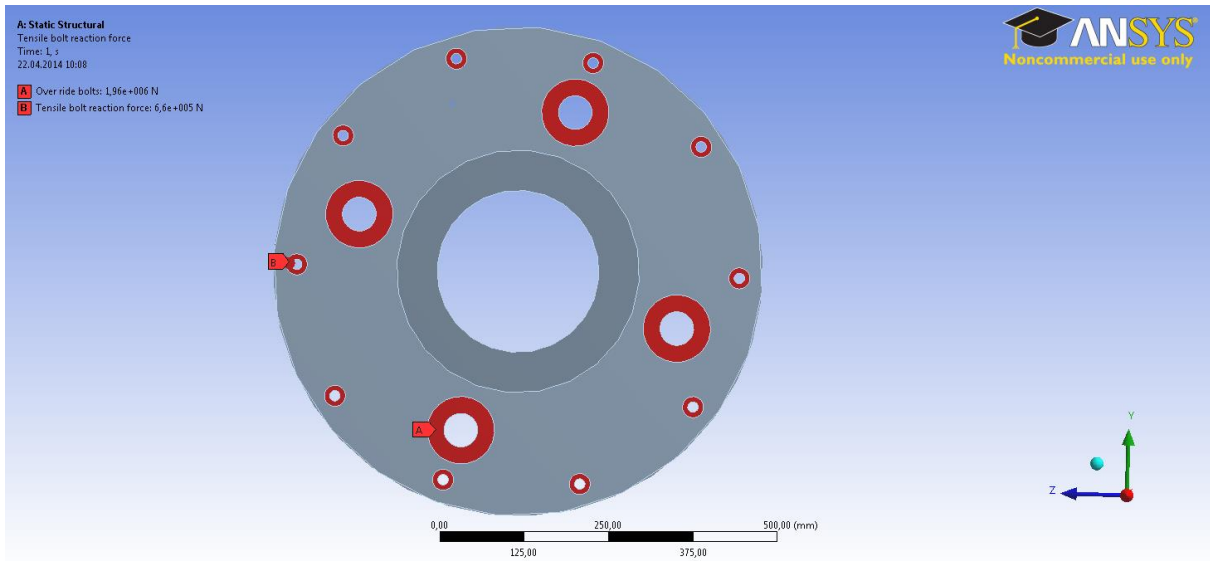


Figure 3.13 Reaction forces from the bolt pretension

By not including all the bolts in the model, there are fewer elements for the program to solve. There would be a total of 14 bolts (10 tension bolts and 4 over-ride cylinders) if all were included. By reducing the number of elements in the model the solving will become quicker. Only the tensile bolts most exposed to the bending moment are included. A more accurate result would be obtained by including all 10 + 4 bolts in the simulation, but the “no bolt simulation” method provides a good approximation. (Montgomery, 2002, p.15)

**Pretension values:**

Information supplied from FMC Technologies about the pretension values are given in table 3.16.

Table 3.16 Pretension values to be used in ANSYS workbench

	Number of bolts	Pretension for each bolt
Tensile bolts	10	66kN
Over-ride cylinders	4	490kN

The assembly of the joint is only held together by friction and bolts. When performing the ANSYS workbench simulations with the semi-pressurized over-ride function, the pretension of the bolts will not be equal to zero. If a large axial force is applied to the joint with zero pretension from the over-ride bolts, the tensile bolts might yield immediately. Because of this, the over-ride bolts must always have some pretension. In the semi-pressurized over-ride function simulation, the pretension of the over-ride bolts combined with the pretension from the tensile bolts shall equal the effective tension in the riser. For the second simulations where the over-ride function is activated. The over-ride bolts will have the maximum pretension described in table 3.16.

### Capacity of the tensile bolts

The maximum tension force that can be applied to each tensile bolt prior to yielding is calculated from the data in table 3.15.

$$T_{bolt} = R_{p0,2}A = 634MPa \cdot \frac{(15,6mm)^2}{4} \cdot \pi = 121kN$$

The tensile bolts already have a pretension of 66kN, hence this must be subtracted. The additional axial load capacity of each bolt is:

$$121kN - 66kN = 55kN$$

Since there are ten bolts, the axial capacity of the joint when held together by the tensile bolts is:

$$10bolts \cdot 55kN = \underline{550kN}$$

### 3.8.4 TENSILE BOLTS

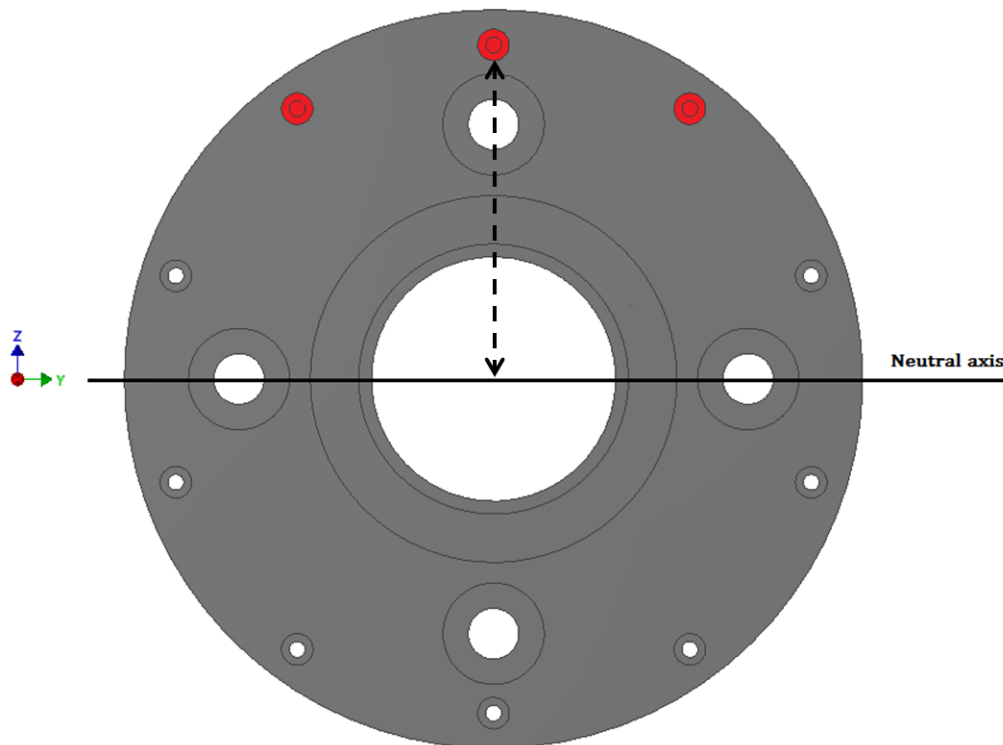


Figure 3.14 Location of the three tensile bolts in the model

Three tensile bolts are included in the model. These are located where the largest displacement occurs; furthest from the neutral axis. The bending moment is placed about the y-axis. The tensile bolt furthest away from the y-axis is subjected to the largest displacement and thus tensile stress. The placements of the tensile bolts are shown in figure 3.14.



### 3.8.5 SIMULATION

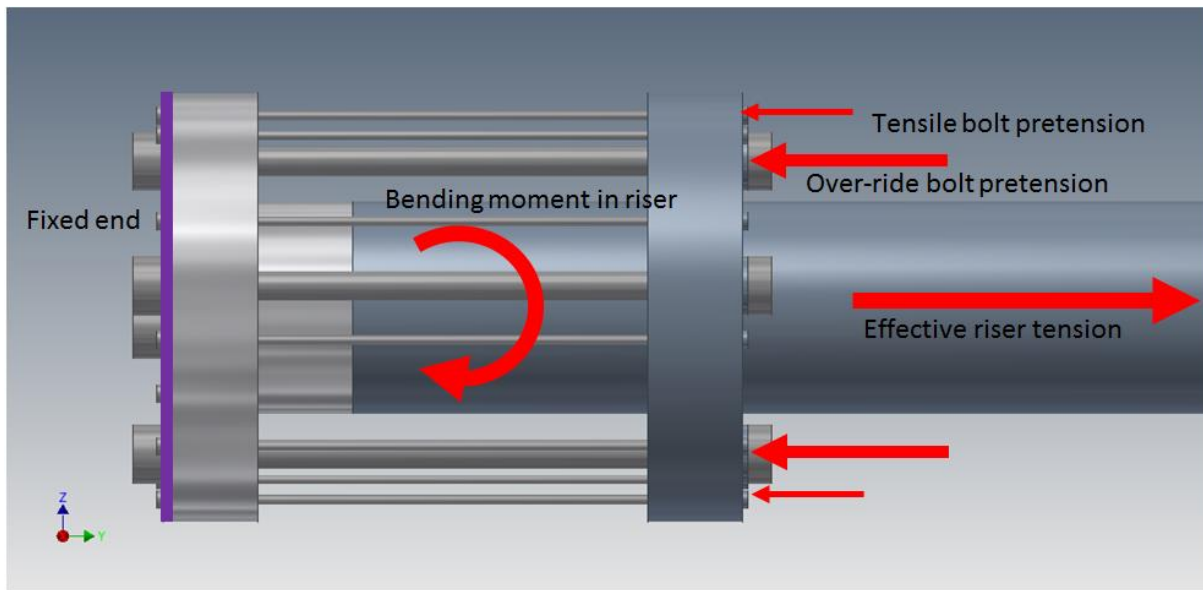


Figure 3.15 Forces applied to the joint in ANSYS.

The loading condition for the model is shown in figure 3.15. Since the pretension for the tensile bolts are given, they will be constant for all simulations. The purpose of the simulations is to see how the strength of the joint increase with larger pressure in the over-ride cylinders. One model will test the joint when the over-ride cylinders are fully-pressurized, so the over-ride bolts will have the maximum pretension. The other model will use a semi-pressurized version of the over-ride cylinders; hence this uses over-ride bolts with lower pretension. When applying a tension and a bending moment to the joint the simulations will show when the tensile bolts begin to yield. It is the magnitude of the bending moment applied to the joint that is of greatest interest. If the joint using fully-pressurized over-ride cylinders can withstand a larger bending moment than the semi-pressurized joint, the actual effect of the over-ride function with respect to bending moment can be proven.

# 4. RESULTS

This chapter presents the results from the simulations performed, as well as calculations of the strength of the workover riser.

## 4.1 SENSITIVITY ANALYSIS

Four sensitivity tests were performed in order to ensure that the correct data points were used. What duration each simulation would require to ensure that the optimal time step was chosen. The effect of sea current versus no sea current to find which conditions is the most critical to the system and which points along the riser were subjected to the largest loads. The results are shown in the latter.

### 4.1.1 TIME STEP SENSITIVITY TEST

To decide the correct time step for the OrcaFlex simulations a sensitivity analysis was performed. A 52m riser section with  $H_s = 5m$  and  $T_z = 16s$  was tested and the maximum bending moment in the riser was plotted. Different time steps were tested to see when the bending moment converged towards one value. If too short time step is chosen for the simulation, the result would be inaccurate. If the time step is too large the simulation will take unnecessary long time to perform. The results from the sensitivity analysis are shown in figure 4.1.

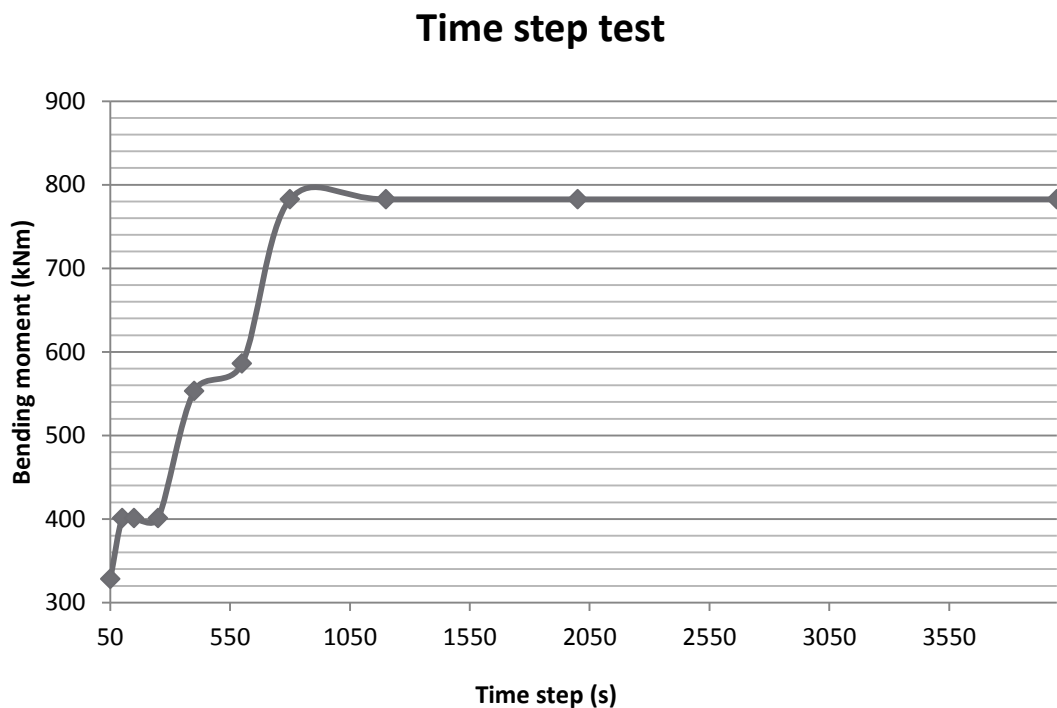


Figure 4.1 Sensitivity analysis of the time step in OrcaFlex

The time step test shows that the bending moment converge towards a fixed value for around 800s.

$$Time\ step = 800s$$

#### 4.1.2 CURRENT SENSITIVITY TEST

The current will generate a constant lateral force on both riser and equipment, but may also have a damping effect on the system. This damping may prevent harmonic motion from becoming too large. The maximum bending moment in the riser was plotted for  $5s \leq T_z \leq 20s$  for one model with current of  $0,5m/s$  and another model with zero current. The results are shown in figure 4.2.

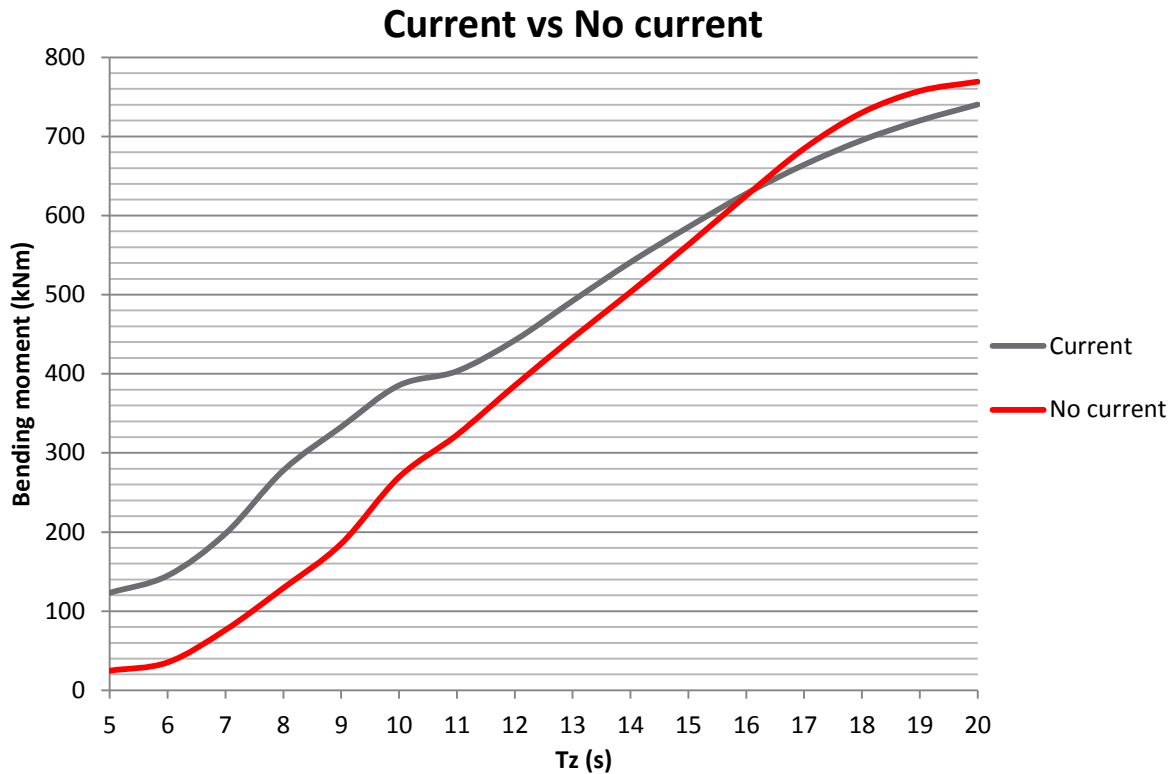


Figure 4.2 Comparison of bending moment in the riser with and without sea current

Figure 4.2 shows that the “no current” situation gives a larger bending moment in the riser when  $T_z > 16s$ . This is due to the natural period of the system being large. When the waves have a period close to the natural period of the equipment stack the current will damp the harmonic motion of the system. For shorter wave periods where harmonic motion is not likely to occur, the current increase the bending moment in the riser. Since there are no waves with  $T_z > 16s$  in the scatter diagram, the installation with sea current is going result in larger bending moments in the riser. The OrcaFlex simulation will therefore have a sea current present.

$$Sea\ current = 0,5\ m/s$$

#### 4.1.3 POINT OF MAXIMUM BENDING MOMENT

Figure 4.3 shows the distribution of bending moment along a 39m riser in  $H_s = 4$  and  $T_z = 12$ . For all simulations performed, the maximum bending moment was always found at the top end of the riser. Due to this, all values for bending moment that will be presented are found at the top of the riser.

### Bending moment along the riser

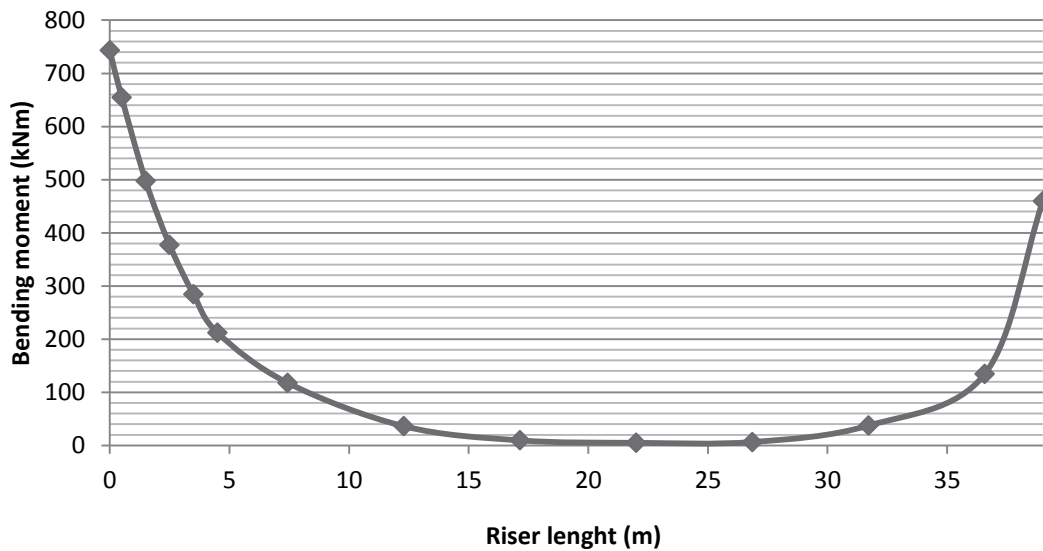


Figure 4.3 Distribution of bending moment along the workover riser

$$M_{max} \text{ occurs at riser length} = 0$$

#### 4.1.4 POINT OF MAXIMUM EFFECTIVE RISER TENSION

### Effective tension along the riser

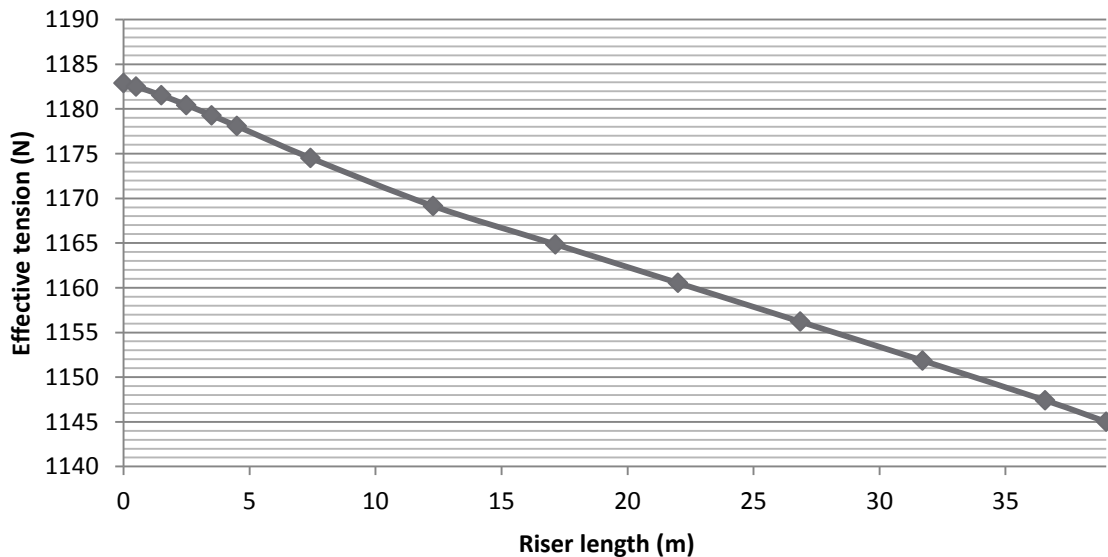


Figure 4.4 The distribution of effective tension along the riser

The distribution of maximum tension along the riser is shown in figure 4.4. The tension has a close to linear distribution, with the largest tension occurring at riser length =0m. This trend was seen in every simulation performed.

$$T_{max} \text{ occurs at riser length} = 0$$

## 4.2 RESULTS OF THE DYNAMIC SIMULATIONS

### 4.2.1 TEST 1 – RESULTS FOR THE 26M RISER SIMULATION (2<sup>ND</sup> JOINT DEPLOYED)

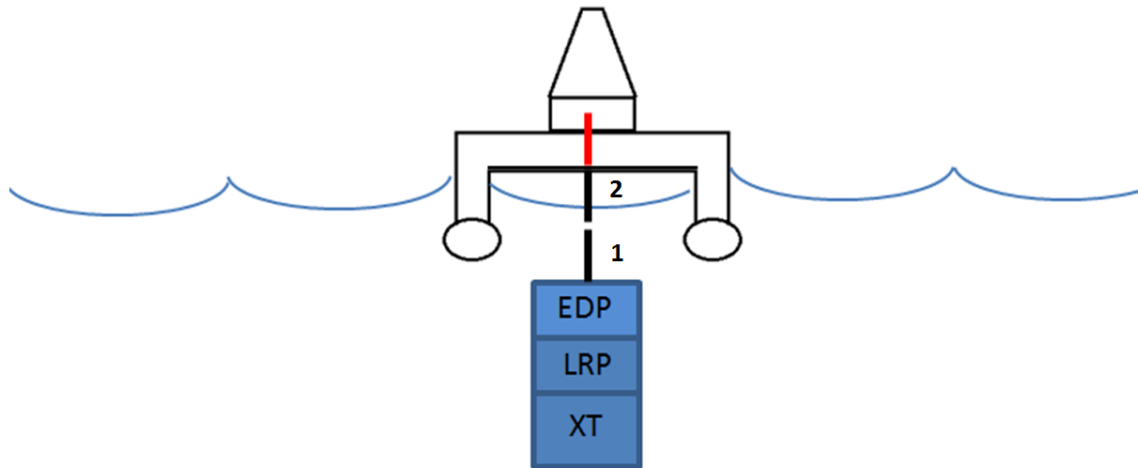


Figure 4.5 The workover vessel with two riser joints deployed.

The first OrcaFlex simulation tested the loads in a 26m riser section deployed from the workover vessel. While the third joint is being connected at the deck, the deployed riser section is exposed to loads due to the motion of the vessel and the equipment package. A sketch of the scenario is seen in figure 4.5.

#### BENDING MOMENT

It was shown that the maximum bending moment for the riser always occur at the top; the connection point between the riser and vessel. Table 4.1 shows the maximum bending moments at the top of the riser during the 800s simulation. For each significant wave height, the bending moment in the riser increase with longer wave periods. This is due to the long waves being closer to the natural period of the system. For  $T_z$  above 10 seconds the increase in bending moment is close to linear.

Table 4.1 Maximum bending moment in the riser for different waves – test 1

		Maximum bending moment (kNm)														
		Tz (sec)														
		2	3	4	5	6	7	8	9	10	11	12	13	14	15	16
Significant wave height Hs (m)	5,0					674	894	836	1176	1303	1786	1830	1972	2103	2227	2333
	4,5				323	548	725	853	1084	1435	1557	1686	1838	1970	2080	2171
	4,0				290	466	583	843	933	1298	1400	1547	1699	1829	1934	2014
	3,5				301	436	494	738	1016	1125	1256	1405	1553	1678	1777	1849
	3,0			172	231	304	461	623	866	979	1110	1254	1395	1515	1608	1670
	2,5			163	252	313	469	631	723	834	956	1090	1222	1335	1419	1472
	2,0			148	183	257	434	507	590	684	790	909	1028	1131	1206	1249
	1,5		111	136	177	267	330	395	457	528	611	706	806	894	957	991
	1,0	103	110	123	161	201	245	287	328	374	427	490	558	621	667	690
	0,5		104	111	126	146	167	188	207	229	254	282				

## Bending moment vs Tz

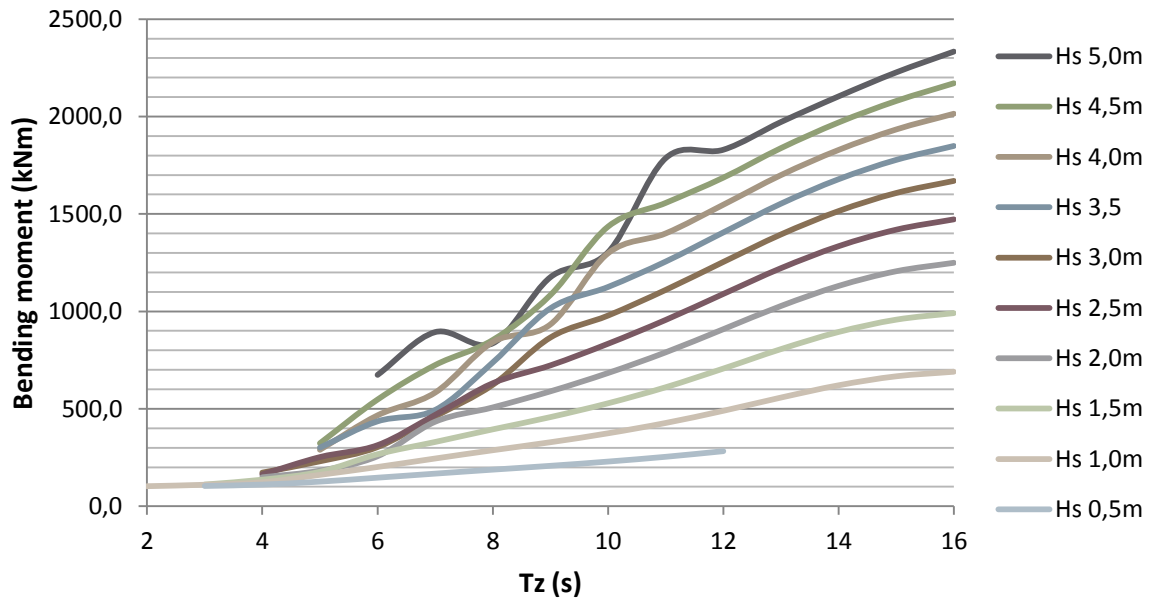


Figure 4.6 The bending moment as a function of wave period (26m test)

Figure 4.6 shows how the bending moment increase with larger zero up-crossing periods for each significant wave height.

## Bending moment vs Hs

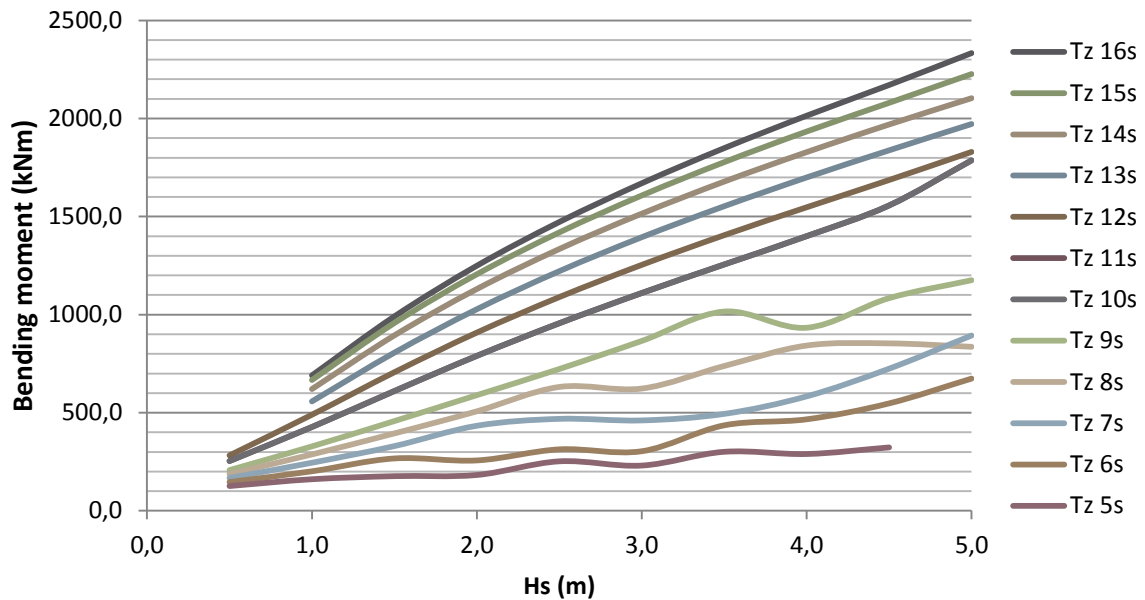


Figure 4.7 The bending moment as a function of the significant wave height (26m test)

The bending moment as a function of the significant wave height is shown in figure 4.7.

## EFFECTIVE TENSION

Table 4.2 Maximum effective riser tensions for different waves – test 1

		Maximum effective tension (kN)														
		Tz (sec)														
		2	3	4	5	6	7	8	9	10	11	12	13	14	15	16
Significant wave height Hs (m)	5,0					1284	1301	1234	1321	1256	1389	1365	1352	1345	1303	1267
	4,5				1151	1220	1233	1259	1289	1305	1333	1315	1302	1296	1263	1233
	4,0				1144	1188	1180	1240	1202	1300	1280	1267	1256	1251	1224	1198
	3,5				1154	1168	1164	1189	1220	1234	1230	1220	1212	1209	1186	1163
	3,0			1072	1111	1108	1127	1157	1186	1188	1184	1170	1170	1167	1149	1130
	2,5			1061	1096	1105	1096	1145	1142	1144	1141	1135	1129	1128	1114	1099
	2,0			1046	1055	1071	1096	1099	1102	1104	1101	1096	1091	1090	1081	1069
	1,5		1000	1033	1044	1059	1061	1065	1066	1067	1064	1060	1057	1056	1050	1042
	1,0	980	997	1013	1024	1029	1031	1034	1034	1033	1031	1028	1025	1025	1022	1017
	0,5		989	996	1000	1003	1004	1005	1005	1004	1002	1001				

It was shown that the largest effective riser tension occurs at the top of the riser. Table 4.2 shows the maximum effective riser tension for the 26m riser.

### 4.2.2 TEST 2 – RESULTS FOR THE 39M RISER SIMULATION (3<sup>RD</sup> JOINT DEPLOYED)

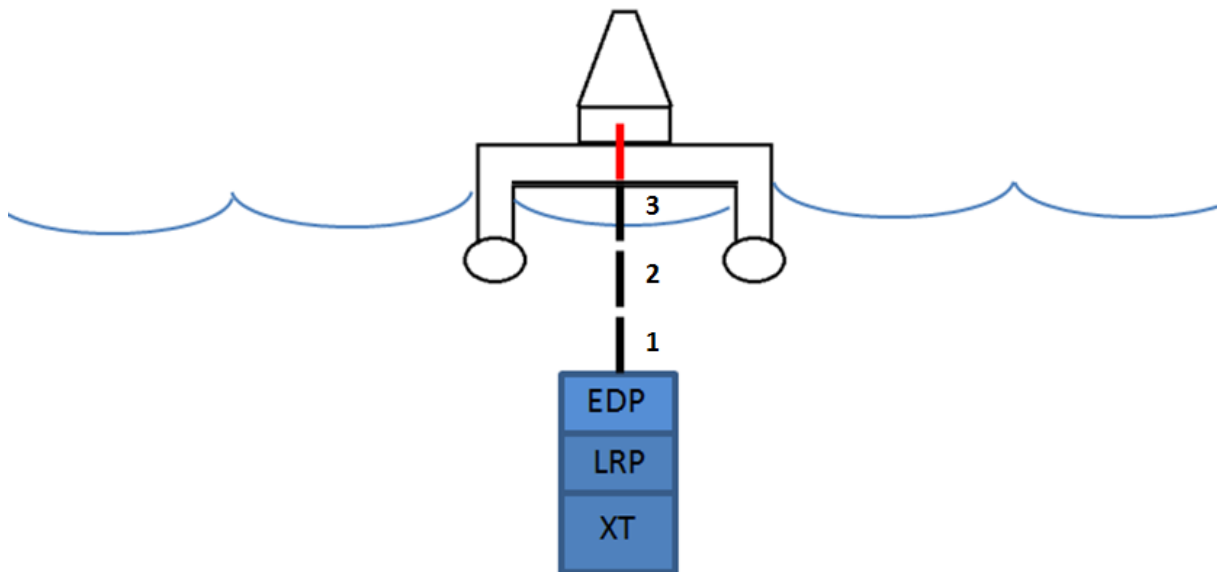


Figure 4.8 The workover vessel with three riser joints deployed

Figure 4.8 illustrates the second dynamic simulation. The 39m riser is suspended of the vessel with the equipment stack attached at the end. This simulates a situation where three riser joint have been deployed and the fourth joint is being connected at the deck.

## BENDING MOMENT

Table 4.3 Maximum bending moments in the riser for different waves – test 2

		Maximum bending moment (kNm)														
		Tz (sec)														
		2	3	4	5	6	7	8	9	10	11	12	13	14	15	16
Significant wave height Hs (m)	5,0					182	287	364	502	639	850	899	978	1063	1138	1208
	4,5				143	148	266	382	474	642	753	820	900	982	1056	1125
	4,0				133	158	233	370	466	614	674	744	820	899	970	1038
	3,5				137	165	228	327	459	539	600	665	737	811	879	944
	3,0			143	126	144	219	287	415	469	525	584	649	717	782	843
	2,5			119	123	137	226	304	354	402	449	500	556	617	676	733
	2,0			114	117	144	212	258	297	336	373	414	460	511	562	611
	1,5		115	108	114	145	180	213	242	271	298	328	362	400	440	478
	1,0	111	106	104	110	129	151	172	190	209	226	245	267	292	317	342
	0,5		102	102	105	113	123	133	142	151	160	169				

The largest value for the bending moment for each sea state is plotted in table 4.3. All the values are in kNm. Figure 4.9 shows the correlation between bending moment and wave period.

### Bending moment vs Tz

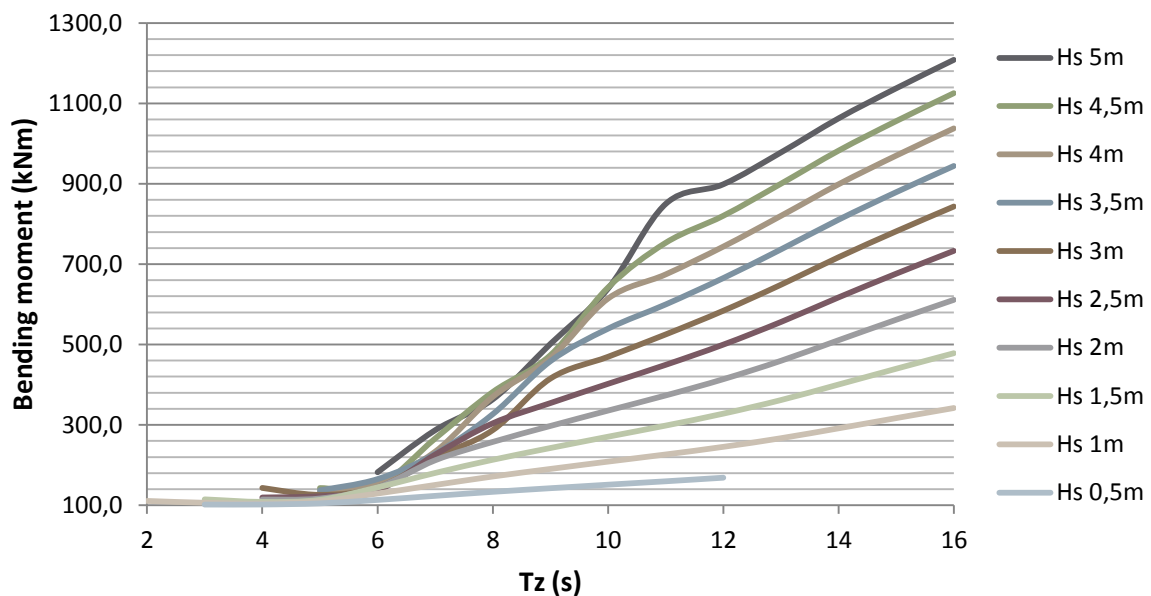


Figure 4.9 The bending moment as a function of wave period (39m test)

The bending moment decrease with lower wave heights as expected. Figure 4.10 shows how the bending moment in the riser increases with the larger significant wave height.



## Bending moment vs Hs

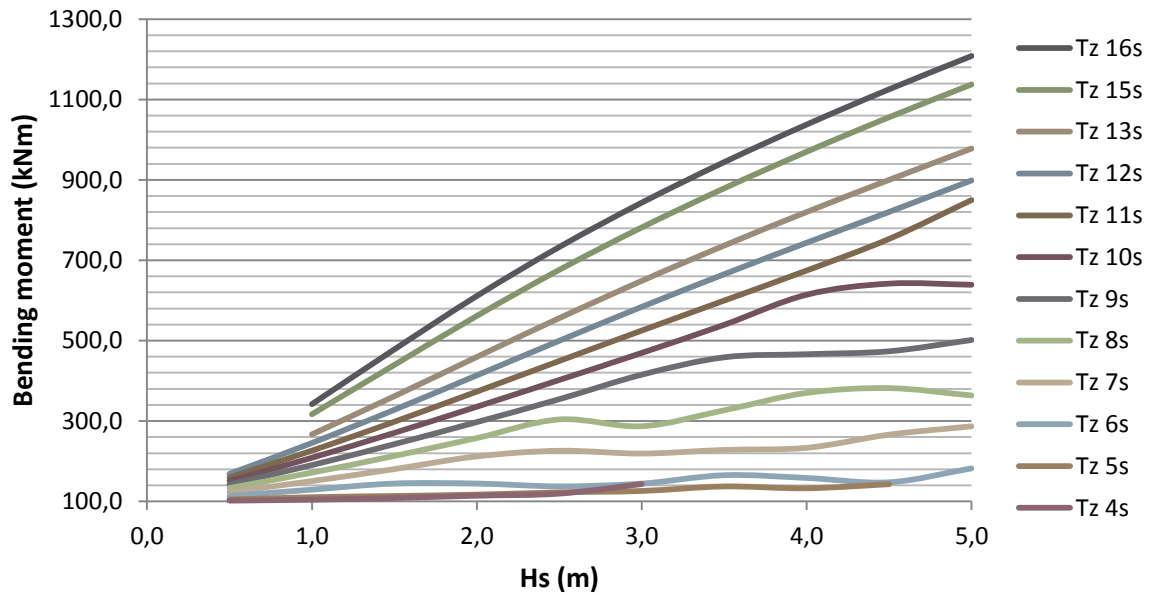


Figure 4.10 The bending moment as a function of the significant wave height (39m test)

### EFFECTIVE TENSION

The maximum effective tension along the riser is always at the top. Table 4.4 shows the riser tension for all wave conditions tested. From the table it can be shown that the difference between the maximum tension for the longest and highest wave compared with the shortest and smallest wave, is approximately 200kN. This is a minor difference compared to the bending moment table.

Table 4.4 Maximum effective riser tensions for different waves – test 2

		Maximum effective tension (kN)														
		Tz (sec)														
		2	3	4	5	6	7	8	9	10	11	12	13	14	15	16
Significant wave height Hs (m)	5,0					1091	1155	1152	1191	1164	1261	1247	1231	1228	1221	1210
	4,5				1037	1079	1132	1153	1184	1206	1229	1214	1201	1199	1193	1184
	4,0				1032	1068	1104	1154	1132	1205	1194	1183	1172	1170	1166	1158
	3,5				1032	1065	1090	1125	1145	1164	1162	1153	1144	1143	1140	1133
	3,0			1010	1020	1047	1076	1096	1129	1134	1133	1125	1117	1117	1114	1109
	2,5			1005	1024	1046	1065	1096	1100	1106	1105	1098	1091	1092	1090	1086
	2,0			1002	1013	1032	1061	1069	1076	1080	1078	1073	1067	1068	1067	1063
	1,5		992	1000	1013	1034	1041	1048	1053	1055	1054	1049	1045	1046	1044	1042
	1,0	993	991	997	1009	1018	1023	1028	1030	1032	1031	1027	1024	1025	1024	1022
	0,5		991	994	999	1004	1006	1008	1009	1010	1009	1007				

### 4.2.3 TEST 3 – RESULTS FOR THE 52M RISER SIMULATION (4<sup>TH</sup> JOINT DEPLOYED)

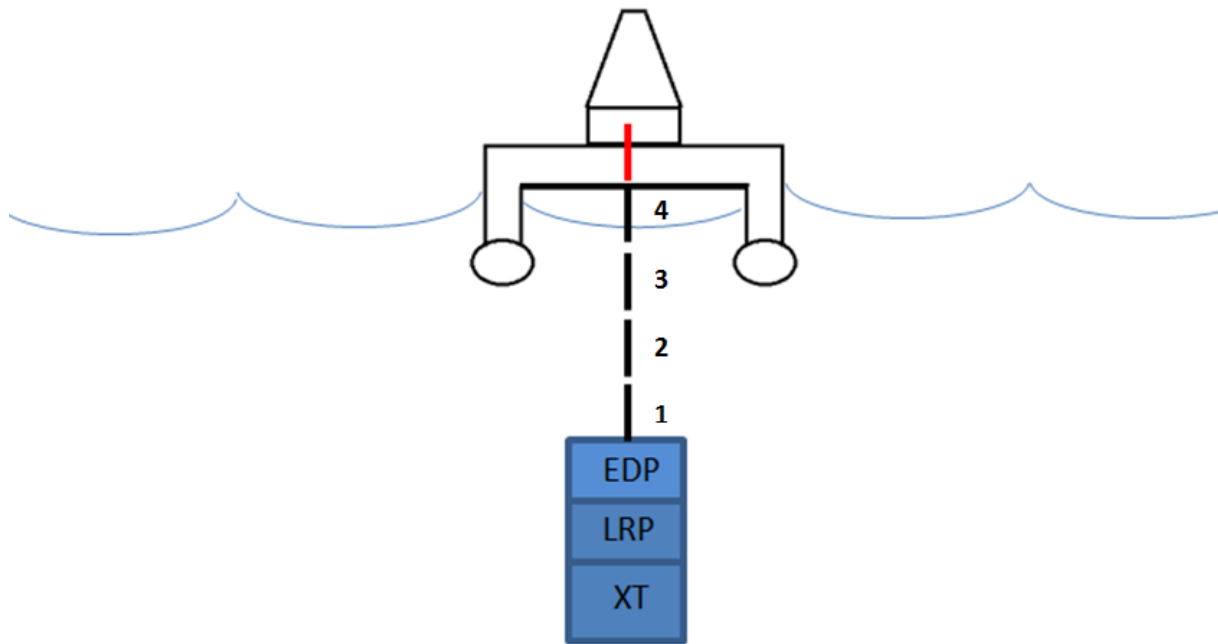


Figure 4.11 The workover vessel with four riser joints deployed

Figure 4.11 shows how the second dynamic simulation is performed. This illustrates a case where the fourth riser joint has been deployed and the fifth joint is being connected topside.

### BENDING MOMENT

Table 4.5 Maximum bending moments in the riser for different waves – test 3

		Maximum bending moment (kNm)														
		Tz (sec)														
		2	3	4	5	6	7	8	9	10	11	12	13	14	15	16
Significant wave height Hs (m)	5,0					191	178	212	303	400	514	564	621	683	736	783
	4,5				145	151	158	222	271	374	468	515	569	628	678	722
	4,0				136	144	155	207	293	376	423	467	517	571	618	660
	3,5				148	131	141	199	275	338	378	419	463	512	555	594
	3,0			142	126	127	143	189	262	299	335	370	408	451	489	525
	2,5			121	124	122	156	196	230	262	291	320	352	388	422	453
	2,0			116	116	117	144	174	200	225	248	271	297	325	352	378
	1,5		113	110	111	116	132	153	172	190	207	224	242	263	283	302
	1,0	106	107	105	108	109	120	133	145	157	168	179	190	203	216	229
	0,5		102	103	104	105	109	115	121	127	132	137				

Table 4.5 shows that the bending moment in the riser is considerably reduced compared to the first dynamic simulation model from test 1. This is due to the effect of the waves which decreases exponentially with water depth. All values are in kNm.

## Bending moment vs Tz

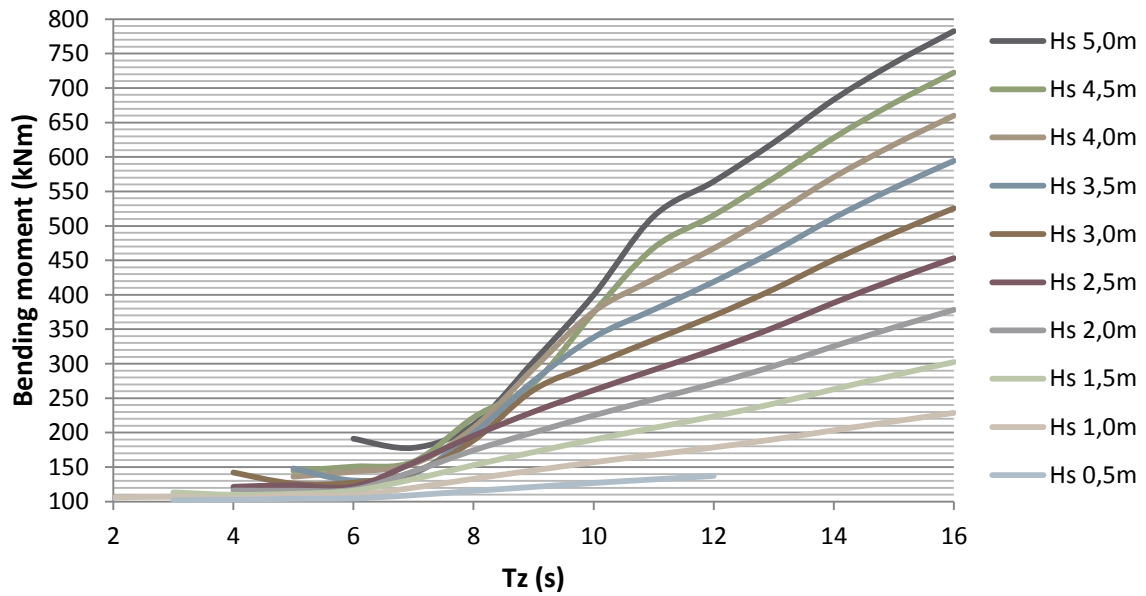


Figure 4.12 The bending moment as a function of wave period (52m test)

The bending moments as a function of zero up-crossing periods are shown in figure 4.12.

## Bending moment vs Hs

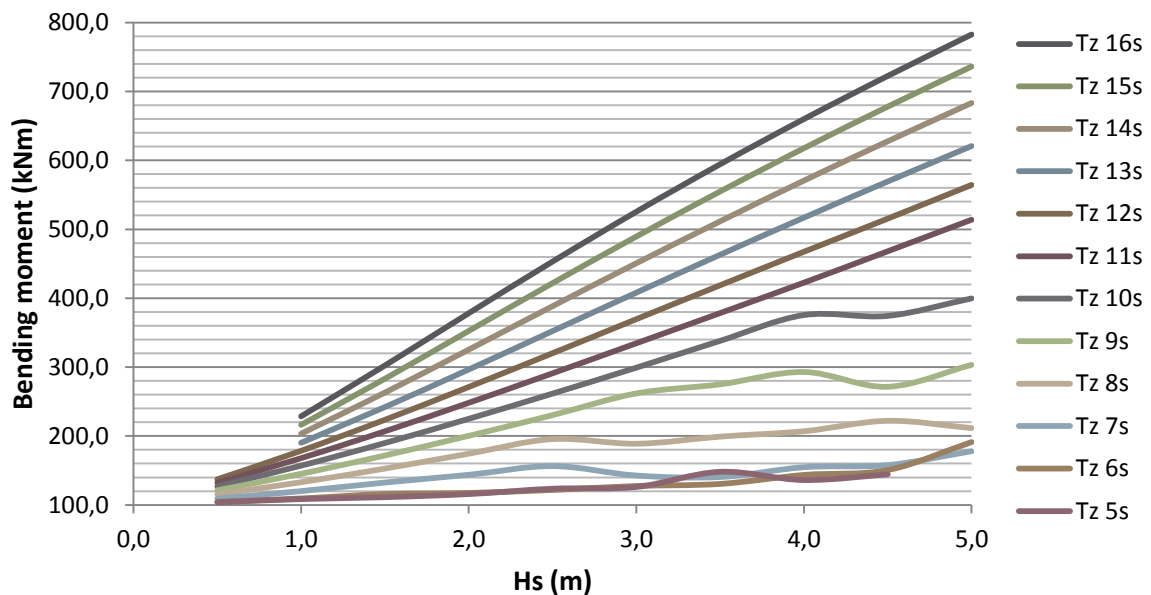


Figure 4.13 The bending moment as a function of the significant wave height (52m test)

Figure 4.13 shows the bending moment as a function of the significant wave height.

## EFFECTIVE TENSION

Table 4.6 shows the effective tension for the 52m riser.

Table 4.6 Maximum effective riser tensions for different waves – test 3

		Maximum effective tension (kN)															
		Tz (sec)															
		2	3	4	5	6	7	8	9	10	11	12	13	14	15	16	
Significant wave height Hs (m)	5,0					1052	1110	1125	1152	1142	1214	1204	1191	1191	1187	1180	
	4,5				1020	1051	1097	1127	1153	1170	1190	1179	1168	1169	1166	1159	
	4,0				1020	1041	1083	1127	1117	1170	1164	1155	1146	1147	1145	1139	
	3,5				1020	1042	1074	1104	1121	1140	1139	1133	1124	1126	1124	1119	
	3,0			1011	1014	1035	1065	1080	1110	1116	1117	1111	1104	1106	1104	1100	
	2,5			1009	1015	1034	1060	1082	1088	1095	1095	1090	1084	1086	1085	1081	
	2,0			1007	1011	1029	1055	1061	1070	1075	1075	1070	1065	1067	1066	1063	
	1,5		1002	1006	1013	1032	1040	1045	1051	1055	1055	1051	1047	1049	1048	1046	
	1,0	1003	1001	1003	1012	1021	1027	1030	1034	1036	1036	1033	1031	1032	1031	1030	
	0,5		1001	1002	1006	1011	1013	1015	1017	1018	1018	1016					

### 4.2.4 TEST 4 – RESULTS FOR THE 65M RISER SIMULATION (5<sup>TH</sup> JOINT DEPLOYED)

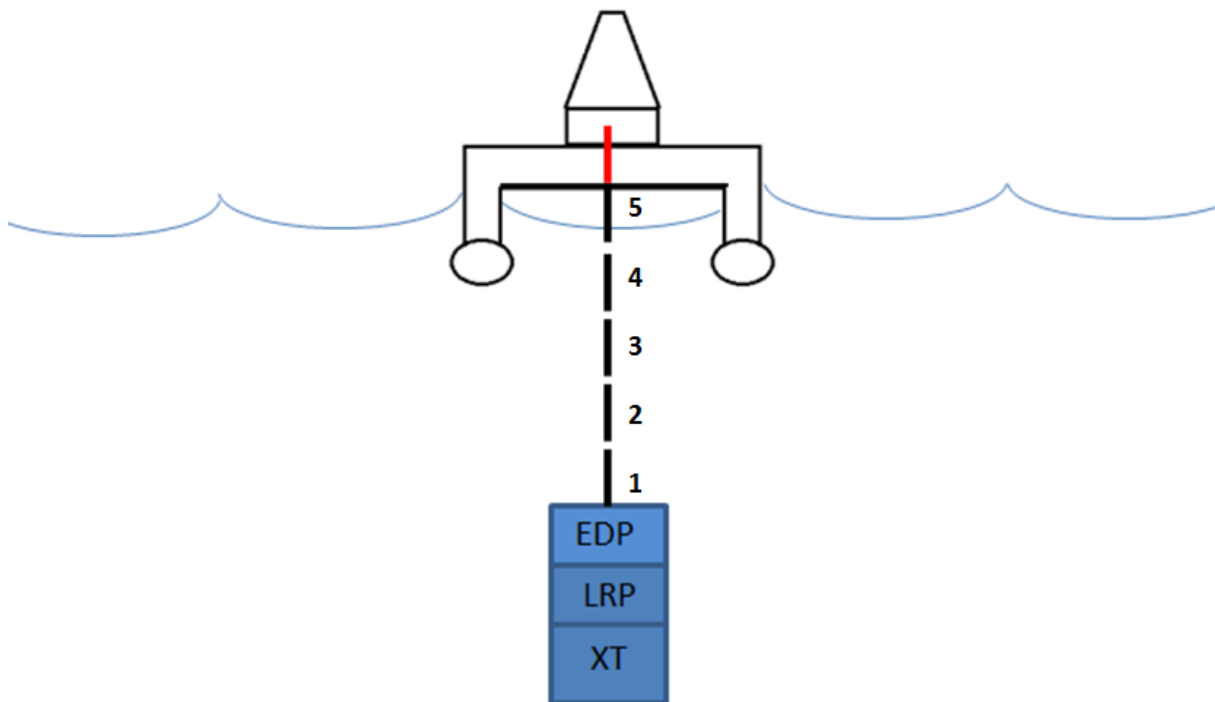


Figure 4.14 The workover vessel with five riser joints deployed

Test 3 uses a 65m long workover riser, this is the case when five riser joints have been deployed and the sixth joint is being connected topside, as seen in figure 4.14. This was the longest riser length tested in OrcaFlex.

## BENDING MOMENT

Table 4.7 Maximum bending moments in the riser for different waves – test 4

		Maximum bending moment (kNm)														
		Tz (sec)														
		2	3	4	5	6	7	8	9	10	11	12	13	14	15	16
Significant wave height Hs (m)	5,0					205	171	180	215	280	355	404	450	501	543	577
	4,5				151	164	155	181	216	253	333	371	414	460	499	531
	4,0				133	150	152	173	207	264	304	339	377	419	454	483
	3,5				157	135	141	155	192	244	276	306	339	376	408	435
	3,0			153	130	133	133	155	191	220	247	273	302	334	361	385
	2,5			126	122	123	128	147	173	197	219	240	264	290	314	334
	2,0			120	115	120	122	137	156	174	192	209	227	248	266	282
	1,5		120	112	112	115	116	126	139	153	166	178	191	206	220	231
	1,0	110	115	109	106	108	110	110	116	125	134	142	150	158	167	176
	0,5		104	104	105	105	106	106	108	112	116	120	124			

The values for the bending moment in table 4.7, continues the trend of the decreasing effect from the waves. It is worth noticing that the bending moment for the  $H_s = 0,5$  simulation has hardly changed for any of the four tests. This is due to the steady current that does not decline with water depth. When the effect from the waves is almost not present, it is the force applied by the current that creates a bending moment in the riser. By assuming that the current has the same value throughout the water depth, the force exerted on the equipment stack will be constant. As the riser is lowered down, this constant force will result in an increasing bending moment at the top section of the suspended riser. So as the bending moment from the waves gradually decreases, bending moment from the current force increases. All values are in kNm.

### Bending moment vs Tz

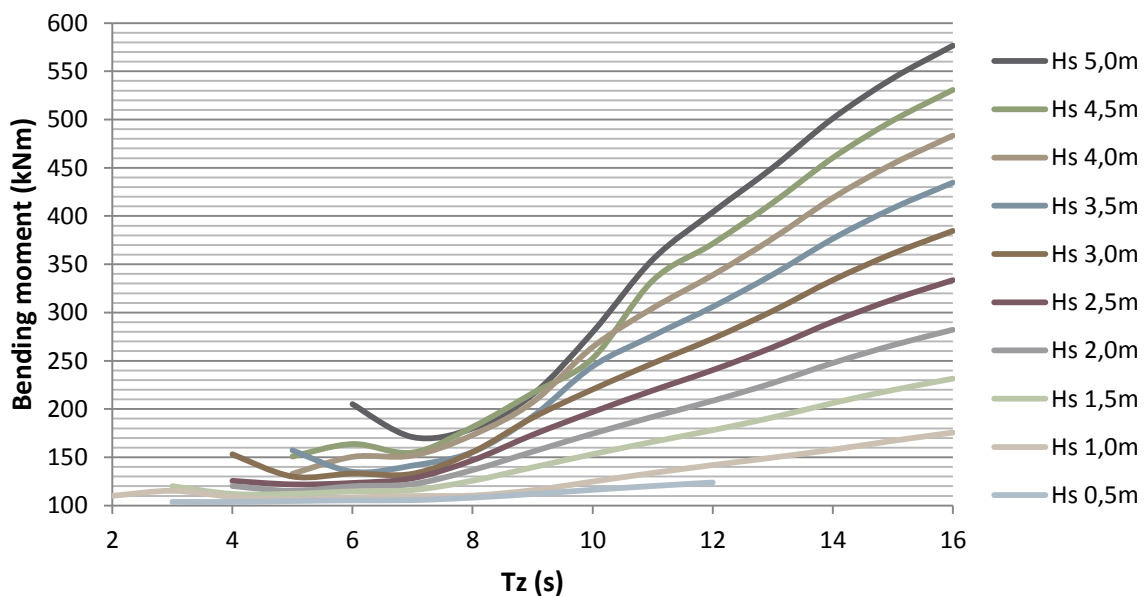


Figure 4.15 The bending moment as a function of wave period (65m test)

The bending moments as a function of the zero up-crossing periods are shown in figure 4.15.

## Bending moment vs Hs

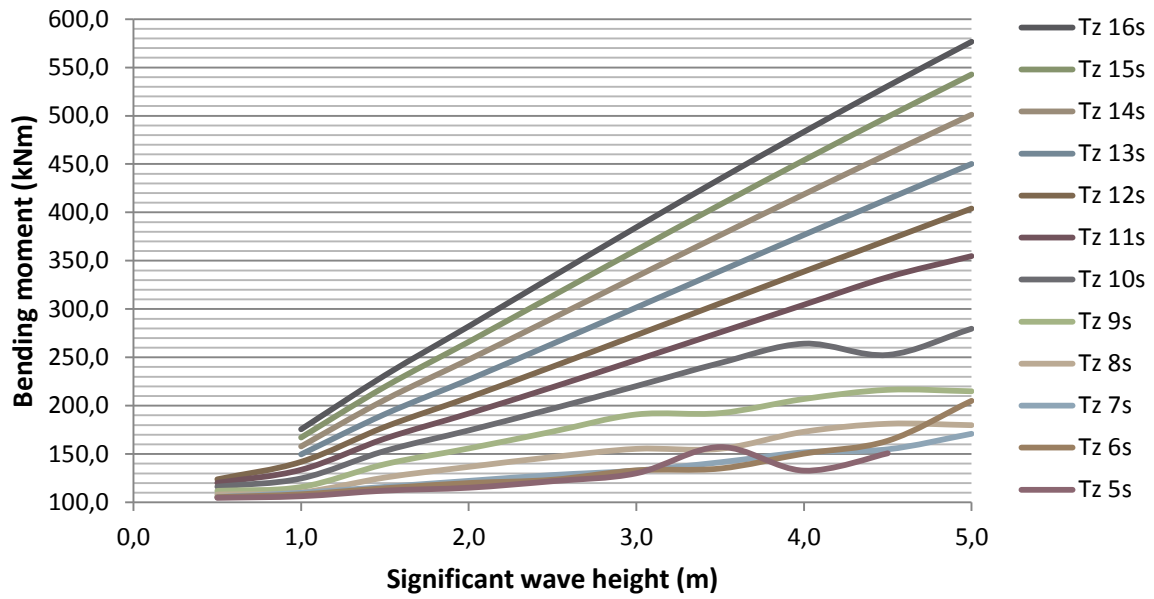


Figure 4.16 The bending moment as a function of the significant wave height (65m test)

The maximum bending moment in the riser as a function of the significant wave height is shown in figure 4.16.

### EFFECTIVE TENSION

The values for the maximum effective tension for the 65m riser are shown in table 4.8.

Table 4.8 Maximum effective riser tensions for different waves – test 4

		Maximum effective tension (kN)															
		Tz (sec)															
		2	3	4	5	6	7	8	9	10	11	12	13	14	15	16	
Significant wave height Hs (m)	5,0					1047	1097	1118	1138	1135	1193	1185	1173	1179	1176	1170	
	4,5				1024	1048	1087	1118	1142	1156	1174	1164	1155	1160	1158	1152	
	4,0				1025	1043	1078	1118	1111	1156	1152	1144	1136	1142	1140	1134	
	3,5				1025	1041	1073	1099	1114	1131	1132	1126	1119	1123	1122	1117	
	3,0			1024	1022	1037	1066	1078	1104	1112	1113	1108	1101	1106	1104	1100	
	2,5			1019	1020	1036	1063	1079	1087	1094	1095	1090	1085	1089	1087	1084	
	2,0			1017	1019	1034	1058	1063	1071	1076	1077	1073	1069	1072	1071	1068	
	1,5		1016	1016	1020	1037	1045	1049	1055	1060	1060	1057	1054	1056	1055	1053	
	1,0	1020	1020	1013	1014	1020	1029	1034	1036	1040	1043	1043	1041	1039	1041	1040	
0,5		1012	1013	1015	1020	1022	1024	1026	1027	1027	1026						

## 4.3 RESULTS FROM ANSYS WORKBENCH

### 4.3.1 RESULTS OF THE SEMI-PRESSURIZED OVER-RIDE FUNCTION TEST

Table 4.9 shows the magnitude of the loads applied to the joint in ANSYS workbench. These loads apply for the semi-pressurized over-ride function test that studies the strength of the joint when the over-ride bolts has a low pretension.

Table 4.9 Data table for the semi-pressurized Over-ride function test

Semi-pressurized Over-ride function test				
	Number of bolts	Location	Magnitude	Cumulative pretension
Tensile bolts reaction force	10	Washer head of tensile bolts	66kN	660kN
Over-ride bolts reaction force	4	Washer head of over-ride bolts	135kN	540kN
Effective riser tension	-	Face of lower joint section	-	1200kN
Tensile bolts pretension	3	Head of bolts	66kN	198kN
Bending moment	-	Lower section face (Y-axis)	400kNm	400kNm

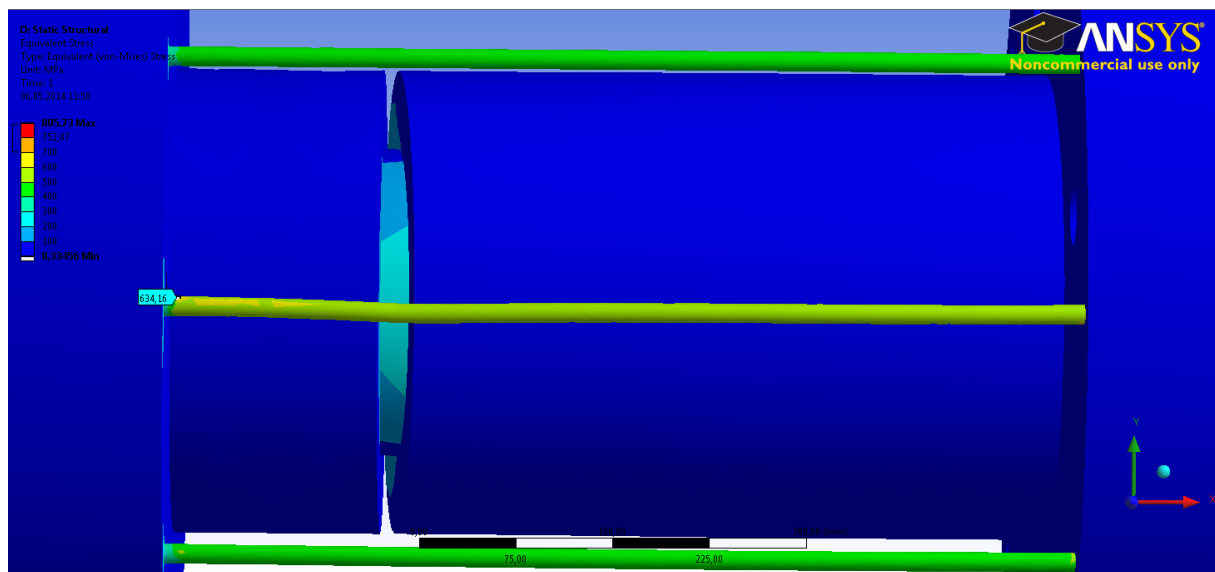


Figure 4.17 Yielding of tensile bolt at 400kNm

The ANSYS workbench simulation revealed that yielding of the tensile bolt furthest away from the neutral axis began at 400kNm. The stress distribution is shown in figure 4.17.

$$M_{max} = 400kNm$$

### 4.3.2 RESULTS OF THE FULLY-PRESSURIZED OVER-RIDE FUNCTION TEST

Table 4.10 shows the loads that were applied to the joint when studying the effect of the over-ride function when its maximum pretension is used.

Table 4.10 Data table for the Active Over-ride function test

Fully-pressurized Over-ride function test				
	Number of bolts	Location	Magnitude	Cumulative pretension
Tensile bolts reaction force	10	Washer head of tensile bolts	66kN	660kN
Over-ride bolts reaction force	4	Washer head of over-ride bolts	490kN	1960kN
Effective riser tension	-	Face of lower joint section	-	1200kN
Tensile bolts pretension	3	Head of bolts	66kN	198kN
Bending moment	-	Lower section face (Y-axis)	620kNm	620kNm

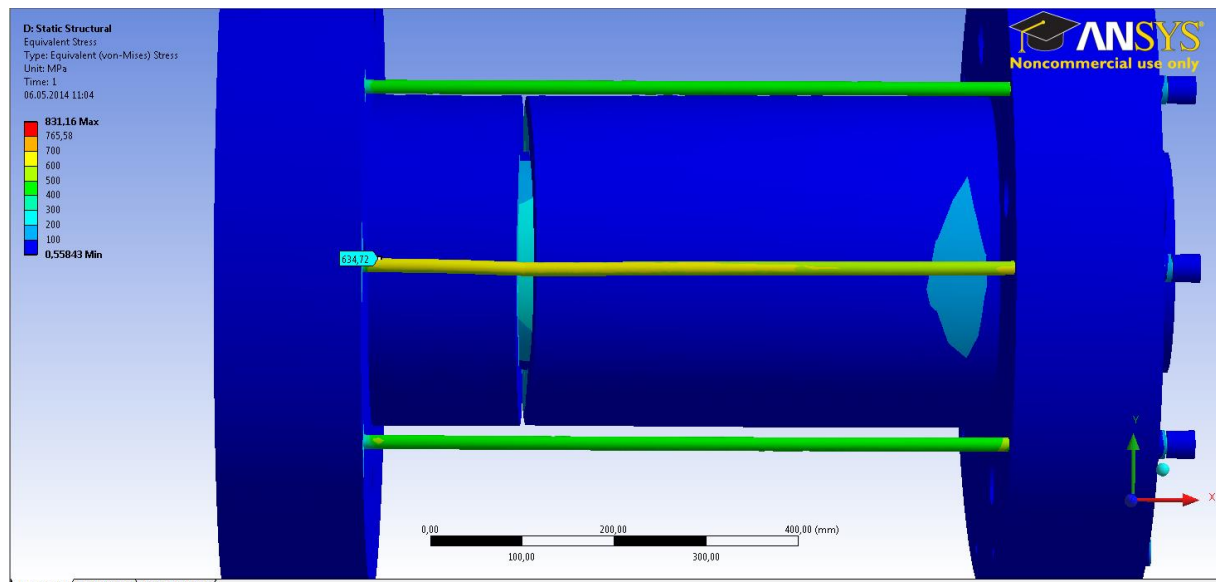


Figure 4.28 Yielding of tensile bolt at 620kNm

When the over-ride bolt pretension was at full capacity, the yielding of the most outer tensile bolt began at 620kNm. The result of the test is shown in figure 4.18.

$$M_{max} = 620kNm$$

### 4.4 WEATHER WINDOW

The results from the ANSYS workbench simulations showed that the maximum bending moment that could be applied to the joint before the tensile bolts began to yield was 400kNm when using the over-ride cylinders were semi-pressurized. The capacity of the joint increased to 620kNm when the four over-ride cylinders were fully pressurized. This is an increase of 55%. Combining these limits with the data tables obtained from the OrcaFlex simulation, it is possible to determine when installation is acceptable and when it is not. The matrices in tables 4.11-4.14 are color coded to show which sea states that are acceptable for installation of the workover system.



#### 4.4.1 INSTALLATION WINDOW FOR THE TSJ AS THE 2<sup>ND</sup> RISER JOINT

Table 4.11 Installation window for the TSJ as the 2<sup>nd</sup> joint

		Installation window - TSJ on 2nd riser joint														
		Tz (sec)														
		2	3	4	5	6	7	8	9	10	11	12	13	14	15	16
Significant wave height Hs (m)	5,0					21	544	985	1928	737	488	200	89	0	10	1
	4,5				9	118	1241	1221	2312	943	593	283	114	0	8	0
	4,0				84	373	2175	1472	2994	1202	754	286	130	0	24	6
	3,5				550	792	2716	1703	4095	1257	868	280	91	0	29	4
	3,0			4	1413	1202	3465	2362	4776	1478	799	330	130	0	25	10
	2,5			128	2984	1626	4847	3351	5021	1509	725	261	111	0	39	11
	2,0			625	3447	1676	5814	2866	4210	1020	469	230	85	0	31	11
	1,5		38	2263	5478	3604	8972	3391	3918	706	329	163	94	0	25	13
	1,0	1	264	1792	5037	2225	4450	1442	1268	260	109	46	34	0	10	2
	0,5		8	38	72	69	107	35	14	3	1	1				

Installation acceptable
Installation acceptable only for fully-pressurized over-ride cylinders
Installation not acceptable

Table 4.11 shows the sea states that will not lead to plastic damage to the safety joint when it has been installed as the 2<sup>nd</sup> riser joint. The values in the table are taken from the all year scatter diagram and show how many observations that is recorded for each sea state.

#### 4.4.2 INSTALLATION WINDOW FOR THE TSJ AS THE 3<sup>RD</sup> RISER JOINT

Table 4.12 shows which wave conditions that are within the acceptable range for installation when the TSJ is installed as the 3<sup>rd</sup> joint on the workover riser.

Table 4.12 Installation window for the TSJ as the 3<sup>rd</sup> joint

		Installation window - TSJ on 3rd riser joint														
		Tz (sec)														
		2	3	4	5	6	7	8	9	10	11	12	13	14	15	16
Significant wave height Hs (m)	5,0					21	544	985	1928	737	488	200	89	0	10	1
	4,5				9	118	1241	1221	2312	943	593	283	114	0	8	0
	4,0				84	373	2175	1472	2994	1202	754	286	130	0	24	6
	3,5				550	792	2716	1703	4095	1257	868	280	91	0	29	4
	3,0			4	1413	1202	3465	2362	4776	1478	799	330	130	0	25	10
	2,5			128	2984	1626	4847	3351	5021	1509	725	261	111	0	39	11
	2,0			625	3447	1676	5814	2866	4210	1020	469	230	85	0	31	11
	1,5		38	2263	5478	3604	8972	3391	3918	706	329	163	94	0	25	13
	1,0	1	264	1792	5037	2225	4450	1442	1268	260	109	46	34	0	10	2
	0,5		8	38	72	69	107	35	14	3	1	1				

Installation acceptable
Installation acceptable only for fully-pressurized over-ride cylinders
Installation not acceptable

#### 4.4.3 INSTALLATION WINDOW FOR THE TSJ AS THE 4<sup>TH</sup> RISER JOINT

The weather window for installation with respect to the TSJ is larger when the joint is installed as the 4<sup>th</sup> riser joint. Since the riser is longer, the equipment package is less exposed to the wave forces. Less wave forces on the equipment stack means less bending moment in the riser and so there are more waves acceptable for installation. Table 4.13 shows which wave conditions that allow for installation of the equipment stack with the TSJ as a 4<sup>th</sup> link, without any plastic damage to any of the joint's tensile bolts.

Table 4.13 Installation window for the TSJ as the 4<sup>th</sup> joint

Installation window - TSJ on 4th riser joint																
		Tz (sec)														
		2	3	4	5	6	7	8	9	10	11	12	13	14	15	16
Significant wave height Hs (m)	5,0					21	544	985	1928	737	488	200	89	0	10	1
	4,5				9	118	1241	1221	2312	943	593	283	114	0	8	0
	4,0				84	373	2175	1472	2994	1202	754	286	130	0	24	6
	3,5				550	792	2716	1703	4095	1257	868	280	91	0	29	4
	3,0			4	1413	1202	3465	2362	4776	1478	799	330	130	0	25	10
	2,5			128	2984	1626	4847	3351	5021	1509	725	261	111	0	39	11
	2,0			625	3447	1676	5814	2866	4210	1020	469	230	85	0	31	11
	1,5		38	2263	5478	3604	8972	3391	3918	706	329	163	94	0	25	13
	1,0	1	264	1792	5037	2225	4450	1442	1268	260	109	46	34	0	10	2
0,5		8	38	72	69	107	35	14	3	1	1					

Installation acceptable
Installation acceptable only for fully-pressurized over-ride cylinders
Installation not acceptable

#### 4.4.4 INSTALLATION WINDOW FOR THE TSJ AS THE 5<sup>TH</sup> RISER JOINT

For the 65m riser, installation will be acceptable for all wave conditions as long as the over-ride function is active. When the over-ride cylinders are semi-pressurized there are 14 wave conditions that lead to plastic deformation of the tensile bolts. Table 4.14 shows which conditions that are acceptable for installation.

Table 4.14 Installation window for the TSJ as the 5<sup>th</sup> joint

Installation window - TSJ on 5th riser joint																
		Tz (sec)														
		2	3	4	5	6	7	8	9	10	11	12	13	14	15	16
Significant wave height Hs (m)	5,0					21	544	985	1928	737	488	200	89	0	10	1
	4,5				9	118	1241	1221	2312	943	593	283	114	0	8	0
	4,0				84	373	2175	1472	2994	1202	754	286	130	0	24	6
	3,5				550	792	2716	1703	4095	1257	868	280	91	0	29	4
	3,0			4	1413	1202	3465	2362	4776	1478	799	330	130	0	25	10
	2,5			128	2984	1626	4847	3351	5021	1509	725	261	111	0	39	11
	2,0			625	3447	1676	5814	2866	4210	1020	469	230	85	0	31	11
	1,5		38	2263	5478	3604	8972	3391	3918	706	329	163	94	0	25	13
	1,0	1	264	1792	5037	2225	4450	1442	1268	260	109	46	34	0	10	2
0,5		8	38	72	69	107	35	14	3	1	1					

Installation acceptable
Installation acceptable only for fully-pressurized over-ride cylinders
Installation not acceptable

## 4.5 SUMMARY OF RESULTS

Table 4.15 shows the amount of the time that installation of an EDP, LRP and Xmas tree stack can be performed when using the workover riser as a running tool. The table shows when the installation can be performed depending on which point along the riser the TSJ have been installed. The table compares the availability for the joint when the over-ride cylinders are semi-pressurized and when they are fully pressurized. This was calculated by summarizing all the observations done at the acceptable wave conditions and dividing them by the total number of observations that have been performed in the scatter diagram.

Table 4.15 Availability for installation of EDP, LRP and Xmas tree at Draugen

Percentage of time that installation can be performed				
	Telescopic Safety Joint installed as joint no.			
	2	3	4	5
TSJ with over-ride at full capacity	58,1 %	87,9 %	91,3 %	91,4 %
TSJ with reduced over-ride pretension	36,4 %	71,2 %	88,5 %	91,1 %
Increased availability for over-ride function	21,7 %	16,7 %	2,8 %	0,3 %

## 4.6 STRENGTH OF THE RISER

No matter how efficient the over-ride function might be, installation will not be possible if the workover riser cannot cope with the increased load conditions. To see whether the safety joint will limit the weather window for installation, hand calculations was performed to find out which bending moment result in yielding of the workover riser. This is done using the equation for uniaxial Von-Mises stress (Gelgele, 2010, p.24)

$$\sigma_{Von-Mises} = \sqrt{(\sigma_b + \sigma_t)^2 + 3\tau^2} \quad (4.1)$$

Where:

- $\sigma_b$  is the bending stress [MPa]
- $\sigma_t$  is the axial stress [MPa]
- $\tau$  is the shear stress [MPa]

### Axial stress

The axial stress is calculated from the formula:

$$\sigma_t = \frac{T_{max}}{A} \quad (4.2)$$

Where:

- $A$  is the cross sectional area of the workover riser [ $mm^2$ ]

Dimension from table 3.2 gives the cross sectional area:

$$A = \frac{(219^2 - 178^2)}{4} \cdot \pi = 1,28 \cdot 10^4 mm^2$$

The effective riser tension used for the ANSYS simulations was  $T_{max} = 1200kN$ , hence:

$$\sigma_t = \frac{T_{max}}{A} = 94MPa$$

### Shear stress

The maximum shear stress that occurred in the riser during installation when two riser joint were deployed are shown in table 4.16. The green section shows where the installation is acceptable when the over-ride cylinders are fully pressurized. The maximum shear force that occurs within this area is 169kN. The riser must be able to withstand this shear force in order to not be the bottle neck of the operation.

Table 4.16 Shear force in the workover riser

		Maximum shear force (kN)															
		Tz (sec)															
		2	3	4	5	6	7	8	9	10	11	12	13	14	15	16	
Significant wave height Hs (m)	5,0					196	266	240	343	366	527	529	575	621	661	695	
	4,5				91	157	209	246	312	417	443	478	526	571	607	636	
	4,0				82	133	166	238	258	367	392	433	479	523	556	583	
	3,5				84	123	139	210	287	312	348	390	434	474	506	530	
	3,0			48	64	85	127	176	240	270	306	346	387	425	454	475	
	2,5			46	70	88	131	175	199	230	263	300	338	373	399	416	
	2,0			41	51	71	120	140	163	188	218	251	284	315	338	352	
	1,5		31	38	49	74	91	109	126	146	169	195	223	249	267	278	
	1,0	29	31	34	45	56	68	79	91	103	118	136	155	173	186	193	
	0,5		29	31	35	41	46	52	57	63	70	78					

$$S_{max} = 169kN$$

The shear stress is found using  $S_{max}$  instead of  $T_{max}$  in Eq.4.2:

$$\tau = \frac{S_{max}}{A} = 13MPa$$

### Bending stress

$$\sigma_b = \frac{My}{I} \quad (4.3)$$

Where:

- $y$  is the distance from the neutral line to the point furthest from the center [ $mm$ ]
- $I$  is the moment of inertia [ $mm^4$ ]

$$I = \frac{(OD^4 - ID^4)}{64} \cdot \pi \quad (4.4)$$

Using riser dimensions from table 3.2, the moment of inertia is calculated from Eq.4.4:

$$I = 6,25 \cdot 10^7 mm^4$$

$$y = \frac{OD}{2} = 110mm$$

### Maximum allowable bending moment in the riser

According to workover riser data from Shell the yield strength of the riser can be up to  $724\text{MPa}$ . Using this limit as the maximum allowable Von-Mises stress in the riser, the maximum allowable bending moment can be calculated.

Combining Eq.4.1 with Eq.4.3 the maximum allowable bending moment can be written as:

$$M = \frac{(\sqrt{(\sigma_{\text{Von-Mises}})^2 - 3\tau^2} - \sigma_t)I}{y}$$

Inserting all calculated values gives an allowable bending moment for the workover riser of:

$$M = \frac{(\sqrt{(724\text{MPa})^2 - 3(13\text{MPa})^2} - 94\text{MPa})}{110\text{mm}} \cdot 6,25 \cdot 10^7 \text{mm}^4$$

$$M = 355\text{kNm}$$

# 5. CONCLUSIONS

## 5.1 DISCUSSION

To sum up the result from the simulations; the strength of the joint increased when maximum hydraulic pressure was applied to the over-ride cylinders as opposed to the semi-pressurized test. The tensile bolts in the semi-pressurized joint began yielding at 400kNm. This increased by 55% to 620kNm when the over-ride function was fully pressurized. As far as the weather window is concerned, there was an increase in availability for performing installation of the workover system when using the full capacity of the over-ride system. The Telescopic Safety Joint appears to be very robust. To put these numbers into perspective, hand calculations showed that the allowable bending moment in an OD 8 5/8", ID 7" workover riser would be in the vicinity of 355kNm. It is likely that the workover riser would rupture before damage would occur to the safety joint and thus the safety joint do not limit the weather window for installation of the workover system. In fact, the results from this thesis would suggest that the safety joint would be able to perform just as well with reduced hydraulic pressure to the over-ride cylinders, or even a reduced system all together. It should be noted that a large pretension for the over-ride cylinders may protect the tensile bolts from the increased axial load and may prevent them from taking fatigue damage during the installation face. A comparison between the strength of the joint for different pressurized over-ride cylinders versus the workover riser is seen in figure 4.19. A TSJ without an active over-ride function is not included as it would not be able to withstand 1200kN of tension.

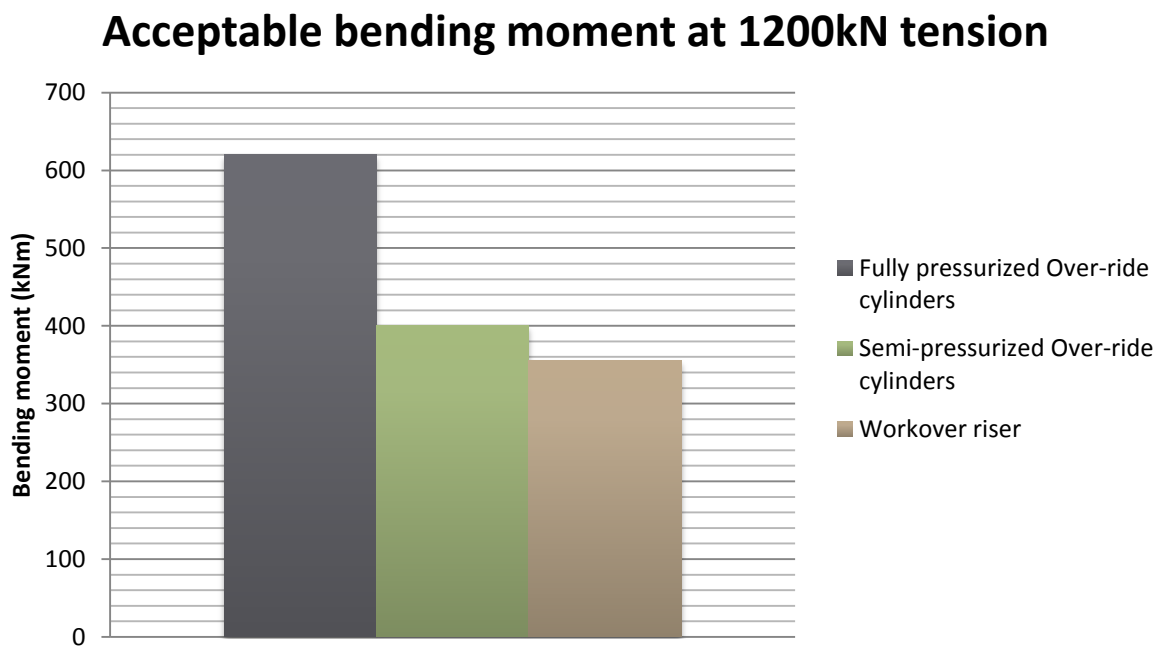


Figure 5.1 Acceptable bending moment for TSJ vs workover riser

It should also be made clear that the over-ride function certainly would be a requirement when the safety joint is to be installed in the workover riser. If no over-ride function were present, the tensile bolts would rupture immediately after the deployment of the joint due to axial forces alone. Section 3.8.3 showed that the joint could withstand an additional axial force of 550kN before the bolts began to yield. From OrcaFlex it was seen that the effective riser tension never dropped below 990kN for any of the simulations.

Whether the safety joint should be installed as the second, third, fourth, etc. -joint should be decided based upon each individual workover. The over-ride cylinders are not functional during operation, thus the joint is more vulnerable to axial and bending forces at this stage. The bending moment in the riser usually has two bending maxima, where one of these is located close to the bottom. The actual location and magnitude of this will depend upon several factors including top tension, weight of riser, water depth and vessel drift-off. The TSJ should be situated close to the bottom where the axial tension is lower, but not at the location of one of the bending maxima. It would therefore be recommended that calculations are performed for each individual workover case before deciding where to locate the safety joint. The strength and pretension of the bolts must be adjusted to suit the position where the joint is installed so that they rupture at the correct top tension.

## 5.2 CONCLUSIONS

The conclusions of this thesis are that the over-ride function would be a requirement when performing installation of an EDP, a LRP and a Xmas tree when using the workover riser as a running tool. This over-ride function provides sufficient increased strength of the joint so that the joint itself does not become a limiting factor when performing workover installation. The ANSYS simulations performed here indicated that the effect of the over-ride function is so great the strength of the joint exceeds that of the workover riser.

## 5.3 RECOMMENDATIONS FOR FUTURE WORK

Several simplifications were done in order to complete all the simulations performed in this thesis. If more accurate data values for the loading conditions are required, a good way to begin would be improve the model of the equipment stack in OrcaFlex. The true EDP, LRP and Xmas tree has a quite complex geometry and its volume, drag- and mass coefficients may differ from the ones used in these simulations.

The ANSYS workbench model was based on a crude work drawing and does not contain all details of the true joint. Better result might be obtained if a full model of the joint was created with all external cylinders included, as well as all the physical bolts.

Due to problems with the software on the computer used at the University of Stavanger, error messages repeatedly appeared when trying to alter the mesh of the model. These error messages did not appear when the same alterations were done using ANSYS workbench 14.0 at a different computer. Due to this, only the auto generated tetrahedral mesh setting was used for the simulations. It is acknowledged that the quality of the ANSYS simulations can be discussed due to this. It would be recommended to focus on different mesh settings for more thorough analysis at a later stage.

## REFERENCE LIST

- A/S Norske Shell (2009) "Offshore Metocean Design and Operational Criteria – Draugen Platform" Vol 10. Restricted document.
- Azar J.J., Soltveit. R.E. (1978) "A Comprehensive Study of Marine Drilling Risers" American Institute of Mining Metallurgical and Petroleum Engineers Inc. - SPE 7200
- Baker R.J (1991) "Improved Heave Compensation". Paper presented at the SPE/IADC Drilling Conference, Amsterdam, 11-14 March 1991. -SPE/IADC 21961
- Det Norske Veritas Recommended Practice C-205., (2010) "Environmental Conditions and Environmental Loads"
- Det Norske Veritas Recommended Practice H-103., (2011) "Modelling and Analysis of Marine Operations"
- Finnemore. E.J & Franzini. J.B. (2002) "Fluid Mechanics with Engineering Applications". 10<sup>th</sup> edition. McGraw-Hill.
- FMC Technologies (2014) "Safety Joint Test and Presentation; System Description" Unpublished presentation. FMC Safety Joint Team, Notodden.
- Gelgele, H.L. (2010), Compendium "Dimensjonering av Maskinelementer" from the course "BIM150 Maskinelementer" [Compendium], University of Stavanger, Department of Mechanical and Structural Engineering and Materials Science
- Gudmestad. O.T., (2013) Lecture notes from the course "MOM480 - Marine Technology and Design" at the University of Stavanger Spring of 2013
- Guo. B., Song. S., Ghalambor. A., Lin. T.R., (2014) "Offshore Pipelines: Design, Installation, and Maintenance". 2<sup>nd</sup> edition. Elsevier Inc
- ISO 19902:2007., (2011) "Petroleum and natural gas industries -- Fixed steel offshore structures"
- Montgomery. J., (2002) "Methods for Modeling Bolts in the Bolted Joint", presented at the 2002 International ANSYS Conference
- NORSOK D-002., (2000). "System Requirements Well Intervention Equipment" Rev. 1
- Offshore.no (March 2014), "Alt klart for Rodriguez" [Internet], Offshore.no AS. Available at: [http://www.offshore.no/sak/36592\\_alt\\_klart\\_for\\_rodriguez](http://www.offshore.no/sak/36592_alt_klart_for_rodriguez) [March, 2014]
- Orcina.com (January 2, 2014) "Orcaflex" [Internet], Orcina Ltd. Available at: <http://www.orcina.com/SoftwareProducts/OrcaFlex/index.php> [February 2014]
- Statoil (1998) "Accident cause found" [Internet], Statoil ASA. Available at: <http://www.statoil.com/en/NewsAndMedia/News/1998/Pages/AccidentCauseFound.aspx> [May, 2014]
- Stewart. R.H, (November 15, 2006) "Ocean Waves" [Internet], Texas A&M University, Department of Oceanography. Available at: [http://oceanworld.tamu.edu/resources/ocng\\_textbook/chapter16/chapter16\\_04.htm](http://oceanworld.tamu.edu/resources/ocng_textbook/chapter16/chapter16_04.htm) [March, 2014]



Subsea1.com (September 5, 2010) "Workover systems" [Internet], Ibruk as. Available at:  
[http://subsea1.com/index/page?keyword=workover\\_completion\\_system](http://subsea1.com/index/page?keyword=workover_completion_system) [February 2014]

Tømmermo. B.O., Tandberg. G., Carlsen. H.P., Carlsen. T.Ø., Muff. A.D., Løvland T.A., Orekåsa. R., Sundkvist. A., Sørensen. A. & Lerstang. J. (2014). "Pressure Balanced Telescopic Riser Safety Joint". Paper presented at the Offshore Technology Conference, Houston, May 5-8, 2014. OTC 25147-MS